ลักษณะสมบัติการเร่งปฏิกิริยาแสงของไททาเนียมไดออกไซด์ที่เจือธาตุต่างๆและปรับสภาพด้วยกระบวนการไฮโดรเทอร์มัลภายใต้การกระตุ้นด้วยแสงที่มองเห็น

นางสาวฐาปนันท์ พุทธา

วิทยานิพนธ์นี้เป็นส่วนหนึ่งของการศึกษาตามหลักสูตรปริญญาวิทยาศาสตรดุษฎีบัณฑิต
สาขาวิชาการจัดการสิ่งแวดล้อม (สหสาขาวิชา)
บัณฑิตวิทยาลัย จุฬาลงกรณ์มหาวิทยาลัย
ปีการศึกษา 2552

PHOTOCATALYTIC CHARACTERISTICS OF TITANIUM DIOXIDE DOPED WITH VARIOUS ELEMENTS AND HYDROTHERMAL TREATMENT UNDER VISIBLE-LIGHT ACTIVATION

Miss Thapanan Putta

A Dissertation Submitted in Partial Fulfillment of the Requirements
for the Degree of Doctor of Philosophy Program in Environmental Management
(Interdisciplinary Program)
Graduate School
Chulalongkorn University
Academic Year 2009

Thesis Title	PHOTOCATALYTIC CHARACTERISTICS OF TITANIUM DIOXIDE DOPED WITH VARIOUS ELEMENTS AND HYDROTHERMAL TREATMENT UNDER VISIBLE-LIGHT ACTIVATION
By	Miss Thapanan Putta
Field of Study	Environmental Management
Thesis Advisor	Associate Professor Jin Anotai, Ph.D.
Thesis Co-Advisor	Professor Ming-Chun Lu, Ph.D.

Accepted by the Graduate School, Chulalongkorn University in Partial Fulfillment of the Requirements for the Doctoral Degree

..... Dean of the Graduate School
(Associate Professor Pornpote Piumsomboon,Ph.D.)

THESIS COMMITTEE

..... Chairman
(Chantra Tongcumpou, Ph.D.)

..... Thesis Advisor
(Associate Professor Jin Anotai, Ph.D.)

..... Thesis Co-Advisor
(Professor Ming-Chun Lu, Ph.D.)

..... Examiner
(Nyein Nyein Aung, Ph.D.)

..... Examiner
(Pichet Chaiwiwatworakul, Ph.D.)

..... External Examiner
(Associate Professor Duangrat Inthorn, Ph.D.)

ฐาปนันท์ พุทธา : ลักษณะสมบัติการเร่งปฏิกิริยาแสงของไททาเนียมไดออกไซด์ที่เจือธาตุต่างๆและปรับสภาพด้วยกระบวนการไฮโดรเทอร์มัลภายใต้การกระตุ้นด้วยแสงที่มองเห็น (PHOTOCATALYTIC CHARACTERISTICS OF TITANIUM DIOXIDE DOPED WITH VARIOUS ELEMENTS AND HYDRO-THERMAL TREATMENT UNDER VISIBLE-LIGHT ACTIVATION) อ. ที่ปรึกษาวิทยานิพนธ์หลัก: รองศาสตราจารย์ ดร. จินต์ อโณทัย, อ. ที่ปรึกษาวิทยานิพนธ์ร่วม: Professor Ming-Chun Lu, Ph.D., 119 หน้า.

ในงานวิจัยนี้ สารเร่งปฏิกิริยาแสงไททาเนียมไดออกไซด์ชนิดใหม่ที่เจือทังสเตนและปรับสภาพด้วยกระบวนการไฮโดรเทอร์มัลได้ถูกพัฒนาและทดสอบความไวปฏิกิริยาของการเร่งปฏิกิริยาแสงโดยใช้ 2-คลอโรฟีนอลเป็นสารเป้าหมาย วิธีการสังเคราะห์และสภาวะที่เหมาะสมได้แจกแจงไว้อย่างละเอียด สารเร่งปฏิกิริยาแสงนี้สามารถถูกกระตุ้นอย่างมีประสิทธิภาพภายใต้การฉายแสงสีฟ้าและมีความไวปฏิกิริยาเกือบเทียบเท่ากับ Degussa P-25 ที่ผลิตเพื่อการค้าภายใต้การฉายแสงอัลตราไวโอเล็ต โดย 2-คลอโรฟีนอลที่ 0.01 มิลลิโมลาร์สามารถถูกกำจัดได้ทั้งหมดภายใน 120 และ 90 นาทีด้วยกระบวนการเร่งปฏิกิริยาแสงที่ใช้ไททาเนียมไดออกไซด์เจือทังสเตนร้อยละ 0.5 โดยโมลและปรับสภาพด้วยกระบวนการไฮโดรเทอร์มัลภายใต้การฉายแสงสีฟ้าและ Degussa P-25 ภายใต้การฉายแสงอัลตราไวโอเล็ตตามลำดับ โครงสร้างผลึกซึ่งเป็นตัวแปรสำคัญที่ควบคุมพฤติกรรมการตอบสนองของไททาเนียมไดออกไซด์ภายใต้การฉายแสงอัลตราไวโอเล็ตไม่มีผลกระทบที่สำคัญภายใต้การฉายแสงที่มองเห็น จลนพลศาสตร์การเร่งปฏิกิริยาแสงของการออกซิเดชั่น 2-คลอโรฟีนอลด้วยไททาเนียมไดออกไซด์ที่เจือทังสเตนร้อยละ 0.5 และปรับสภาพด้วยกระบวนการไฮโดรเทอร์มัลภายใต้การฉายแสงสีฟ้าสามารถอธิบายได้ด้วยแบบจำลองของ Langmuir-Hinshelwood โดยมีค่า k_r และ K เท่ากับ 3.00×10^{-4} มิลลิโมลาร์/นาที และ 239.13 ต่อมิลลิโมลาร์ ตามลำดับ

สาขาวิชา การจัดการสิ่งแวดล้อม ลายมือชื่อนิสิต Thapanan Patta

ปีการศึกษา 2552 ลายมือชื่อ อ.ที่ปรึกษาวิทยานิพนธ์หลัก

ลายมือชื่อ อ.ที่ปรึกษาวิทยานิพนธ์ร่วม

5087805720: MAJOR ENVIRONMENTAL MANAGEMENT
KEYWORDS: TITANIUM DIOXIDE / PHOTOCATALYSIS / VISIBLE-LIGHT / 2-CHLOROPHENOL

THAPANAN PUTTA: PHOTOCATALYTIC CHARACTERISTICS OF TITANIUM DIOXIDE DOPED WITH VARIOUS ELEMENTS AND HYDROTHERMAL TREATMENT UNDER VISIBLE-LIGHT ACTIVATION. THESIS ADVISOR: ASSOCIATE PROFESSOR JIN ANOTAI, Ph.D., THESIS CO-ADVISOR: PROFESSOR MING-CHUN LU, Ph.D., 119 pp.

In this study, a new tungsten-doped titanium dioxide photocatalyst with hydrothermal treatment has been developed and tested for its photocatalytic activity by using 2-chlorophenol as the target compound. The synthetic procedure and optimum conditions were described in details. This photocatalyst could be effectively activated by blue-light irradiation and its activity was almost comparable to those of the commercial Degussa P-25 under ultraviolet irradiation. 2-chlorophenol at 0.01 mM could be removed completely in 120 and 90 minutes by the photocatalysis using 0.5% by mole tungsten-doped titanium dioxide with hydrothermal treatment under blue-light irradiation and the P-25 under ultraviolet irradiation, respectively. Crystalline structure which is a very important factor controlling the response behavior of the titanium dioxide under ultraviolet irradiation did not have any significant effect under visible-light irradiation. Photocatalytic kinetics of 2-chlorophenol oxidation by the 0.5% tungsten-doped titanium dioxide with hydrothermal treatment under blue-light irradiation could be sufficiently explained by the Langmuir-Hinshelwood model with k_r and K of 3.00×10^{-4} mM/min and 239.13 1/mM, respectively.

Field of Study: Environmental Management Student's Signature Thapanan Putta
Academic Year: 2009 Advisor's Signature
Co-Advisor's Signature

ACKNOWLEDGEMENTS

I would like to gratefully acknowledge my thesis advisor, Assoc. Prof. Dr. Jin Anotai and my thesis co-advisor, Prof. Dr. Ming-Chun Lu, for their encouragement, invaluable support, and guidance. Their comments and suggestions not only provide valuable knowledge but broaden perspective in practical applications as well. Special gratitude goes to all committee members, Dr. Chantra Tongcumpou, Dr. Nyein Nyein Aung, Dr. Pichet Chaiwiwatworakul and Assoc. Prof. Dr. Duangrat Inthorn for providing invaluable advices and their insightful suggestions.

This work was supported in part by a grant from the National Center of Excellence for Environmental and Hazardous Waste Management (NCE-EHWM) Program, Thailand. Without these financial supports, my achievement could not become true.

Thanks to the Department of Environmental Engineering, King Mongkut's University of Technology Thonburi in Bangkok of Thailand and the Department of Environmental Resources Management, Chia-Nan University of Pharmacy and Science in Tainan of Taiwan for providing the worth opportunity for me to do my great research.

Also I would like to thanks The National Nanotechnology Center, Thailand, (NANOTEC) in supportive for Point of zero charge analysis of my catalyst.

Special thanks to my beloved family, my friends and others for supportiveness, understanding, encouragement, and patient support throughout my entire study and believed in me.

CONTENTS

Page

Page

LIST OF TABLES

Page

LIST OF FIGURES

Page

Page

CHAPTER I

INTRODUCTION

1.1 Research Rationale

Semiconductor photocatalysis has been proven to be a high efficient process for environmental remediation, air purification, deodorization, sterilization, and water treatment (Fujishima and Honda., 1972; Hoffmann et al., 1995). Among the semiconductor photocatalysts, titanium dioxide (TiO_2) is the most preferred and has been extensively studied for environmental purification applications because of its physical and chemical stability, good characteristics of powerful oxidation strength, non-toxicity and inexpensiveness (Ao et al., 2008). Unfortunately, major drawbacks in the popularization of TiO_2 are the large band gap (3.2 eV) which requires high activated energy and limiting the photocatalytic activity of TiO_2 only to the ultraviolet region and the high recombination rate of the electron-hole pair.

Many researchers have consistently attempted to improve the TiO_2 light-activated property. The first and most common modification is to stretch its absorptivity down to the visible range which is abundant in solar light. Visible light energy accounts for 42% of the solar spectra compared with only 3% of the ultraviolet portion. Since, solar energy is clean, renewable, and ideally inexpensive, using solar energy to perform the photocatalytic processes has become the researchers' long-time dream. The second modification, which is also of interest by several researchers, is to reduce the electron recombination rate. Several main approaches have been investigated to achieve these purposes. Firstly, doping TiO_2 with transition metal to introduce defects into the TiO_2 lattice in the band-gap of TiO_2 to inhibited the phase transformation and assists the charge separation efficiency (Xu et al., 2004; Murakami et al., 2008; Lorret et al., 2009; and Wang, Chen et al., 2009). Secondly, couple TiO_2 with other semiconductors in order to enhance the charge separation in the photocarrier generation process (Albonetti et al., 2008; Xiao et al., 2008). The third possibility is to modify TiO_2 by surface deposition of noble metal to decrease charge carrier recombination by providing an electron sink (Chen, Ku and Kuo, 2007).

Many techniques have been used to produce the TiO_2 doped various elements, co-precipitation, and chemical vapor deposition (Stakheev, Shpiro and Apijok, 1993; Khouw et al., 1994) but sol-gel process is considered as one of the most promising alternatives. This is because it presents a number of advantages such as low calcination temperature, flexibility of processing, and homogeneity at molecular level. This method allows obtaining the anatase phase, which has high activity in photocatalytic applications (Fox and Dulay, 1993; Kato et al., 1994), at low temperature. Hydrothermal processing represents an alternative to the calcination for the crystallization of titanium under mild temperatures. It has been widely applied in the synthesis of zeolites and in the production of advanced ceramic powders with ultrafine particle size. In the hydrothermal treatment, grain size, particle morphology, crystalline phase, and surface chemistry can be controlled via processing variables such as nature of solvent, pH, reaction temperature and pressure, aging time and also additive. Typically, under various hydrothermal conditions, products of TiO_2 with different morphologies and micro structural forms have been yielded.

This research mainly focused on the improvement of TiO_2 photoactivity in the visible range by doping with several transition or noble metals as well as treating with hydrothermal treatment. 2-chlorophenol was selected as the target compound because it is an important toxic chemical commonly present in wastewater. It has wide applications as a biocide and disinfectant, and is an intermediate product in the manufacture of pesticides, dyestuffs and preservatives. Similar to other chlorinated aromatic compounds, 2-chlorophenol can adversely impact the ecosystem, either directly or indirectly, and can function as a carcinogenic agent (Ilisz et al., 2002). This has led to an increasing demand for efficient and economical treatment for 2-chlorophenol. The photocatalytic oxidation behavior of 2-chlorophenol revealed as a result of this research will provide valuable information for future 2-chlorophenol treatment.

1.2 Objectives

The main objective of this study is to use the sol-gel process to synthesize TiO_2 doped with various elements which can be activated by the visible-light. The specific objectives of this study are:

1. To study the photocatalytic activity of TiO_2 doped with various elements by using 2-chlorophenol as an organic probe.

2. To studies the optical and structural properties of TiO_2 doped with various elements by using BET, SEM, XRD, XRF, UV-VIS spectrophotometer and Point of zero charge (pzc) methods.

1.3 Hypothesis

Doping and hydrothermal treatment can expand the photocatalytic activity of TiO_2 down to the visible light region.

1.4 Scopes of the Study

All experiments in this research were conducted in the laboratory scale. The scopes of this work were as follows:

1. Sol-gel and hydrothermal technique was used to synthesize TiO_2
2. All the photocatalytic processes were done with synthetic wastewater using 2-chlorophenol as an organic probe.
3. All the photocatalytic experiments were conducted at 1 atm and 25ºC.

1.5 Obtained Results

This research provides valuable information on the synthetic TiO_2 which could be activated by visible light. This visible-light activated TiO_2 is a very useful photocatalyst and can be applied in the field practice with lower operative cost due to no need of an expensive UV light irradiation. The fundamental knowledge in the TiO_2 synthesis can serve as a solid platform for further improvement. In addition, the kinetics of 2-chlorophenol photodegradation by TiO_2 with visible-light irradiation is also included which can be applied to treat 2-chlorophenol contaminated wastewater in the future.

CHAPTER II

BACKGROUNDS AND LITERATURE REVIEWS

2.1 Theoretical Backgrounds

2.1.1 Advanced Oxidation Processes

Advanced oxidation processes (AOPs) represent an alternative approach, including ultraviolet (UV) radiation, ozone, and hydrogen peroxide, either individually or in combination, which is used to destroy hazardous organic contaminants. The AOPs technologies can refer to two stage of sequential reaction. The first is the formation of the strong oxidants such as hydroxyl radicals (•OH) and the second is the reaction of these oxidants with organic/inorganic pollutants. However, the term of AOPs refers specifically to processes in which oxidation of organic contaminant occurs via •OH. The •OH is a powerful oxidant, short lived, highly reactive, and a non-selective oxidant which can oxidize many pollutants. These radicals react with pollutants and lead to degradation reaction. In some cases, AOPs can lead to complete oxidation of organic contaminants resulting in carbon dioxide (CO_2) and water (H_2O) without generating any harmful byproducts. Application of AOPs can cover many fields such as detoxification of persistent organic pollutants (POPs), disinfection and purification of contaminated air and wastewater steam, oxidative degradation of organic compounds, bactericidal and non-biodegradable compounds.

2.1.2 Photocatalytic Process

Photocatalysis is one of the AOPs. It consists of two words, the first word is “photo” which is light; and the second is “catalyst” which is the process by which the rate of a chemical reaction is increased by mean of the addition of species known as a catalyst to the reaction. Therefore, photocatalysis means the process which requires irradiation to initiate the catalytic reaction, without the radiation, the reaction cannot proceed. This technique is very useful for the degradation of non-biodegradable organics or toxic pollutants. Moreover, they are much more efficient than the conventional techniques such as coagulation, precipitation, adsorption on activated

carbon and which lead to the complete mineralization and also detoxicification of pollutants, and in the case of halogenous compounds to the formation of halogenous ions purification. Lhomme, Brosillon and Wolbert (2008) investigated photocatalytic degradation of pesticides in pure water and a commercial agricultural solution on titanium dioxide (TiO_2) coated media.

2.1.3 Titanium Dioxide

2.1.3.1 Titanium Dioxide in Industrial Applications

Titanium dioxide, also known as titanium (IV) oxide or titania, is the naturally occurring oxide of titanium with the chemical formula TiO_2. In the industrial work, it is the most widely used white pigment because of its brightness and very high refractive index. This pigment is used extensively in plastics, paints, coatings, papers, inks, and other applications for its UV resistant properties where it acts as a UV absorber, efficiently transforming destructive UV light energy into heat. When deposited as a thin film, its refractive index and color make it an excellent reflective optical coating for dielectric mirrors and some gemstones. TiO_2 is even used in food stuffs, for instance in the wrapping of salami, as well as medicines (i.e. pills and tablets) and toothpaste. In cosmetic and skin care products such as sunscreens, lipsticks, body powder, and soap.

2.1.3.2 Titanium Dioxide in Environmental Applications

In environmental works, starting in the late 1960s, TiO_2 began with photoelectrochemical solar energy conversion and then shifted into the area of environmental photocatalysis, including self-cleaning surfaces, and most recently into the area of photoinduced hydrophilicity, which involves not only self-cleaning surfaces, but also antifogging ones. One of the most interesting aspects of TiO_2 is that the types of photochemistry responsible for photocatalysis and hydrophilicity are completely different, even though both can occur simultaneously on the same surface (Fujishima, Rao and Tryk, 2000). TiO_2 is the most preferable photocatalyst because of its physical and chemical stability and non-toxicity. It is well known as a photocatalyst for water and air treatment as well as for catalytic production of gases. Also in development is a paving stone that uses the catalytic properties of TiO_2 to remove nitrogen oxide from the air, breaking it down into more environmentally

benign substances that can then be washed away by rainfall. Other experiments with TiO_2 Son, Ko and Zoh (2009) investigated kinetics and mechanism of photolysis and TiO_2 photocatalysis of triclosan. The results were compared in TiO_2 only in the dark condition, photolysis, and TiO_2 photocatalysis with a UV-A lamp. TiO_2 photocatalysis more effectively degraded and mineralized triclosan compared to TiO_2 only and photolysis conditions.

2.1.3.3 Properties of Titanium Dioxide

TiO_2 is consisted of two band gaps; the first is valence band (VB), the highest occupied band full of electron, and the second band is conduction band (CB), the lowest unoccupied band. The bands are separated by different energy level which is called "band gap energy." As the TiO_2 absorbs energy greater than band gap energy, it will produce electron and hole pairs. The electron of the VB of TiO_2 becomes excited when illuminated by light. The excess energy of this excited electron promoted the electron to the CB of TiO_2 therefore creating the negative-electron (e^-) and positive-hole (h^+) pair (Equation (2.1)). This stage is referred as the semiconductor's "photo-excitation" state. Wavelength of the light necessary for photo-excitation of 3.2 eV (band gap energy) is 380 nm. The h^+ of TiO_2 could pull an electron from OH- or water molecule to form •OH as shown in Equations (2.2) and (2.3). The e^- reacts with oxygen molecule to form super oxide anion ($•O^-_2$) (Equation (2.4)). This $•O^-_2$ powerful oxidizing agents will disintegrate and rearrange the structure of the organic pollutants and convert them into CO_2 and H_2O. The photo-excitation of electron and hole pairs can recombine as e^- returns to its original state. Therefore, it should have electron acceptor, for example O_2 to obstruct the recombination. The overall process is illustrated in Figure 2.1 below.

$$TiO_2 + h\nu \longrightarrow e^- + h^+ \quad (2.1)$$

$$h^+ + OH^-(\text{surface}) \longrightarrow •OH \quad (2.2)$$

$$h^+ + H_2O \longrightarrow •OH \quad (2.3)$$

$$O_2 + e^- \longrightarrow •O^-_2 \quad (2.4)$$

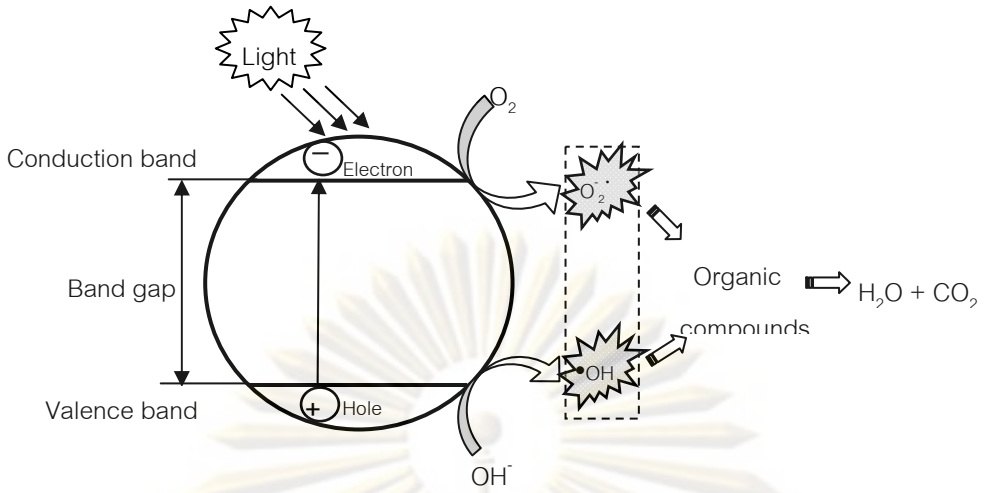

Figure 2.1 Schematic of photocatalytic process.

Normally, TiO_2 crystallizes have three polymorphic forms which are anatase, rutile, and brookite, as shown in Figure 2.2. Rutile and anatase have been used as the catalysts in heterogenous photocatalysis while brookite is usually found only in mineral ores. The photocatalytic activities of these two crystals mainly depend on their structure. Rutile will be more stable at high temperatures while anatase will be more stable at low temperatures. The structure of TiO_2 will depend largely on the calcination temperature. Wetchakun and Phanichphant, (2008) concluded that the anatase to rutile transformation occurred at a temperature between 700 ºC and 800 ºC.

The properties of anatase and rutile such as crystalline form, gibbs free energy, and density are the same or nearly the same. However, the structure between rutile and anatase are different thus makes them differ slightly in crystal habit. The band gap energy of anatase is 3.2 eV, which corresponds to UV light (380 nm), while the band gap energy of rutile is 3.0 eV corresponding to violet light (413 nm). The difference in band gap comes from the level of conduction band edge of anatase which is higher than that of rutile by about 0.2 eV. The VB energies for anatase and rutile are similar and both of them can generate VB hole and sequentially the •OH. On the other hand, the CB energy for rutile is closely than anatase to the potential required to reduce water to hydrogen gas. Therefore, the photogenerated CB electrons and VB holes of rutile can easily recombine with each other before they can do anything useful unlike in the case of anatase. Typically, the TiO_2 can be used in two forms: suspension or immobilized. The anatase type of TiO_2 generally shows a higher photoactivity than another type of TiO_2 by comparison of physical properties as shown in Table 2.1.

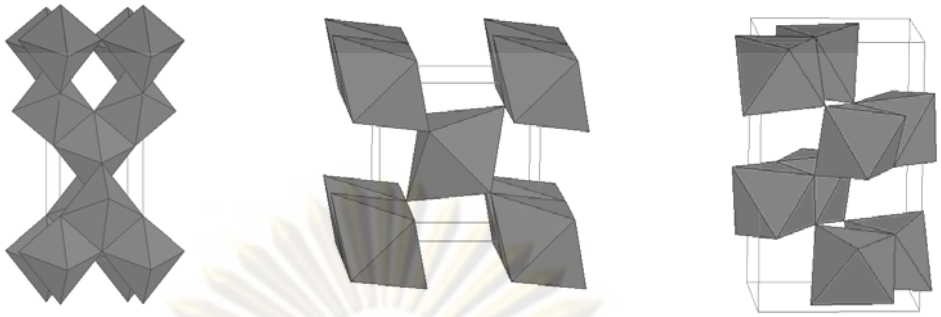

a) anatase **b) rutile** **c) brookite**

Figure 2.2 Crystallize form of TiO_2 (Smyth, 2009).

Table 2.1 Comparison between rutile and anatase.

Properties	Rutile	Anatase
Crystalline form	Tetragonal system	Tetragonal system
Band gap energy (eV)	3.0	3.2
Gibb free energy (kcal/mole)	-212.6	-211.4
Melting point (ºC)	1858	Change to rutile at high temperature (~800)
Hardness (Mohs)	6.0-7.0	5.5-6.0
Permittivity	114	31
Density (g/cm^3)	4.250	3.894
Lattice constant a (Å)	4.58	3.78
Lattice constant c (Å)	2.95	9.49

2.1.3.4 Photocatalysis of Doped Titanium Dioxide

Recently, TiO_2 has been utilized as a photocatalyst for environmental remediation such as air-purification, deodorizing, sterilization, self-cleaning and water treatment. However, it is facing with two major limits in real practice. Firstly, TiO_2 requires UV of the wavelength (λ) less than 380 nm, whose energy exceeds the band gap of 3.2 eV of the anatase crystalline phase; hence, utilizing only a very small fraction of sunlight, which is only 3% of UV portion. Secondly, TiO_2 has a high

recombination rate of electron-hole pairs because it has wide band gap energy. The mechanism of TiO_2 photocatalysis mainly depends on the semiconductor interfacial redox reactions of electrons and holes. The efficiency of TiO_2 photocatalysis is low for its application because the photogenerated electron-hole pairs recombine rapidly after excitation leading to low charge carrier transfer rate on semiconductor surface.

Recently, most of the research is focused on improving the TiO_2 properties. It is generally recognized that the improved photocatalysts should allow the use of the main part of solar spectrum or even the illumination of interior lighting. Therefore, the major aim in the development of TiO_2-based materials is to extend the photoactivity from 3.2 eV into visible light range in order to utilize solar light more efficiently (Yang et al., 2008). Efforts have been made using chemical or physical methods, to enhance the photocatalytic activity of TiO_2 through modification of crystal structure, crystal size and surface area with different group of elements such as transition metal ions (Hathway et al., 2009; Saepurahman, Abdullah and Chong, 2010), non-metallic atoms (Todorova et al., 2008) and noble metals (Zhang X., Zhang F. and Chan, 2006).

2.1.3.5 Synthesis Titanium Dioxide Process

2.1.3.5.1 Sol-Gel Process

Sol-gel process is a flexible solution process for making ceramic and glass materials. In general, the sol-gel process involves the transition of a system from a liquid “sol” (mostly colloidal) into a solid “gel” phase. Applying the sol-gel process, it is possible to fabricate ceramic or glass materials in a wide variety of forms: ultrafine or spherical shaped powders, thin film coatings, ceramic fibers, microporous inorganic membranes, monolithic ceramics and glasses, or extremely porous aerogel materials. Among the available techniques, for instance co-precipitation, vapor deposition, etc., the sol-gel process is undoubtedly the simple (Chao et al., 2003) and the cheap one (Sonawane, Kale and Dongare, 2004).

The sol-gel processing for TiO_2 synthesis refers to the hydrolysis and condensation of alkoxide-based precursors such as tetra(n-butoxyl) titanium ($Ti(O\text{-}Bu)_4$). The reactions involved in the sol-gel chemistry started form the hydrolysis, water and alcohol condensation reaction of metal alkoxides as shown in

Equations (2.5) to (2.7), lead to the formation of new phase (sol-gel) can be described as follows:

$$\text{Ti-O-R} + H_2O \longrightarrow \text{Ti-OH} + \text{R-OH (hydrolysis)} \quad (2.5)$$

$$\text{Ti-O-H} + \text{HO-Ti} \longrightarrow \text{Ti-O-Ti} + H_2O \text{ (water condensation)} \quad (2.6)$$

$$\text{Ti-O-R} + \text{OH-Ti} \longrightarrow \text{Ti-O-Ti} + \text{R-OH (alcohol condensation)} \quad (2.7)$$

Sol-gel method of synthesizing nanomaterials is very popular amongst chemists and is widely employed to prepare oxide materials and can be characterized by a series of distinct steps as follows:

-Step 1: Formation of different stable solutions of the metal alkoxide or solvated metal precursor (the sol).

-Step 2: Gelation resulting from the formation of an oxide- or alcohol-bridged network (the gel) by a polycondensation or polyesterification reaction that results in a dramatic increase in the viscosity of the solution.

-Step 3: Aging of the gel (Syneresis), during which the poly-condensation reactions continue until the gel transforms into a solid mass, accompanied by contraction of the gel network and expulsion of solvent from gel pores. Phase transformations may occur concurrently with syneresis. The aging process of gels can exceed 7 days and is critical to the prevention of cracks in gels that have been cast.

-Step 4: Drying of the gel, when water and other volatile liquids are removed from the gel network. This process is complicated due to fundamental changes in the structure of the gel. The drying process has itself been broken into four distinct steps: (i) the constant rate period; (ii) the critical point; (iii) the falling rate period; and (iv) the second falling rate period. If isolated by thermal evaporation, the resulting monolith is termed a xerogel. If the solvent (such as water) is extracted under supercritical or near super critical conditions, the product is an aerogel.

-Step 5: Dehydration, during which surface-bound R-OH groups are removed, there by stabilizing the gel against rehydration. This is normally achieved by calcining the monolith at temperatures up to 800^{o}C.

-Step 6: Densification and decomposition of the gels at high temperatures (T>800ºC). The pores of the gel network are collapsed, and remaining organic species are volatilized.

The typical steps that are involved in sol-gel processing are shown in the schematic diagram below (Figure 2.3). Navarrete et al. (1996) investigated on the effect of preparation conditions on sol-gel mix and found to be the determining factor in the textural properties of the solids. The hydrolysis catalyst used was an important factor on the specific surface area, acidity and basicity as well as activity. In the gelation and age of gel step, the reactions were impracticably slow room temperature, often requiring several days to reach completion. For this reason, acid or base catalysts were added to the formulation. The amount and type of catalyst used played important roles in the microstructural, physical and optical properties of the final aerogel product. Acid catalysts could be any protic acid such as H_2SO_4, and HCl. Basic catalyst usually uses ammonia or more commonly ammonia and ammonium fluoride. Aerogels prepared with acid catalysts often showed more shrinkage during supercritical drying and might be less transparent than base catalyzed aerogels.

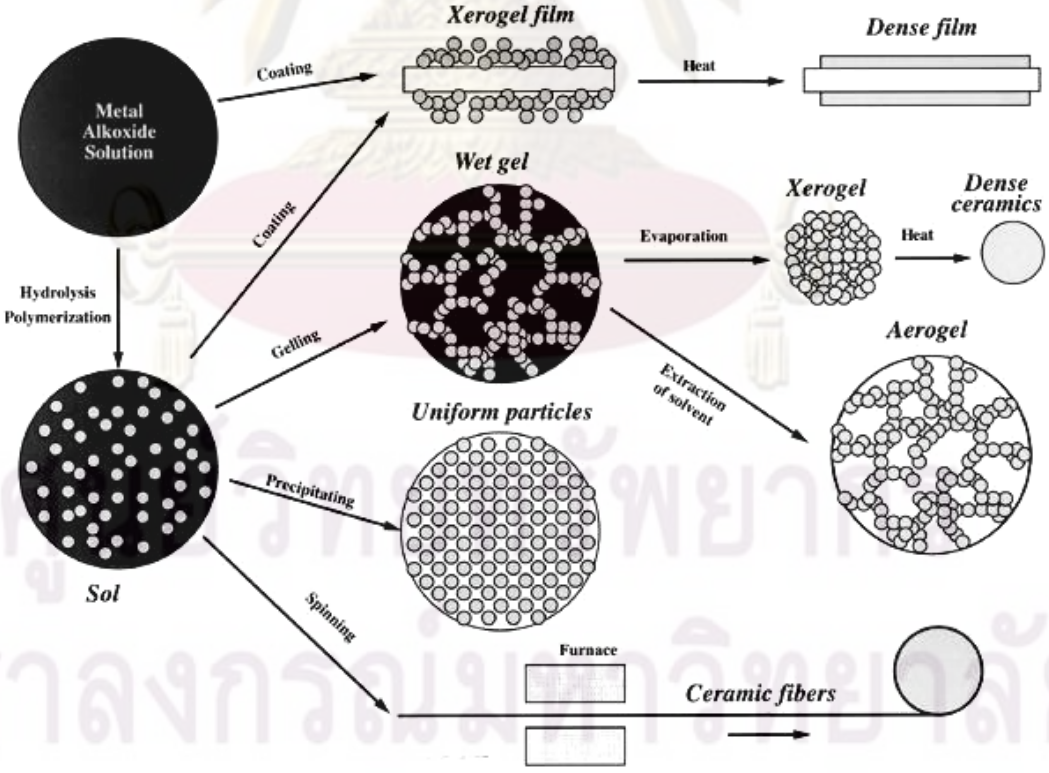

Figure 2.3 Mechanism of sol-gel process (Chemat Technology, 2010).

2.1.3.5.2 Hydrothermal Process

Hydrothermal synthesis can be defined as a method of synthesis of single crystals which depends on the solubility of minerals in hot water under high pressure. The crystal growth is performed in an apparatus called “autoclave”. Possible advantages of the hydrothermal method over other types of crystal growth include the ability to create crystalline phases which are not stable at the melting point. Also, materials which have a high vapor pressure near their melting points can also be grown by the hydrothermal method. The method is also particularly suitable for the growth of large good-quality crystals while maintaining good control over their composition.

In general, hydrothermal synthesis is a prospective method to obtain nanocrystalline titanium particles, where polymorphism, particle size and crystallinity could be controlled under high pressure. Moreover, it is a low temperature technique for materials development, widely applied in industrial processes for ceramic synthesis. The hydrothermal technique requires autoclave instrumentation and relies on the extensive heating of the nanoparticles diluted over an aqueous solution or slurry. The way to modification nanoparticle size and specific active area importantly affects the desired properties of the photocatalysts by varying the surface to volume ratio, by affecting the photo excited charge transfer and by influencing the surface hydroxyl concentration. The hydrothermal procedure of titanium powder at relatively low temperature ensures finely modification the properties of the modified titanium particles by only varying the duration of the treatment without the danger of the anatase phase transformation to rutile. Thus, optimum properties like increased roughness and complexity of the photocatalyst surfaces, and amplified hydroxyl content per unit area can be combined with improved interconnection of the nanoparticles and adhesion to the substrate. Control of the above factors by fine tuning of the autoclave parameters can lead to efficient immobilized titanium photocatalysts (Kontos et al., 2005).

2.1.4 Adsorption Isotherm

Photocatalytic decomposition rate is influenced by many factors such as activity and surface area of photocatalyst, adsorption and desorption of reactants/products. In the photodegradation process of TiO_2, the disappearance of the pollutant depends on two mechanisms, pollutants adsorb on the TiO_2 surface and

oxidation reaction by the •OH. Both mechanisms occur on the TiO_2 surface. For this reason, the adsorption of organic molecules on the TiO_2 plays an important part in the photocatalytic process. Therefore, it is important, in the first step, to determine the isotherm of adsorption.

2.1.4.1 Langmuir Adsorption Isotherm

Langmuir adsorption isotherm was developed by Irving Langmuir in 1916 to describe the dependence of the surface coverage of an adsorbed gas on the pressure of the gas above the surface at a fixed temperature. The basic idea behind the Langmuir model is the coverage of the surface by a monomolecularic layer. The Langmuir adsorption isotherm was developed by assuming:

- A fix number of accessible sites are available on the adsorbent surface, all which have the same energy.
- Adsorption is reversible. Equilibrium is reached when the rate of adsorption of molecule onto the surface is the same as the rate of desorption of molecule from the surface. The rate at which of adsorption proceeds is proportional to the driving force, which is the difference between the amount of adsorbed at a particular concentration and the amount that can be adsorbed at that concentration. At the equilibrium concentration, this difference is zero.
- Adsorption is monolayer or unilayer.

Langmuir adsorption isotherm can be written as Equation (2.8):

$$q_e = \frac{q_{max} bC}{bC + 1} \tag{2.8}$$

where "q_e" represents moles of adsorbate per unit weight of adsorbent, "b" is rate constant ratio between adsorption and desorption, "q_{max}" is maximum moles of adsorbate per unit weight of adsorbent, and "C" is adsorbate aqueous concentration. This Equation is a linear line when plotted inverse q_{max} and inverse concentration rewritten as Equation (2.9):

$$\frac{1}{q_e} = \frac{1}{q_{max} b}\left(\frac{1}{C}\right) + \left(\frac{1}{q_{max}}\right) \tag{2.9}$$

2.1.4.2 Freundlich Adsorption Isotherm

The most multisite adsorption isotherm for rough surface is the Freundlich adsorption isotherm. This isotherm is used commonly to describe the adsorption characteristics of activated carbon used in water and wastewater treatment. Freundlich adsorption isotherm is defined as shown in Equation (2.10) and its linearized form is illustrated in Equation (2.11):

$$q_{max} = K_F C^{\frac{1}{n}} \tag{2.10}$$

$$\log q_e = \log K_F + \frac{1}{n}\log C \tag{2.11}$$

where "K_F" and "n" are constants for a given adsorbate and adsorbent at the particular temperature.

2.1.5 Langmuir-Hinshelwood Expression

Langmuir-Hinshelwood expression is one of kinetic model that widely used to analyze the heterogeneous photocatalytic oxidation, especially in the presence of pre-adsorption or dark adsorption prior the irradiation (Roa et al., 2003; Vargas and Núñez, 2008; Merabet, Bouzazab and Wolbert, 2009; Tsai et al., 2009). This model was developed base on the assumption of no competition with reaction byproducts. The photocatalytic oxidation of organic pollutant over TiO_2 should comply with the following Equation (2.12):

$$r = -\frac{dC}{dt} = \frac{k_r KC}{1 + KC} \tag{2.12}$$

where "r" is the reaction rate for the oxidation of organic pollutant ($mM.min^{-1}$), "k_r" is the specific reaction rate constant for the oxidation of organic pollutant ($mM.min^{-1}$), "K" is the equilibrium adsorption constant of organic pollutant (mM^{-1}), and "C_0" is the initial concentration of organic pollutant (mM). This Equation is a linear line when plotted between inverse initial rate and inverse concentration as shown in Equation (2.13). Slope ($1/k_rK$) and interception ($1/k_r$) are positive.

$$\frac{1}{r} = \frac{1}{k_r} + \frac{1}{k_r K}\frac{1}{C} \qquad (2.13)$$

The constants, k_r and K, can be obtained from the intercept and slope of the line formed when "1/r" is plotted against "1/C". The integrated form of Equation (2.12) is shown in Equation (2.14):

$$t = \frac{1}{k_r K}\ln\left(\frac{C}{C_0}\right) + \frac{1}{k_r}(C_0 - C) \qquad (2.14)$$

Plotting between "$t_{1/2}^{*}$" and initial concentration of organic pollutant should be a linear line as in the following Equation (2.15)

$$t_{1/2}^{*} = \frac{0.5C_0}{k_r} + \frac{\ln 2}{k_r K} \qquad (2.15)$$

Where "$t_{1/2}^{*}$" is the half-life when there is no competitive effect from intermediates.

2.1.6 Properties of 2-Chlorophenol

2-Chlorophenol or ortho-chlorophenol is a benzene that is substituted with hydroxyl group (-OH) in first position and covalently bonded chlorine atoms in second or ortho position. 2-Chlorophenol is produced by electrophilic halogenation of phenol with chlorine. It has a medicinal smell and is a slightly acidic liquid. According to the Notification of the Ministry of Industry No. 6 (1997), 2-chloro-phenol is classified as a toxic hazardous waste and the industrial effluent standard for 2-chlorophenol is less than 1 mg/L. 2-Chlorophenol has been used as a biocide and disinfection and is also used as an intermediate in chemical industry. It is toxic to a wide range of organisms. 2-Chlorophenol is also used to preserve wood. It is used as an intermediate in the production of pesticides, dyestuffs and preservative. This chemical compound has an appearance as a light amber liquid at room temperature. 2-Chlorophenol is toxic to plants, fish and invertebrates. It spills have resulted in fish kills. Exposure to large quantities of 2-chlorophenol impairs algae reproduction and primary production. Biodegradation in soils is lightly to be reasonably rapid (day-

weeks) and it binds moderately with soil/sediment particles, however for significant spills to land, leaching to groundwater may be possible. Bioaccumulation of 2-chlorophenol appears to be moderate. Explosive exposure to 2-chlorophenol can effect if swallowed, inhaled, or absorbed through the skin. 2-Chlorophenol may cause long-term adverse effects in the aquatic environment. It may cause eye and skin damage, respiratory tract irritation, central nervous system effects, liver and kidney gastrointestinal system damage. The molecular structure and MSDS are shown in Figure 2.4 and Table 2.2.

In wastewater, 2-chlorophenol represents an important water pollutant and has been named as the priority pollutant by the USEPA. The stability of the C-Cl bond in halo-hydrocarbons is responsible for their toxicity and persistence in the biological environment. The main entry routes of 2-chlorophenol to the aquatic environment are discharges from plants manufacturing it, or from plants, and those employ it as intermediate in the production of higher chlorinated phenols or phenoxy herbicides. Indirect sources include discharges from paper mills as a by-product of chlorine-based bleaching, and from slow microbial breakdown of herbicides during post-application period. The compound is also used as a solvent for extracting sulfur and nitrogen compounds from coal. 2-Chlorophenol is very toxic and poorly biodegradable in water. A wastewater stream containing 2-chlorophenol over 200 mg/l may not be treated effectively by direct biological methods.

There are many researches studied on the oxidation of 2-chlorophenol under photocatalytic, electrocatalytic, and Fenton's oxidation under various conditions to determine the influence of pH and the formation of oxidation intermediates and products. It has been observed that the types and distribution of intermediates was depending largely on the oxidation process and experimental conditions. Catechol and cyclopentadienic acids were reported to be the major intermediates from the degradation of 2-chlorophenol by photolysis whereas phenol, hydroquinone, benzoquinone, chlorohydroquinone, and hydroxyl hydroquinone were identified

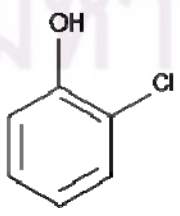

Figure 2.4 2-Chlorophenol molecular structure.

Table 2.2 MSDS of 2-chlorophenol.

Property	Information
Name	2-Chlorophenol / 2-hydroxychlorobenzene/ o-Chlorophenol / 1-chloro-2-hydroxybenzene, o-chlorophenic acid, chlorophenolate
CAS number	95-57-8
Molecular formula	C_6H_5ClO
Molar mass	128.56 g/mol
Appearance	colorless to light brown liquid
Density	1.262 g/cm³, liquid
Melting point	8ºC
Boiling point	173.0 - 175.0 ºC
Flash point	63ºC (closed cup)
Solubility in water	Slightly Soluble (20-25ºC)
Vapor Density	4.4 (Air = 1)
Vapor Pressure	0.3 kPa (20ºC)
Odor Threshold	1.24 ppm

under the photocatalysis. Figure 2.5 shows the photodegradation pathway of 2-chlorophenol as proposed by Ilisz et al. (2002). It starts with the addition of •OH to the aromatic moiety (1) leaded to the formation of chlorodihydroxycyclohexadienyl radical, •OH addition in the para position to 2-chlorophenol (2), followed by H-abstraction (3), leaded to chlorohydroquinone, while addition in ortho position (4), followed by chlorine-abstraction from the bezene ring (5) and yielded pyrocatechol. The chlorodihydroxycyclohexadienyl radical formed in the first step may disproportionate into 2-chlorophenol and chlorohydroquinone, accompanied by water elimination (6). Although •OH often seems to be a plausible explanation for heterogeneous photocatalytic transformations observed in the aqueous phase, the possibility of direct hole oxidation can not be excluded. Since direct electron transfer from 2-chlorophenol to a semiconductor (7) could also give a positive radical, which could be converted into an chlorodihydroxycyclohexadienyl radical after nucleophilic water addition (8), or into chlorophenoxyl radical after deprotonation (9). (In the

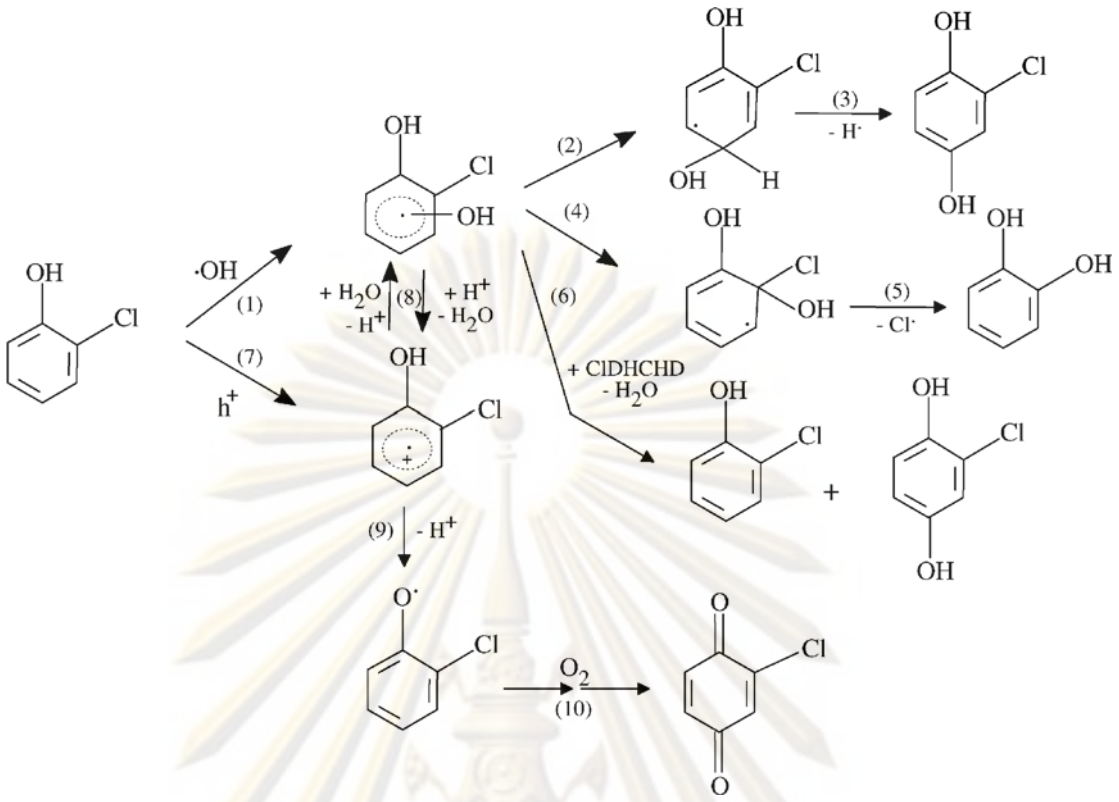

Figure 2.5 Simplified mechanism for the photocatalytic degradation of 2-chlorophenol (Ilisz et al., 2002)

presence of dissolved O_2 the chlorophenoxyl radical may lead to the formation of quinonic derivatives (10)). Since the hydroxylation initiated by either •OH or a surface trapped hole can lead to chlorodihydroxycyclohexadienyl, a distinction between direct hole and •OH oxidation can hardly be accomplished by using only the product distribution. Further oxidation of the aromatic intermediates leads to ring opening and aliphatic products may occur (e.g. carboxylic acids and hydroxylated carboxylic acids). Prolonged irradiation will lead to the total mineralization, producing water, carbon dioxide and hydrochloric acid as final products. It is reported that higher pH discouraged the formation of aromatic intermediates. Moreover, when organochlorine compounds undergo oxidation, they may produce other organochlorine compounds that may be more toxic than the parent compound itself. Due to its widely use, potential pollutant, and hazardous property, 2-chlorophenol was selected as the target compound for evaluating the photocatalytic activity of the synthesized TiO_2 in this study.

2.2 Literature Reviews

2.2.1 Photocatalysis of Doped Titanium Dioxide

Liu, Yang and Li (2006) synthesized the visible-light responsive TiO_2-V_2O_5 photocatalyst by using a binary sol-gel and in-situ intercalation method. The photoactivity of the prepared catalyst under UV and visible light irradiation were evaluated by decolorization of methylene blue solution. The results showed that the composite catalyst displayed a homogeneous anatase phase, and the vanadium pentoxide species was highly dispersed in the TiO_2 phase. The composite catalyst responded to visible light because of the narrowed band gap.

Huang, Sun and Liu (2007) studied about Pt/N-codoped TiO_2 nanotubes and its photocatalytic activity under visible light by photodegradation of Rhodamine B in an aqueous solution. It has been confirmed that Pt/N-codoped TiO_2 nanotubes could be excited by visible light and the recombination rate of electron-hole pairs reduced significantly. The higher visible light activity is due to the co-doping of nitrogen and platinum.

Ishibai et al. (2008) synthesized TiO_2 photocatalyst with Pt-modification which active to visible-light. The results showed that Pt on the surface of TiO_2 increased photocatalytic activity under visible light irradiation, depending on the calcination temperature. The temperature correlated with the light absorption properties of the Pt complex on TiO_2 nanoparticles. It was found that TiO_2 surface structure plays an important role in the formation of Ti-O-Pt bonds resulting in a large visible light absorbance and high photocatalytic activity under visible light irradiation.

Xu et al. (2008) studied the low-temperature preparation of F-doped TiO_2 film and its photocatalytic activity under solar light. The photocatalytic activity was evaluated by decomposing X-3B under artificial solar light. The results showed that the crystallinity of TiO_2 was improved by F-doping. Fluoride ions could prevent the grain growth, and the transformation of anatase to rutile phase was also inhibited. F-doped TiO_2 film exhibited better photocatalytic activity. The high photocatalytic activity of F-doped TiO_2 film may due to extrinsic absorption through the creation of oxygen vacancies rather than the excitation of the intrinsic absorption band of bulk TiO_2.

Lin, Wu and Onn (2008) studied the degradation of 4-chlorophenol in TiO_2, WO_3, SnO_2, TiO_2/WO_3 and TiO_2/SnO_2 systems and found that TiO_2/WO_3 increased the band edge wavelength to 475 nm, gap energy decreased and the specific surfaces area reduced to 2.61 eV. Although the specific surfaces area of TiO_2/WO_3 decreased due to its larger size as compared to either TiO_2 or WO_3, the 4-chlorophenol degradation efficiency significantly increased as compared to single TiO_2 or WO_3 system at 435 nm wavelength. The TiO_2/WO_3 degradation of 4-chlorophenol at 369 nm was inhibited. For TiO_2/SnO_2, the degradation efficiency also suffered at 369 nm, and only slightly increased compared to otherwise hardly 4-chlorophenol degraded in single TiO_2 or SnO_2 system.

2.2.2 Sol-Gel and Hydrothermal Methods

Kontos et al. (2005) prepared mixed anatase-rutile phase nanocrystalline TiO_2 powders by hydrothermal modification used Degussa P-25 as a precursor. The preparation procedure took place at 200 ºC for 1-10 days in an autoclave system with water as the solvent. Thus, different degrees of modification were achieved. After that, TiO_2 water modified nanocrystalline thin films were immobilized on glass substrates by applying a doctor-blade's deposition technique. Methyl orange was used in order to evaluate the photocatalytic efficiency of the modified material. The results show that the photocatalytic activity of the modified films is improved by a two factor when the hydrothermal treatment was extended from 1 to about 4 days in the autoclave system. Scratch tests revealed favorable interconnection of the titanium nanoparticles as well as significantly higher adhesion to the glass substrate for the modified films, in comparison to the original P-25 material.

Carotta et al. (2007) synthesized TiO_2 thick films and powders by two synthetic processes, traditional sol-gel and hydrothermal route. A comparison between two synthetic processes has been performed. They found that in the hydrothermal process, the TiO_2 film was maintained the anatase phase at higher calination temperature with any introduction of foreign elements than traditional sol-gel process. Furthermore, hydrothermal powders show particle size much smaller than sol-gel.

Tian et al. (2009) synthesized S-doped TiO_2 nanoparticles by hydrothermal process and their photocatalytic ability was studied by degradation of methyl orange. The result showed that S-doped TiO_2 photocatalysts at a nanometer scale could be

successfully synthesized at 180ºC by a hydrothermal process, which could achieve the crystalline under a mind condition. The particle size and morphology, and phase/chemical compositions of the S-doped TiO_2 photocatalysts were strongly dependent on the amount of S incorporation in TiO_2. S/TiO_2 sample at 1.5% with a spherical morphology and 30 nm in diameter has the best photocatalytic activity.

2.2.3 Photocatalysis of 2-Chlorophenol and Phenolic Compounds

Shchukin et al. (2004) synthesized nanocrystalline bicomponent TiO_2-In_2O_3 powder and studied the photodegradation of 2-chlorophenol in water. From the results, it found that photocatalytic activity increased with decreasing In_2O_3. The concentration of the main aromatic intermediate products (chlorohydroquinone and catechol) was considerably lower for TiO_2-In_2O_3 photocatalysts than pure TiO_2. On the basis of various characterizations of the photocatalysts, the reasons invoked to explain the photocatalytic activity enhancement due to In_2O_3 included a better separation of photogenerated charge carriers, an improved oxygen reduction and an increased surface acidity inducing a higher extent of adsorption of the aromatics.

Barakat et al. (2005) studied the photocatalytic degradation of 2-chlorophenol by nanoparticles Co-doped TiO_2. The results revealed that Co-doped TiO_2 exhibited high activity for UV-photocatalytic degradation of 2-chlorophenol. The efficiency values of the 2-chlorophenol photodegradation were 93.4% and 96.4% at solution pH of 9 and 12, respectively. The presence of Co ions in the TiO_2 structure caused a significant absorption shift towards the visible region.

Araña et al. (2007) investigated the photocatalytic behavior of different phenolic compounds (catechol, resorcinol, phenol, m-cresol and o-cresol). Their adsorption and interaction types with the TiO_2 Degussa P-25 surface were also studied. Langmuir and Freundlich isotherms were applied in the adsorption studies. The obtained results indicated that catechol adsorption was much higher than those of the other phenolics and its interaction occured preferentially through the formation of a catecholate monodentate. Resorcinol and cresols interacted by means of hydrogen bonds through the hydroxyl group, and their adsorption was much lower than that of catechol. Finally, phenol showed an intermediate behavior with a Langmuir adsorption constant (K) much lower than that of catechol, but a similar interaction. The interaction of the selected molecules with the catalyst surface was evaluated by means of FTIR experiments, which allowed the determination of the probability of

•OH radical attack to the aromatic ring which found to follow the sequence of resorcinol > m-cresol > o-cresol > catechol ≥ phenol.

CHAPTER III

METHODOLOGY

3.1 Materials and Chemicals

3.1.1 Chemicals

-Tetra(n-butoxyl)titanium ($Ti(O\text{-}Bu)_4$) from Fluka was used as the titanium precursor.

-Ethanol (C_2H_5OH) from Merck was use as a solvent to prepare the TiO_2 solution.

-Sodium tungsten dihydrate ($Na_2WO_4 \bullet 2H_2O$) from Fluka was used as the dopant for tungsten doped TiO_2 (W/TiO_2).

-Ammonium fluorine (NH_4F) from Merck was used as the dopant for fluorine doped TiO_2 (F/TiO_2).

-Tetra-amine platinum(II) nitrate ($Pt(NH_4)_4(NO_3)_2$) from Sigma-Aldrich was used as the dopant for platinum doped TiO_2 (Pt/TiO_2).

-Nitric acid (HNO_3), sulfuric acid (H_2SO_4) and phosphoric acid (H_3PO_4) from Merck were used as the acid catalyst to control hydrolysis rate.

-Diethanolamine ($(CH_2OHCH_2)_2NH$) from Carlo Erba was used as the base catalyst to control hydrolysis rate.

-Commercial TiO_2 (Degussa P-25) with the BET surface area of 59.1 m^2/g and average particle diameter of 27 nm was used as a reference for photocatalytic activity comparison.

-2-chlorophenol (C_6H_5OCl) from Fluka was used as the organic probe in phototocatalytic determination.

-Perchloric acid ($HClO_4$) and sodium hydroxide (NaOH) were used to adjust/control the pH during the photocatalysis process.

-All other chemicals were reagent grade.

-All reagents were prepared by using the deionized water.

3.1.2 Reactor

Photocatalytic experiments were conducted in a 1-liter Pyrex beaker placed in a circulating water bath controlled at 25 °C. Magnetic stirrer bar was used to mix the solution. Two-watt light-emitting diode (LEDs), which provide the light in the visible range, i.e., either blue (450-495 nm), green (495-570 nm) or red (620-750 nm), or 4-watt low-pressure mercury UV lamp was placed above the reactor to irradiate the light. pH of the solution was controlled at appropriated value throughout the experiment by pH controller connected with cartridge pump to add acid/base as necessary. A schematic diagram of the photocatalytic reactor is shown in Figure. 3.1.

3.2 Experimental Procedures

Experimental works were divided into two parts**,** i.e., TiO_2 synthesis and determination of the TiO_2 activity.

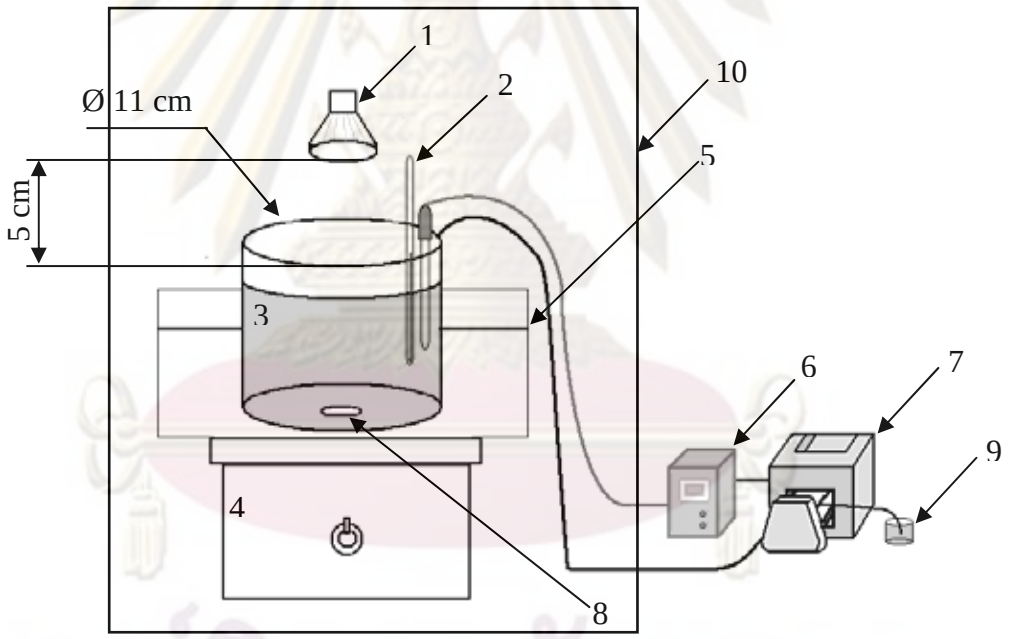

1. LEDs or UV lamp
2. Thermometer
3. Reactor
4. Magnetic stirrer
5. Water bath
6. pH controller
7. Cartridge pump
8. Magnetic stirrer bar
9. NaOH solution
10. Black box

Figure 3.1 Schematic diagram of the photocatalytic reactor.

3.2.1 Titanium Dioxide Synthesis

3.2.1.1 Synthesis of Titanium Dioxide by Sol-Gel Process

In this part, two types of TiO_2 were synthesized by using the sol-gel process. Undoped TiO_2 was prepared according to the procedure of Lin, Tseng and Chen (2006) with some modifications. Doped TiO_2 with tungsten, fluorine and platinum were prepared similarly to the undoped TiO_2 except the dopant at desired ratio was added to the matrix before the catalyst was added. To synthesize W/TiO_2, F/TiO_2, and Pt/TiO_2, $Na_2WO_4{\cdot}2H_2O$, NH_4F, and $Pt(NH_4)_4(NO_3)_2$ were used as the sources of element dopant, respectively. Diagram for TiO_2 synthesis was illustrated in Figure 3.2 and the details were described bellows:

a. Place 70 mL anhydrous ethanol in a 250 mL flask and slowly add 0.05 mole of tetra(n-butoxyl)titanium under the vigorous stirring condition to prepare a clear tetra(n-butoxyl)titanium ethanol solution (Solution I). The flask was then placed in water bath to control the temperature at 4°C for the desired time.

b. At the same time, 20 mL of deionized water was added into 20 mL of anhydrous ethanol alcohol to make the ethanol aqueous solution. In the case of doped TiO_2, the doping compound at the desired mole ratio was added into the ethanol aqueous solution. The mixture was continuously stirred until the doping element was completely dissolved (Solution II).

c. Solution II was dropwise added into Solution I and the precipitates were immediately formed.

d. After 1 hour of continuous stirring, 4 mL of the acid or base catalyst was added into the solution. The mixed liquor was thoroughly mixed to undergo hydrolytic condensation for 3 hours.

e. Hydrolyzed solution was then placed into the oven to dry at 120°C for 2 hours to obtained $Ti(OH)_4$ and then pulverized into powder form.

f. Finally, $Ti(OH)_4$ powder was calcined at the desired temperature for 10 hours to obtain TiO_2.

3.2.1.2 Synthesis of Titanium Dioxide with Hydrothermal Treatment

This part aimed to study the effect of hydrothermal on the synthetic TiO_2 property. Optimum criteria obtained from previous part were used in this

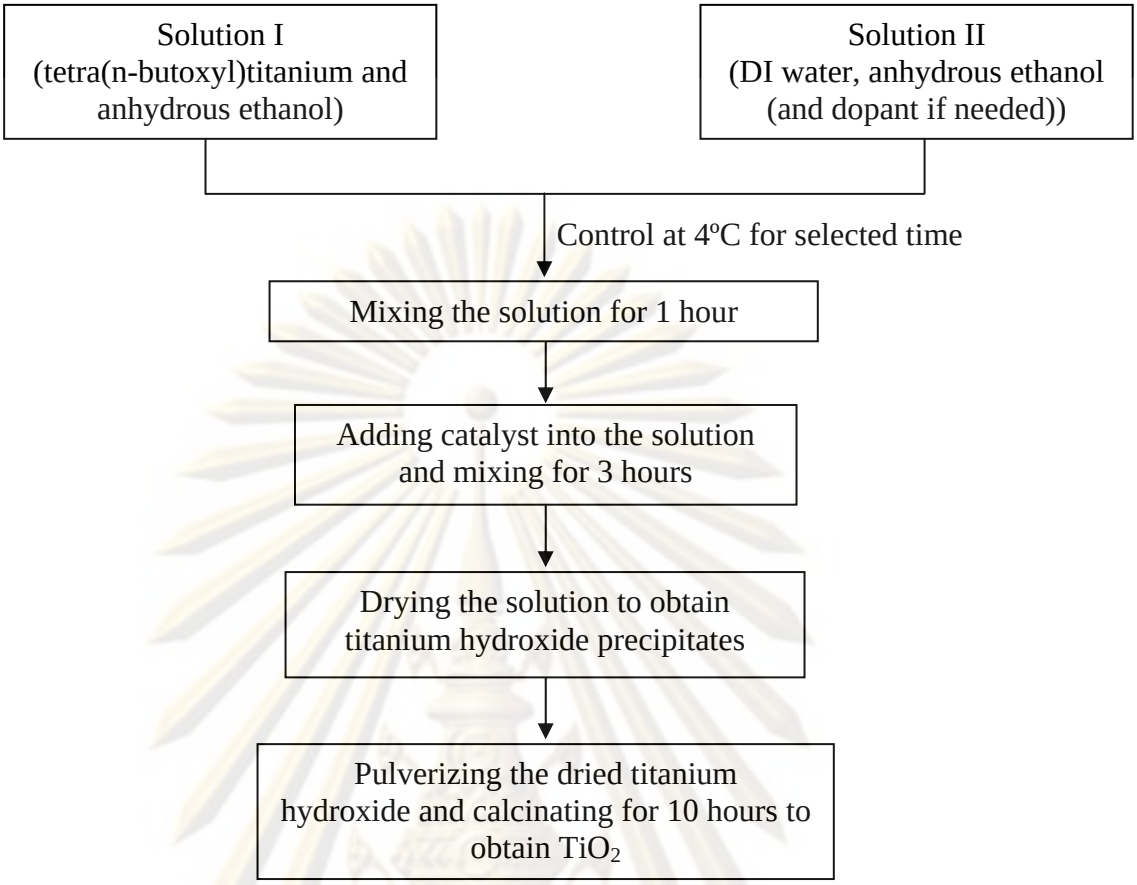

Figure 3.2 Schematic for TiO_2 synthesis by sol-gel method.

hydrothermal section; however, after the hydrolytic condensation for 3 hours, the hydrolyzed solution was sealed and then autoclaved at 121°C and 103.4 kPa for selected time before placing into the oven to dry at 120°C. Overall procedure of TiO_2 synthesis by hydrothermal treatment is illustrated in the Figure 3.3.

3.2.2 Determination of the Titanium Dioxide Activity

Photocatalytic experiments were conducted in a 1-liter Pyrex beaker. At first, the 2-chlorophenol solution with TiO_2 was magnetically stirred in the dark until reaching an adsorption/desorption equilibrium. After that, the irradiation began to initiate the photocatalytic experiment. The disappearance of the 2-chlorophenol, which represented the activity of synthetic TiO_2, was monitored. At a predetermined time, the sample was taken, filtered through a Millipore filter (0.22 μm pores) and analyzed by the UV-VIS spectrophotometer at 510 nm for residual 2-chlorophenol,

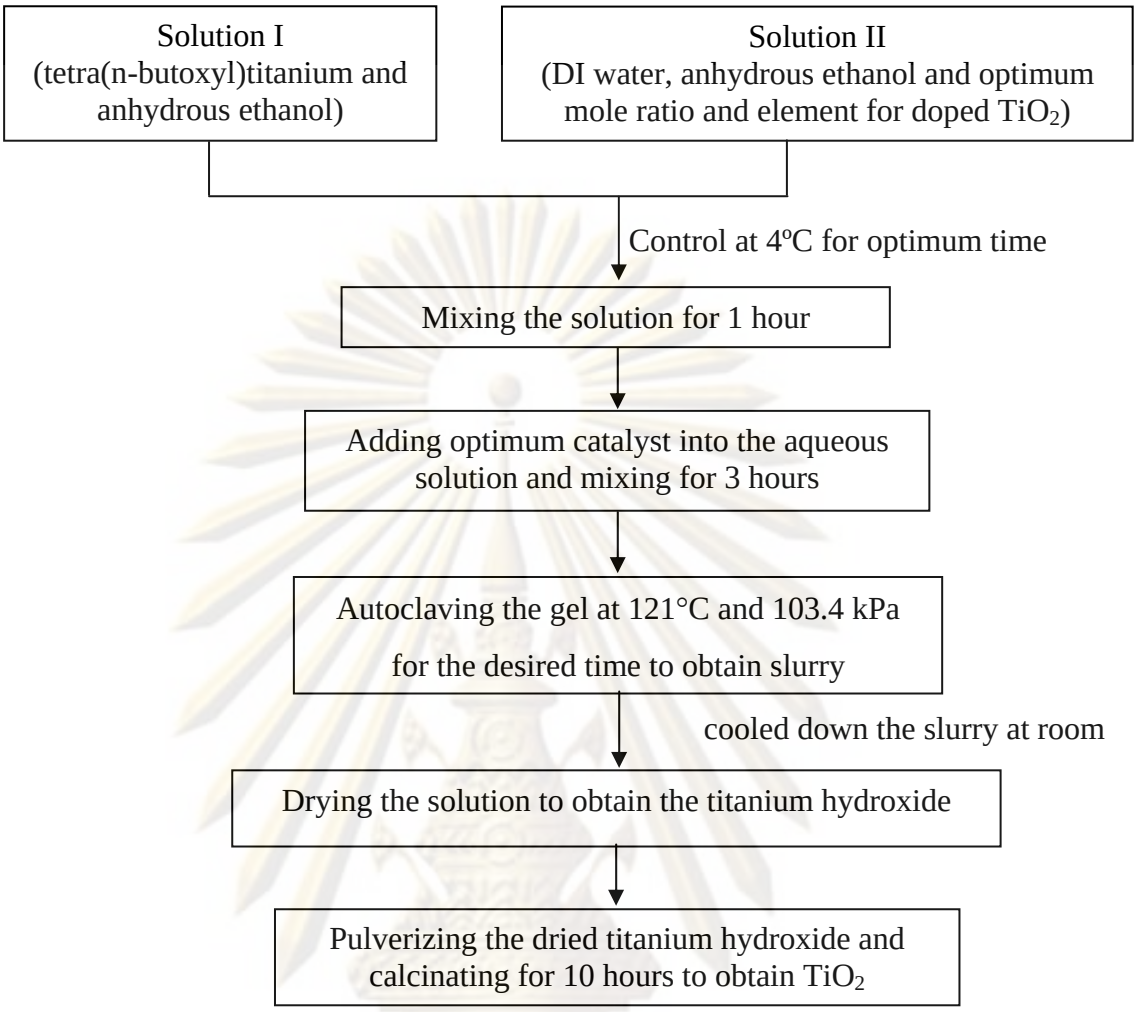

Figure 3.3 Schematic for TiO_2 synthesis by hydrothermal method.

according to the 4-amino-antipyrine colorimetric method (APHA, 1992). Sampling times were 0, 30, 60, 90, 120, 180, 240, 300 and 360 minutes. Solution pH was controlled throughout the experiment. Diagram for the photocatalytic activity test is described in Figure. 3.4.

3.3 Experimental Scenarios

3.3.1 Modification of Titanium Dioxide Synthesis

3.3.1.1 Sol-Gel Process

Key parameters in the sol-gel process which believed to affect the TiO_2 property were investigated including calcination temperature (150, 200, 300, 400, and

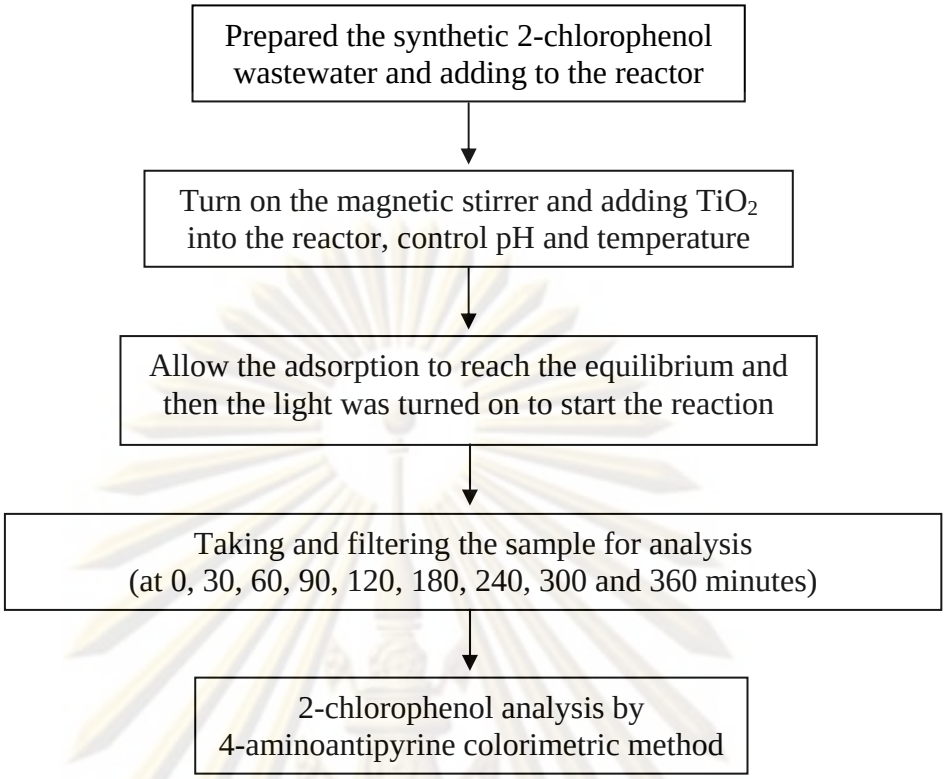

Figure 3.4 Experiment schematic for photocatalytic activity investigation

500°C) and ramp rate (1, 4, and 9°C/min), and sol catalyst type (HNO_3, H_2SO_4, H_3PO_4, and diethanolanime (DEA)). Synthetic TiO_2 under various conditions were tested for their photocatalytic activity using 2-chlorophenol as the target pollutant. Experimental conditions for each scenario are shown in Tables 3.1 to 3.3.

3.3.1.2 Element Doping

In this section, the TiO_2 was synthesized following the optimum conditions obtained from previous part; however, the target dopant (either tungsten, fluorine or platinum) was added to determine the improvement in photocatalytic property.

3.3.1.3 Hydrothermal Treatment

TiO_2 was pretreated by hydrothermal process to further enhance the photocatalytic property. The gel prepared according to the optimum conditions obtained from previous parts was autoclaved for either 2, 3, 4 or 6 hours and the

Table 3.1 Conditions for the study of calcinations temperature effect.

Ramp rate (°C/min)	Catalyst type	Calcination Temp. (°C)
1	HNO_3	150
		200
		300
		400
		500

Table 3.2 Conditions for the study of ramp rate effect.

Ramp rate (°C/min)	Catalyst type	Calcination Temp. (°C)
1	HNO_3	Optimum from Table 3.1
4		
9		

Table 3.3 Conditions for the study of sol catalyst effect.

Ramp rate (°C/min)	Catalyst type	Calcination Temp. (°C)
Optimum from Table 3.12	HNO_3	Optimum from Table 3.1
	H_2SO_4	
	H_3PO_4	
	DEA	

obtained TiO_2 were tested for their photocatalytic activity using 2-chlorophenol as the target compound.

3.3.2 Adsorption Study

It is important to determine the adsorption behavior of the synthetic TiO_2 which principally affects its photocatalytic activity. Table 3.4 shows the conditions used to determine the adsorption isotherm of the synthetic TiO_2.

3.3.3 Photocatalytic Activity Investigation

Photocatalytic activity of the synthetic TiO_2 was investigated under several conditions. The effects of TiO_2 dose, light wavelength, light intensity and pH on 2-

chlorophenol degradation were investigated. Moreover, photocatalytic kinetics of 2-chlorophenol was also determined. The experimental scenarios are shown in Tables 3.5 to 3.9.

Table 3.4 Conditions for characterizing the 2-chlorophenol adsorption onto TiO_2 surface.

TiO_2 dose (g/L)	pH	Temp. (°C)	2-chlorophenol (mM)
1	5	25	0.005
			0.01
			0.03
			0.05
			0.1
			0.2
			0.5
			1.3

Table 3.5 Conditions for characterizing the P-25 catalytic activity under blue and UV light irradiation.

2-chlorophenol (mM)	TiO_2 dose (g/L)	pH	Temp. (ºC)	Light source
0.01	1	5	25	UV
				Blue light

Table 3.6 Conditions for determining the effect of TiO_2 dose under blue light irradiation.

2-chlorophenol (mM)	Temp. (ºC)	TiO_2 dose (g/L)
0.01	25	0.25
		0.5
		1
		1.5

Table 3.7 Conditions for determining the effect of pH on TiO_2 photocatalytic activity.

2-chlorophenol (mM)	Temp. (ºC)	Light color	TiO_2 dose (g/L)	pH
0.01	25	Blue light	Optimum from Table 3.3	5
				6
				7
				8

Table 3.8 Conditions for determining the effect of light wavelength on TiO_2 photocatalytic activity.

2-chlorophenol (mM)	Temp. (ºC)	TiO_2 dose (g/L)	pH	Light color
0.01	25	Optimum from Table 3.3	Optimum from Table 3.4	Blue light
				Green light
				Red light

Table 3.9 Conditions for determining the effect of 2-chlorophenol on TiO_2 photocatalytic activity.

Temp. (ºC)	TiO_2 dose (g/L)	pH	Light color	Light intensity (lamp)	2-chlorophenol (mM)
25	Optimum from Table 3.3	Optimum from Table 3.4	Blue light	1	0.005
					0.01
					0.03
					0.05

3.4 Analytical Methods

3.4.1 Identification of Crystalline Structure

Crystal structure of the synthetic TiO_2 was characterized by the X-ray diffraction spectroscopy (XRD) (D8 Discovery, Bruker-AXS) with Cu Kα radiation (λ = 0.15406 nm) in a 2θ range of 20-80° and a scanning speed of 3°/min.

3.4.2 Identification of Morphology

Surface morphology of the synthetic TiO_2 was characterized by the scanning electron microscopy (SEM) (JEOL, JSM-5410LV).

3.4.3 UV-VIS Absorption Spectra Analysis

Absorption property of the synthetic TiO_2 was evaluated by using a diffuse reflectance scanning spectrophotometer (Perkin Elmer Lambda 35 Spectrophotometer) with the scanning range between 200 and 800 nm.

3.4.4 Point of Zero Charge (pzc) Analysis

Point of zero charge of synthetic TiO_2 was analyzed by using the dynamic light scattering (Malvern ZS90).

3.4.5 Surface Area Analysis

Surface area of synthetic TiO_2 was obtained from nitrogen adsorption isotherm by the Brunauer-Emmett-Teller (BET**)** method following the ASTM standard.

3.4.6 Laser Particle Size Distribution Analysis

Particle size distribution of synthetic TiO2 was analysed by using laser particle size distribution Analyzer model Mastersizer-S.

3.4.7 Elemental Concentration

X-ray fluorescence (XRF) analysis was used to determine the elemental concentration.

3.4.8 Measurement of 2-Chlorophenol

4-aminoantipyrine colorimetric method (APHA, 1992) was used to analyze residual concentration of 2-chlorophenol. One mL of buffer solution, 1 mL of 4-amino-antipyrine solution, and 1 mL of potassium ferric cyanide solution were added into the sample and mixed together to produce a color reaction product. The color intensity representing the 2-chlorophenol concentration was measured by a UV-VIS spectrophotometer at 510 nm.

CHAPTER IV

RESULTS AND DISCUSSION

4.1 Titanium Dioxide Synthesis

4.1.1 Optimizing Sol-Gel Conditions

4.1.1.1 Effect of Calcination Temperature

This experimental part aimed to study effect of calcination temperature on TiO_2 photocatalytic property. Titanium gel was calcined at 150, 200, 300, 400 and 500ºC for 10 hours. Figure 4.1 shows the X-ray diffraction (XRD) patterns of the TiO_2 obtained from different calcination temperatures as compared to the commercial TiO_2 (Degussa P-25). The diffraction angles (2θ) of 25.28 and 27.43 represent the crystal plane of anatase (1 0 1) and rutile (1 1 0). Crystal size can be determined from the Scherrer formula as shown in Equation (4.1):

$$D = \frac{K\lambda}{\beta \cos\theta} \tag{4.1}$$

where λ is the wavelength characteristic of the Cu Kα radiation (λ = 0.154 nm), β is the full width at half maximum of which unit is in radians and θ is the reflecting angle. The full widths at half-maximum of the anatase, brookite, and rutile peaks could be obtained from the XRD pattern; it can be seen from Figure 4.1 that the samples calcined at 200 and 300°C contained only anatase and the crystal sizes were calculated to be 4.029 and 4.284 nm, respectively. As calcination temperature reached to 400°C, a large peak at 2θ of 27.43° and a small peak at 2θ of 25.28° were observed, indicating that the major crystallize phase had transformed from anatase to rutile and the crystal size has been increased to 11.302 nm. At 500°C, the peak at 2θ of 27.43° became predominate; however, greatly reduced at 2θ of 25.28°, suggesting that most of the crystalline had transformed to rutile and the corresponding crystal size has increased to 18.083 nm. Table 4.1 summarizes the crystal sizes of the TiO_2 obtained from this study under various calcination temperatures.

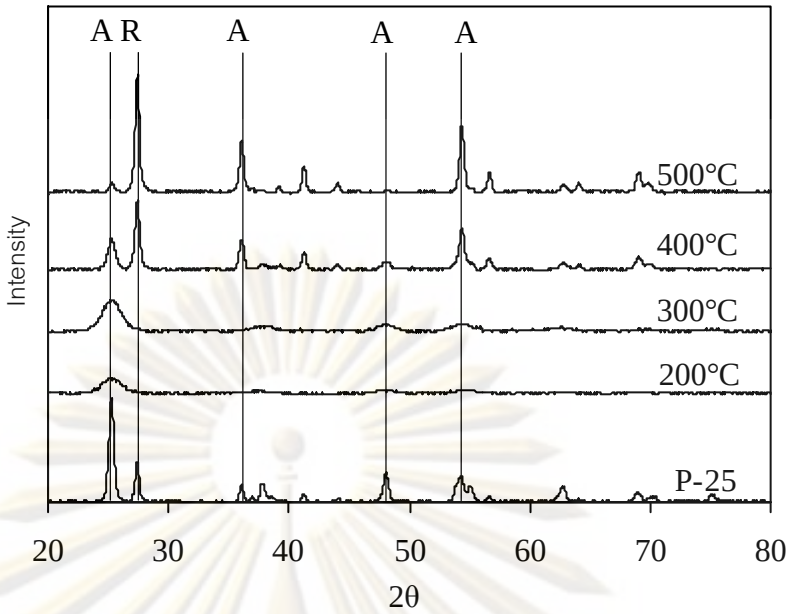

Figure 4.1 XRD patterns of sol-gel synthetic TiO_2 without doping calcined at various temperatures (A and R represents the crystal plane of anatase and rutile, respectively).

Table 4.1 Effect of calcinations temperature on the crystallize size and weight fraction of anatase and rutile phases.

Calcination temp. (ºC)	Crystallize size (nm)	% Anatase	% Rutile
200	4.029	100.00	0
300	4.284	100.00	0
400	11.302	29.09	70.91
500	18.083	93.23	6.77

To quantify the effect of calcination temperature on the phase transformation of the TiO_2, the portions of anatase and rutile were calculated from Equations (4.2), (4.3) and (4.4) by using the integrated intensities of the anatase (1 0 1), rutile (1 1 0), and brookite (1 2 1) peaks obtained from the XRD pattern (Figure 4.1):

$$W_A = \frac{K_A A_A}{K_A A_A + A_R + K_B A_B} \qquad (4.2)$$

$$W_R = \frac{A_R}{K_A A_A + A_R + K_B A_B} \quad (4.3)$$

$$W_B = \frac{K_B A_B}{K_A A_A + A_R + K_B A_B} \quad (4.4)$$

where W_A, W_R, and W_B represent the weight fractions of the anatase, rutile, and brookite phases, respectively. A_A, A_R, and A_B are the integrated intensities of the anatase, rutile and brookite peaks, respectively. The variables K_A and K_B are coefficients with values 0.886 and 2.721, respectively. The summary results were also shown in Table 4.1 which is in agreement with previous discussion.

Furthermore, it was found that the synthetic method and calcined temperature also affected the light absorption ability of the TiO_2. All synthetic TiO_2 obtained in this study could absorb visible light much better than the Degussa P-25 as shown in Figure 4.2 although the Degussa P-25 absorbed better within the UV range. The visible-light absorptivity was the highest at 400 nm (violet light) and declined substantially as the wavelength increased to 800 nm. Visible light absorption ability improved as the calcined temperature increased from 150 to 200°C; however, decreased simultaneously afterward. The presence of carbonaceous species might cause the prepared TiO_2 photocatalyst to be able to respond to the visible light. These carbonaceous species are normally burnt out by the calcination at elevated temperature in typical synthetic procedures as reported by Lettmann et al. (2001) and Lin et al. (2006).

Band gap energy of the TiO_2 can be estimated from the plot of square root of Kubelka Munk function (F(R)) versus photon energy (Asahi et al., 2001). The relation of $(\alpha h\nu)^r$ and $h\nu$ was plotted. The band gap energy of TiO_2 can be determined from the Equation (4.5).

$$\alpha h\nu = A(h\nu - E_g)^r \quad (4.5)$$

where A is a constant, $h\nu$ is the photon energy, E_g represents the band gap energy of material and r is the characteristic of the type of the transition process which is 0.5 for a direct-allowed optical transition and 2.0 for an indirect-allowed optical transition (non direct in case of an amorphous semiconductor). Results are summarized in Table 4.2 which shows that the band gap energies of all synthetic TiO_2 are lower than

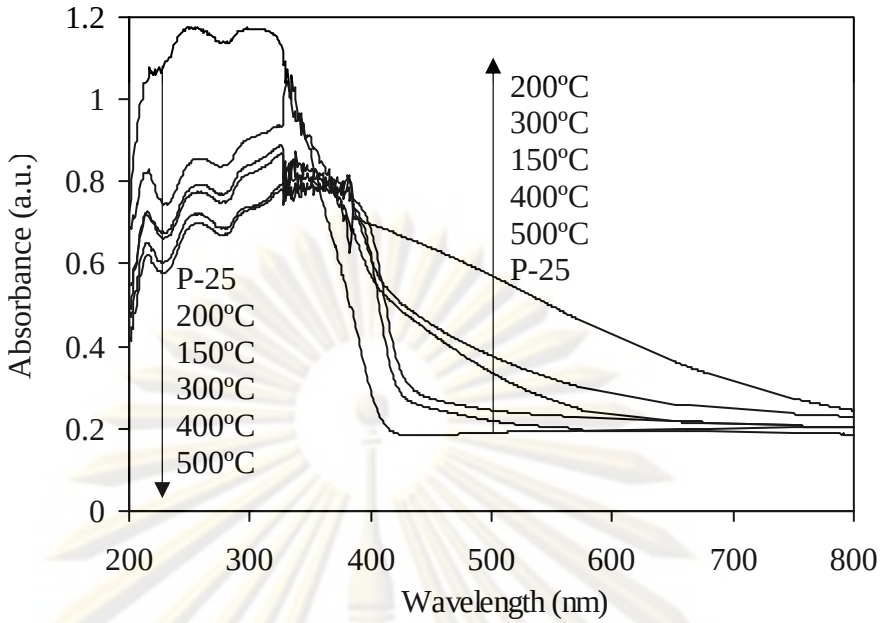

Figure 4.2 UV-VIS absorption spectrograph of sol-gel synthetic undoped TiO_2 calcined at various temperatures.

Table 4.2 Band gap energy of the TiO_2 calcined at various temperatures.

Calcination temperature (°C)	Band gap energy (eV)
150	1.80
200	1.20
300	1.50
400	2.80
500	2.79

Degussa P-25 which is 3.2 eV. The band gap energy was decreased from 3.2 eV to 1.80 and 1.20 eV for the TiO_2 calcined at 150 and 200ºC, respectively. Nonetheless, the band gap increased again as the calcination temperature increased further. At 300ºC, the band gap energy is 1.50 eV and significantly increased to 2.80 and 2.79 eV at 400 and 500 ºC, respectively. This narrower band gap should better facilitate the excitation of an electron to jump from the valance band to conduction band which can result in higher photocatalytic activities. Oxidation of 2-chlorophenol also supported this band gap reduction. The TiO_2 calcined at 200°C had a higher photocatalytic activity under the blue light irradiation than those calcined at 300°C, i.e., 91.8% of 0.01 mM 2-chlorophenol was removed in 6 hours by the TiO_2 calcined at 200°C

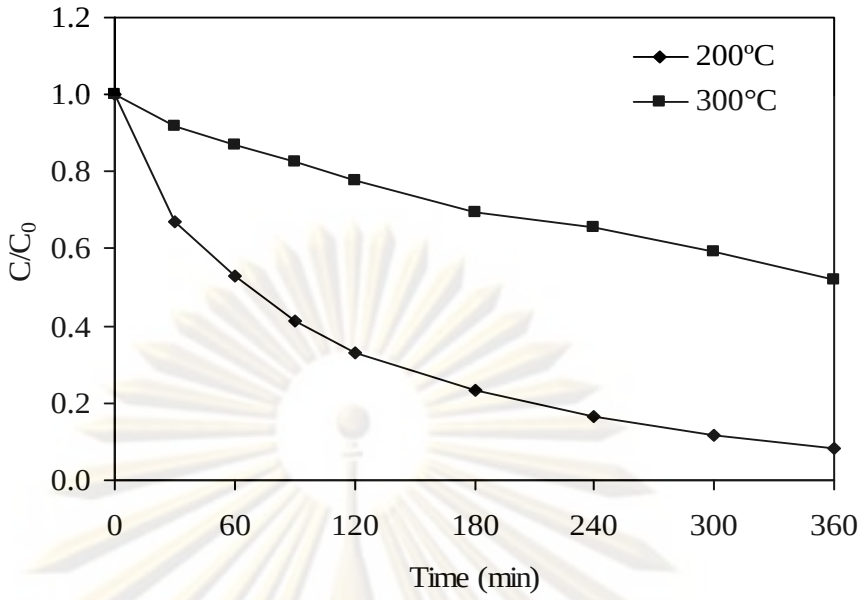

Figure 4.3 Photodegradation of 0.01 mM 2-chlophenol at calcine temperature 200°C and 300°C under blue light irradiation (1g/L TiO_2, pH at 5 and 25°C).

compared to 48.1% of those calcined at 300°C as shown in Figure 4.3. Generally, the Degussa P-25 does not have any significant activity under the visible light irradiation. This implies that the crystal structure formation does not seriously affect the activity of TiO_2 under visible light region as in the case of UV range where anatase has higher absorptivity than rutile and brookite, respectively. According to Figure 4.1, little anatase was formed at the calcinations temperature of 200°C with no other crystal form existed; however, the photocatalytic activity was still exceptional regardless on crystal formation. As a result, the calcination temperature of 200°C was the optimum value for this synthetic method.

4.1.1.2 Effect of Ramp Rate

In this part, all TiO_2 gels were calcined at 300°C but with different ramp rates from 1 to 4 and 9°C/min. Figure 4.4 shows the XRD pattern of synthetic TiO_2 obtained from various ramp rates. At the ramp rate of 1 °C/min, the crystal phase was totally anatase whereas some rutile phase, which has lower UV-VIS photocatalytic activity than anatase, occurred when the ramp rate was increased to 4 and 9°C/min, respectively. It is interesting to observe that the intensity of the main characteristic peak of anatase phase did not change in all samples which indicating that the formation of rutile crystal phase did not from anatase transformation. It is expected

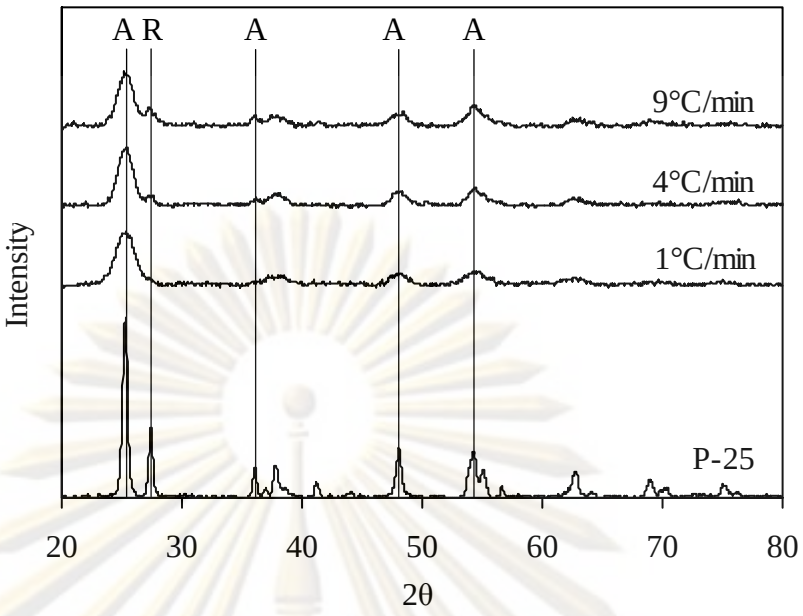

Figure 4.4 XRD pattern of undoped TiO_2 calcined at various ramp rates (A and R represents the crystal plane of anatase and rutile, respectively).

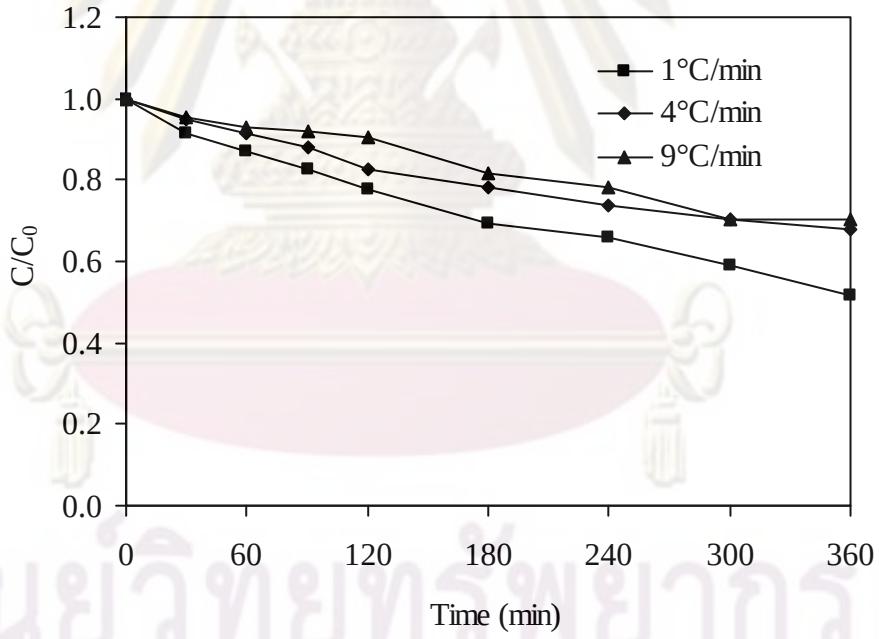

Figure 4.5 Photodegradation of 0.01 mM 2-chlophenol of the TiO_2 at various ramp rate under blue light irradiation (1g/L TiO_2, pH at 5 and 25°C).

that some amorphous TiO_2 were transformed to rutile as a result from high heating rate. Thus, the ramp rate could affect the growth behavior and phase structure of crystal phase similar to the results from Durán et al. (2001), Lei et al. (2009) and Meng et al. (2010). The formation of rutile phase was somehow weakening the

photocatalytic activity of the TiO_2 as represented by the removal efficiency of 0.01 mM 2-chlorophenol, i.e., the TiO_2 calcined at 1° C/min had the highest efficiency of 48.1 as compared to 32.2 and 29.8% of those calcined at 4 and 9° C/min, respectively (Figure 4.5). Thus, the optimum ramp rate for this synthetic method was 1 °C/min.

4.1.1.3 Effect of Dissolution Temperature

This part aimed to study the effect of temperature during the dissolution stage on the photocatalytic activity of the synthetic TiO_2. The dissolution stage included the mixing step of tetra(n-butoxyl) titanium ethanol solution (Solution I) with ethanol aqueous solution (Solution II) and the curing step before the catalyst was added. Several scenarios were performed including no control (no temperature control during the whole dissolution stage), only mixing step (control temperature at 4°C during the mixing of Solution I and Solution II), 30 minutes (control temperature at 4°C during the mixing step and 30 minutes during the curing step), and 1 hour (control temperature at 4°C during the mixing step and the whole 1-hr curing step). The obtained sol was further processed to generate TiO_2 following the optimum conditions obtained from previous sections, i.e., calcination temperature of 200 ºC and ramp rate at 1 ºC/min. From Figure 4.6, the TiO_2 prepared by controlling at 4°C for 30 minutes during the dissolution steps provided the best adsorption spectrum in both UV and visible light regions whereas the other conditions yielded the similar light-adsorption property. Nonetheless, when considering on the photocatalytic activity, it was found that the synthetic TiO_2 prepared by controlling at 4°C for 30 minutes and 1 hour had comparable activities, i.e., 91.8 and 90.4% of the 0.01 mM 2-chlorophenol could be removed in 6 hours, respectively, whereas the TiO_2 from other conditions had lower activity with 87.4 and 71.8% removal efficiency of mix step and no control, respectively, as revealed in Figure 4.7. These results suggested that the tetra(n-butoxyl)titanium is very sensitive to the moisture and the water vapor in the atmosphere; hence, maintaining the tetra(n-butoxyl)titanium during the dissolution stage at low temperature could significantly reduce the reaction with water vapor. By controlling the temperature at 4°C, a clear solution of TiO_2 precursor in ethanol could be achieved. If the temperature was not controlled at 4°C during the dissolution stage, the reaction between tetra(n-butoxyl)titanium and water vapor

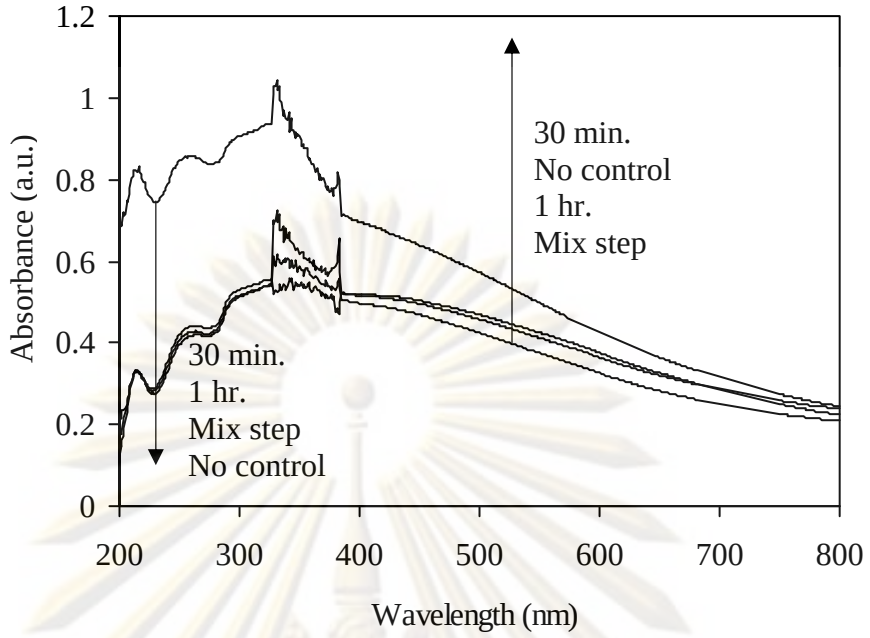

Figure 4.6 UV-VIS absorption spectrograph of sol-gel synthetic undoped TiO_2 at temperature control in dissolution stage.

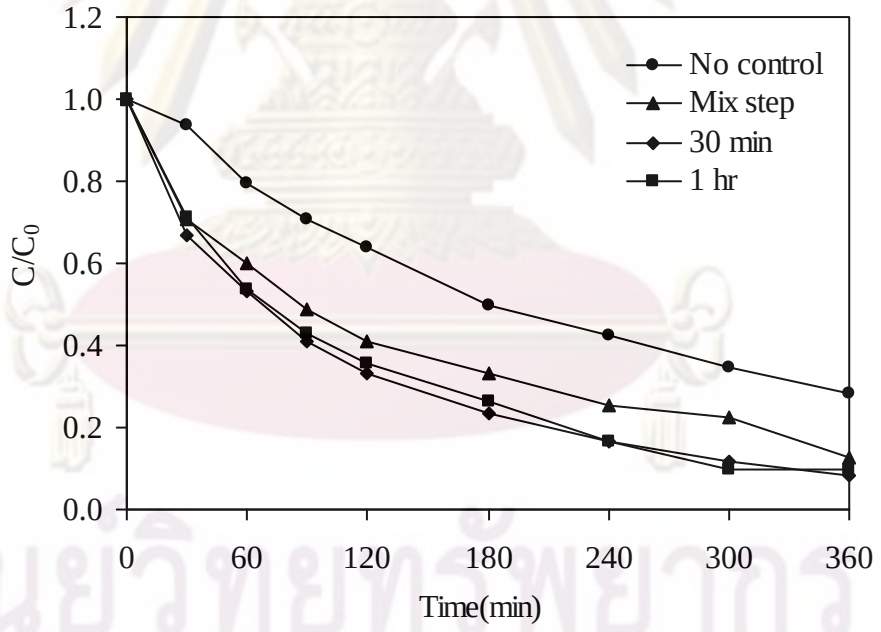

Figure 4.7 Photodegradation of 0.01 mM 2-chlophenol at various temperature and duration time control in dissolution stage under blue light irradiation (1g/L TiO_2, pH at 5 and 25°C).

would occur and white solids would precipitate out and caused failure to the synthesis. Moreover, the low temperature control during dissolution stage could slow down the hydrolysis and polymerization rates resulting in the formation of smaller

particles with more uniformity. As a result from this part, it is necessary to control temperature during the dissolution stage for 30 minutes after the Solution I was completely mixed with Solution II. In conclusion, the optimum conditions for synthesizing the TiO_2 by sol-gel process were dissolution at 4°C for 30 minutes after Solution I and Solution II were completely mixed together, calcinations at 200°C with the ramp rate of 1°C/min.

4.1.2 Enhancement of Visible-Light Photocatalysis by Doping

4.1.2.1 Effect of Doping Element

In this part, the TiO_2 was synthesized by doping with several elements including tungsten (W/TiO_2), fluorine (F/TiO_2), and platinum (Pt/TiO_2) at different mole ratios to enhance their visible-light responses. The optimal conditions from previous section were used. The studied mole ratios of each dopant to Ti are shown in Table 4.3. It is important to note that in the case of Pt/TiO_2, only one mole ratio was investigated since the preliminary result showed that the very expensive platinum was not as effective as other elements in promoting the visible-light absorptivity of the TiO_2 as will be discussed later. The UV-VIS absorption spectra of W/TiO_2, F/TiO_2 and Pt/TiO_2 obtained in this study are shown in Figures 4.8, 4.9 and 4.10, respectively. From Figure 4.8, it was found that tungsten doping enhance the visible light absorptivity of the synthetic TiO_2 though no significant impact in the UV range.

Table 4.3 Mole ratio of dopant to titanium

Dopant	**Mole ratio of dopant to Ti (%)**
Tungsten	$0.1\%W/TiO_2$ $0.5\%W/TiO_2$ $1\%W/TiO_2$
Fluorine	$0.5\%F/TiO_2$ $1\%F/TiO_2$ $2\%F/TiO_2$
Platinum	$1\%Pt/TiO_2$

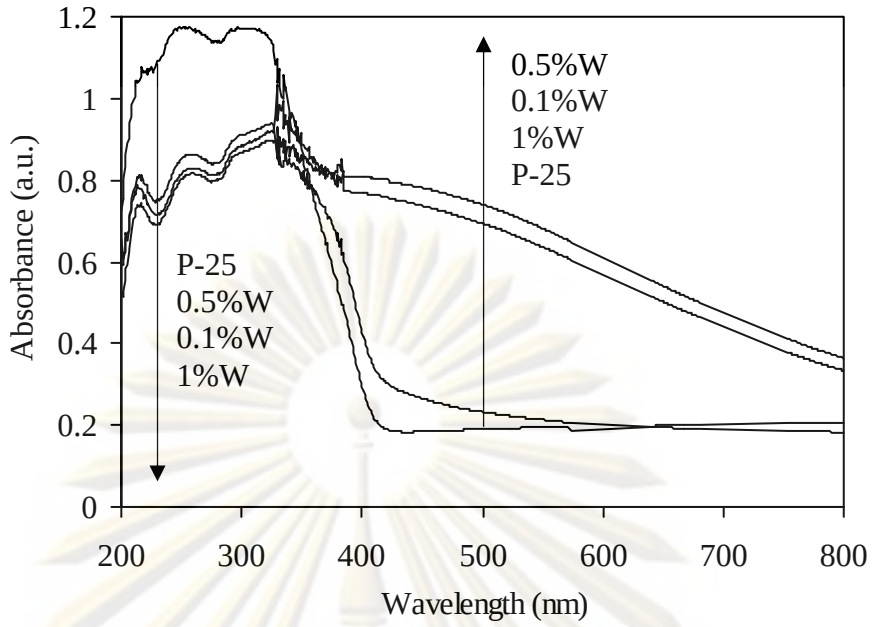

Figure 4.8 Absorption spectrographs of the TiO_2 doped with tungsten under the optimum sol-gel conditions.

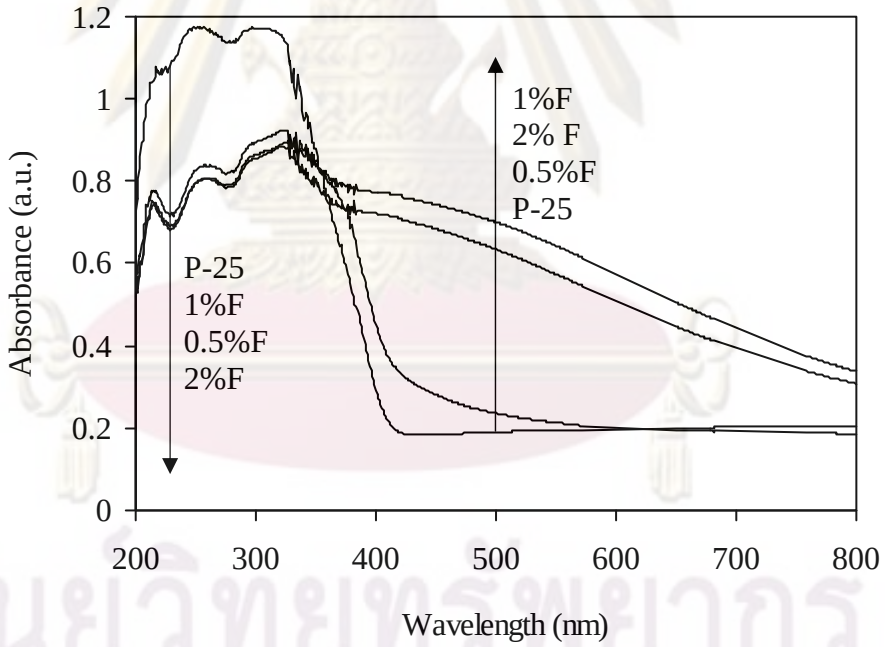

Figure 4.9 Absorption spectrographs of the TiO_2 doped with fluorine under the optimum sol-gel conditions.

The absorption enhancement increased as the W:Ti ratio increased from 0.1 to 0.5%; however, decreased sharply as the ratio increased to 1.0%; thus, the optimum W:Ti ratio was 0.5%. For fluorine doping, the visible light absorptivity increased as the

mole ratio of F:Ti increased from 0.5% to 1%. Nonetheless, the absorbance of visible light of the 2%F/TiO_2 was found to be lower than 1%F/TiO_2. The effect of F:Ti mole ratio was not obvious in the UV range. Therefore, the optimum F:Ti ratio was 1%. Moreover, Figure 4.10 shows the absorptivity of 1%Pt/TiO_2 indicating that 1%Pt/TiO_2 had lower absorbance in UV region but had a higher absorbance in visible light than the P-25. As a result, it can be concluded that all three elements being tested could enhance the absorptivity of the TiO_2 in the visible-light region. Nonetheless, when considering on the effect of element type, it was found that the 0.5%W/TiO_2 was the best followed by 1%TiO_2/F, undoped TiO_2, 1%Pt/TiO_2 and P-25, respectively, as shown in Figure 4.11. The band gap energies of all doped TiO_2 were calculated and shown in Table 4.4. It was found that all dopants impacted the absorptivity property of the TiO_2 and could reduce the band gap energy to be lower than the Degussa P-25 of 3.2 eV. The 0.5%W/TiO_2 had the lowest band gap energy of 1.12 eV causing it to be the easiest catalyst to be activated by visible light.

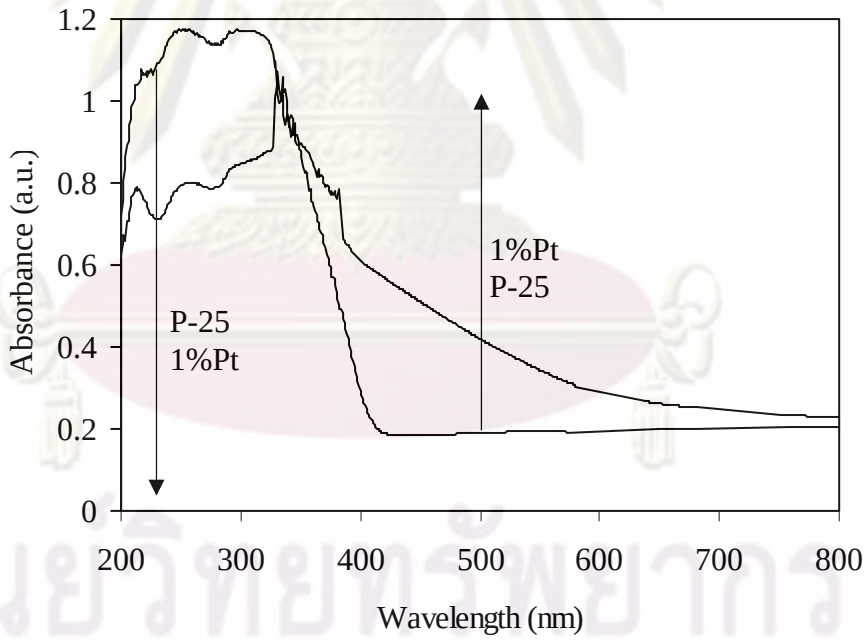

Figure 4.10 Absorption spectrographs of the TiO_2 doped with platinum under the optimum sol-gel conditions.

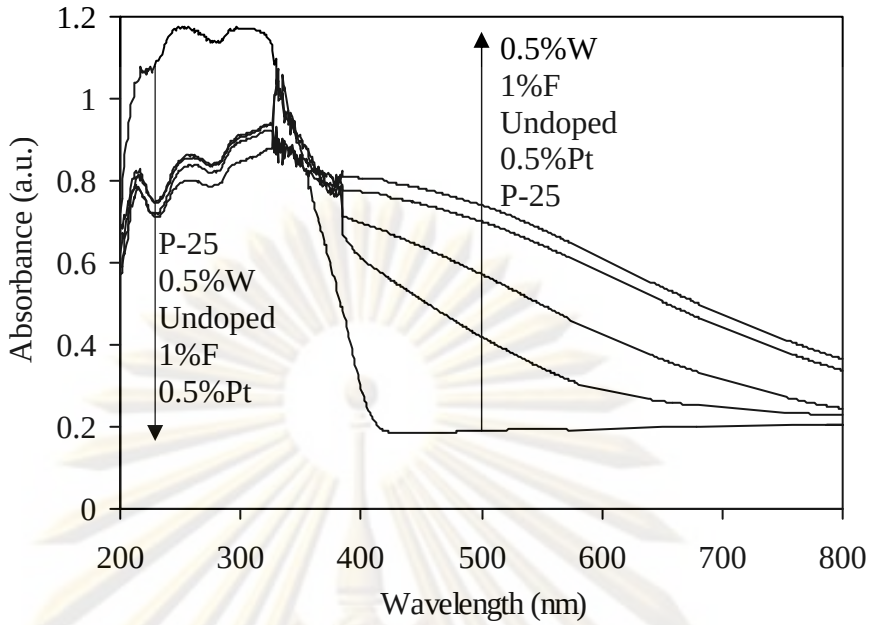

Figure 4.11 Absorption spectrographs of 0.5%W/TiO_2, 1%F/TiO_2 and 0.5%Pt/TiO_2 compare to undoped TiO_2 and Degussa P-25.

Table 4.4 Band gap energy of the doped TiO_2.

Doped TiO_2	**Band gap energy (eV)**
0.1%W/TiO_2	1.20
0.5%W/TiO_2	1.12
1%W/TiO_2	2.85
0.5%F/TiO_2	2.80
1%F/TiO_2	1.13
2%F/TiO_2	1.15
0.5%Pt/TiO_2	1.70

Figure 4.12(a) reveals the results from XRD analysis. It was found that the 0.5%W/TiO_2 apparently had lower the crystal formation than undoped TiO_2 and P-25, chronologically, i.e., much lower anatase peak was detected in the doped sample compared to undoped TiO_2 and P-25. In addition, the refection peak at 2θ of 25.28 which representing the anatase slightly has shifted to a higher angle of 25.40 in the case of undoped TiO_2 and 0.5%W/TiO_2 as shown in Figure 4.12(b). The reflection

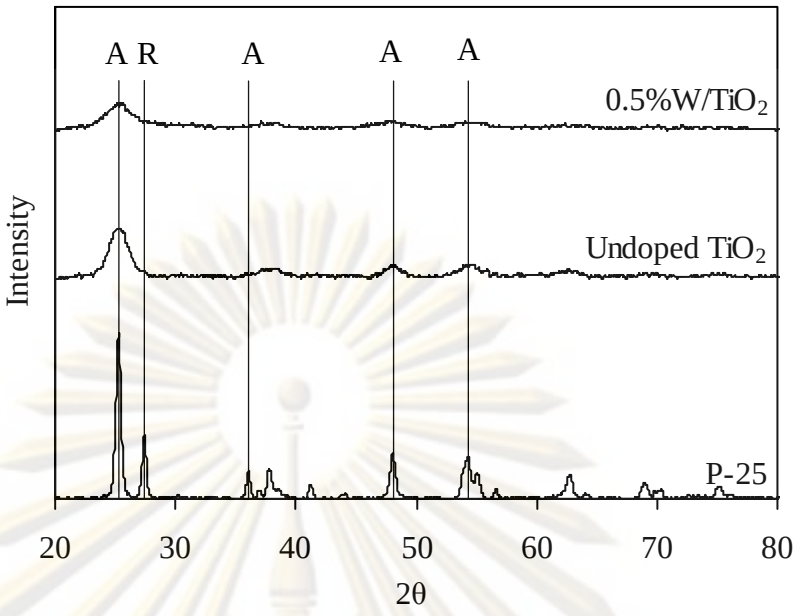

(a)

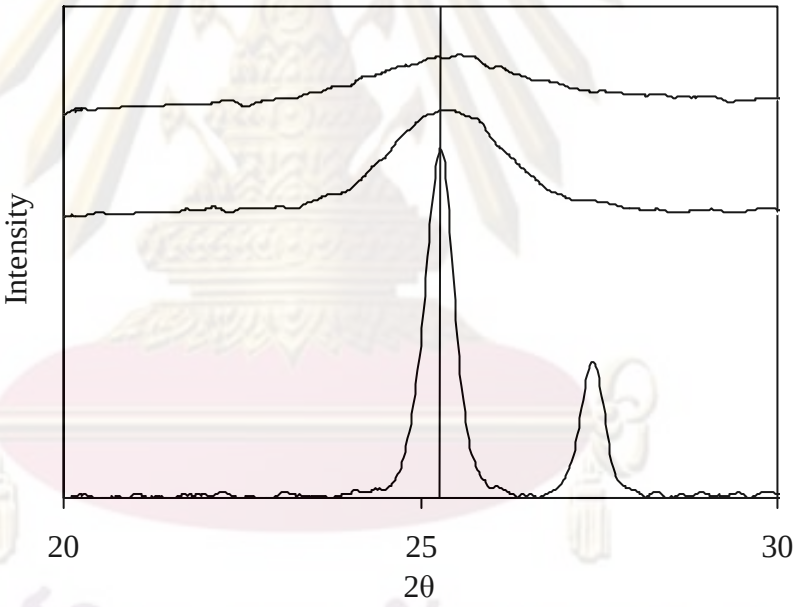

(b)

Figure 4.12 XRD pattern of the 0.5%W/TiO_2 (a) 0.5%W/TiO_2 compared with undoped TiO_2 and Degussa P-25; (b) an enlargement of (a) at 2θ of 25.28 (A and R represents the crystal plane of anatase and rutile, respectively).

peak corresponds to the interlayer spacing of titanium. Thus, the peak shift means a decrease of interlayer spacing. According to Scherrer formula as shown in Equation (4.1), the crystal size was found to be 2.993 nm for 0.5%W/TiO_2. It implied that

tungsten and the sol-gel conditions used in this study retarding the phase transformation and crystal grain growth.

Photocatalytic activity of various TiO_2 synthesized in this study were investigated under the blue light irradiation and the results were illustrated in Figure 4.13. The performance in 2-chlorophenol removal could be arrayed in order of undoped TiO_2 ≈ 0.5%W/TiO_2 > 1%F/TiO_2 > 1%Pt/TiO_2 > Degussa P-25 with the efficiencies of 91.8, 90.5, 51.9, 35.3 and 23.2%, respectively. The high photocatalytic activity of undoped TiO_2 probably because of the existence of carbonaceous species that act as sensitizers as suggested by Lin et al., (2006). However among synthetic TiO_2 the band gap energy of 0.5%W/TiO_2 of 1.12 eV is the lowest. Additionally, the intense absorption and red shift in the visible light range of 0.5%W/TiO_2 (Figure 4.11) implied that more electron hole pairs could be photo- generated under visible-light irradiation. Moreover, from the XRD pattern, it was found that despite low crystalline phases were formed, the 0.5%W/TiO_2 had comparable photoactivity under blue-light irradiation as the undoped TiO_2 but much better than the more crystalline formed P-25. This implies that the photoactivity under

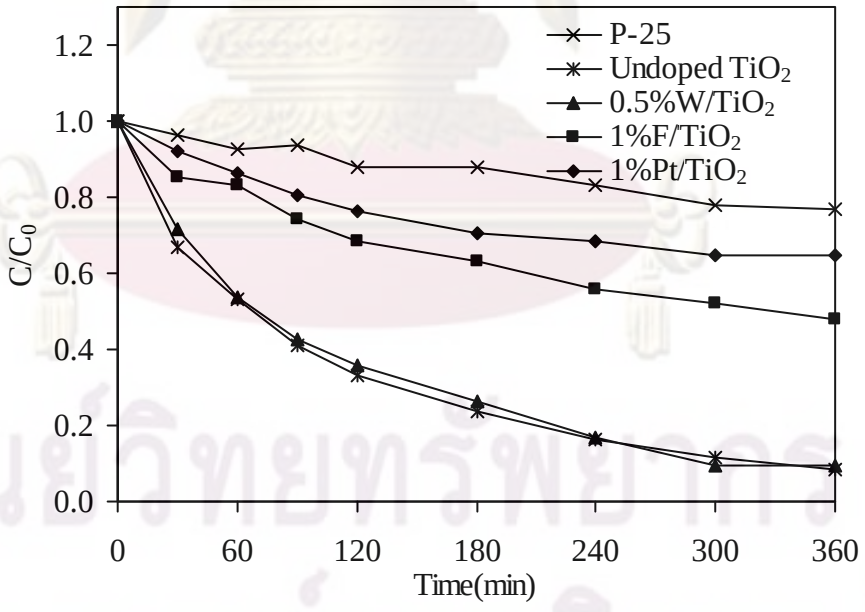

Figure 4.13 Photodegradation of 0.01 mM 2-chlophenol at various doped TiO_2 compare to undoped TiO_2 and Degussa P-25 under blue light irradiation (1g/L TiO_2, pH at 5 and 25°C).

visible light irradiation of the TiO_2 does not depend on crystallinity, i.e., the 0.5%W/TiO_2 with low reflection peak of anatase could effectively serve as the photocatalyst under the visible light irradation. The lowest photocatalytic activity of the Degussa P-25 also corresponded to its lowest visible light absorption ability as shown in Figure 4.11.

4.1.2.2 Effect of Sol Catalyst on 0.5%W/TiO_2

In this part, the optimum 0.5%W/TiO_2 was selected as a medium to study the effect of catalyst type being used during the sol preparation step. From literature reviews, it was found that good catalytic property under UV irradation is governed by two major opposing physical properties, i.e., crystallinity and surface area of the photocatalysts. High crystallinity helps to prolong the recombination rate; hence, strongly increases the activity of the photocatalyst. High surface area helps to facilitate adsorption of the target molecules onto the surface of the catalyst (Kanna and Wongnawa, 2008). From these reasons, 2 types of catalyst using during the sol preparation were tested, i.e., the acid group including HNO_3, H_2SO_4, and H_3PO_4, and the base group in which the diethanolanime (DEA) was used. Figure 4.14 is the adsorption spectrograph of the 0.5%W/TiO_2 powders prepared under DEA and various acid catalysts. The result shows that the acid catalyst type had no effect on the absorptivity in the UV region (λ <400 nm) but had a strong effect to the adsorption in visible region. Among acid catalysts, phosphoric acid was the worst whereas HNO_3 and H_2SO_4 had a mixed impact. For the wavelength greater than 550 nm, the H_2SO_4-catalyzed TiO_2 possessed a better absorptivity whereas the HNO_3-catalyzed TiO_2 was better as the wavelength below 550 nm. On the other hand, the basic DEA showed the lowest absorptivity both in the UV and visible light region. Normally, DEA is used as an inhibitor for the precipitation of oxides and a stabilizing agent on the hydrolysis of the metal alkoxides. Thus, the sol was stable for a long period before it transformed into a gel; hence, aging time should be extended. This application of base catalyst is generally suitable for the preparation of the immobilized TiO_2 but not in this study. The XRD analysis for different acid catalyst types is shown in Figure 4.15 indicating that only the HNO_3-catalyzed TiO_2 had a clear crystal structure (anatase) whereas the H_3PO_4 and H_2SO_4 could not detect any crystal structure since their spectra became broaden. It could be concluded that acid catalyst played an important role during the formation of TiO_2 crystal. Additionally, the photodegradation of 0.05 mM of

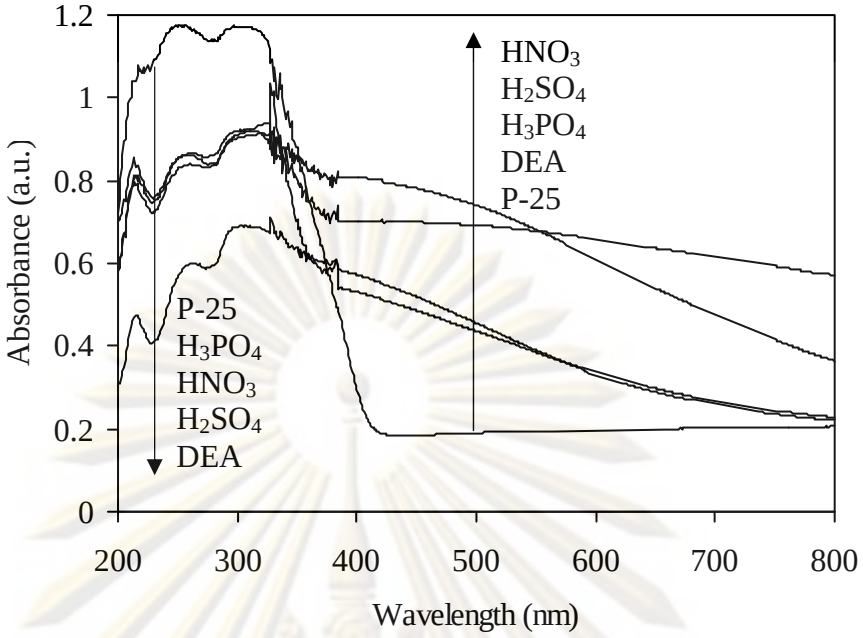

Figure 4.14 Absorption spectrographs of 0.5%W/TiO_2 with different catalyst prepared under optimum conditions.

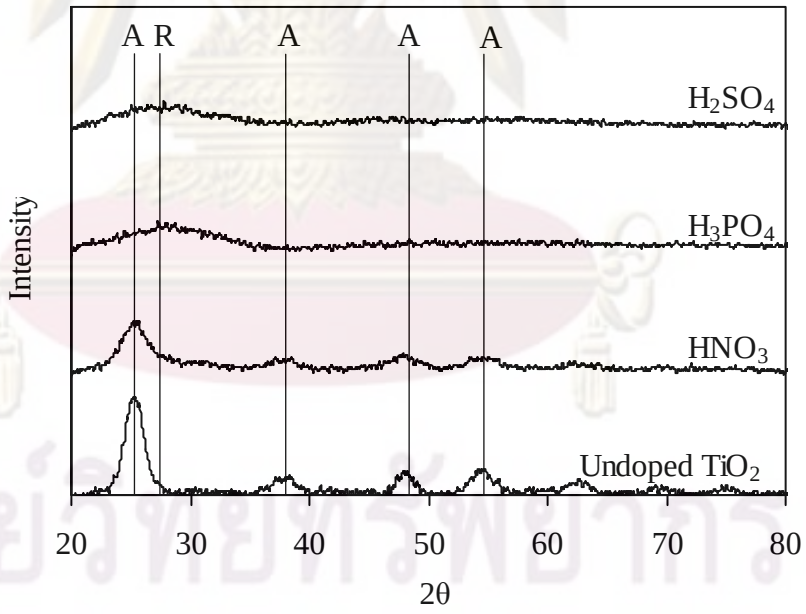

Figure 4.15 Effect of acid catalyst on XRD patterns of the 0.5%W/TiO_2 prepared under the optimum sol-gel conditions (A and R represents the crystal plane of anatase and rutile, respectively).

2-chlorophenol showed that the HNO_3-catalyst TiO_2 had the highest efficiency while H_3PO_4- and H_2SO_4-catalyst TiO_2 were not significantly different as shown in Figure 4.16. Thus, the optimum sol catalyst for this condition was HNO_3.

4.1.2.3 Effect of Hydrothermal Treatment

In this part, hydrothermal treatment was applied by autoclaving the hydrolized mixture before dehydration and calcination to modifies TiO_2 structure rather than sol-gel process only. The sol-gel method is most widely used due to its possible capability in controlling the textural and surface properties of composite oxides. But the calcination process frequently lead to serious particle agglomeration, grain growth, small surface area and phase transformation from anatase to rutile, which all decrease the photocatalytic activity of titanium. The hydrothermal processing represents an alternative to high-temperature calcination for crystallization of titanium hydroxide under mild temperatures. It has been widely applied in the synthesis of zeolites and in the production of advanced ceramic powders with ultrafine particle size. In the hydrothermal treatment, grain size, particle morphology, crystalline phase, and surface chemistry can be controlled via processing variables such as hydrothermal temperature, pressure and time. In this research, the autoclaving

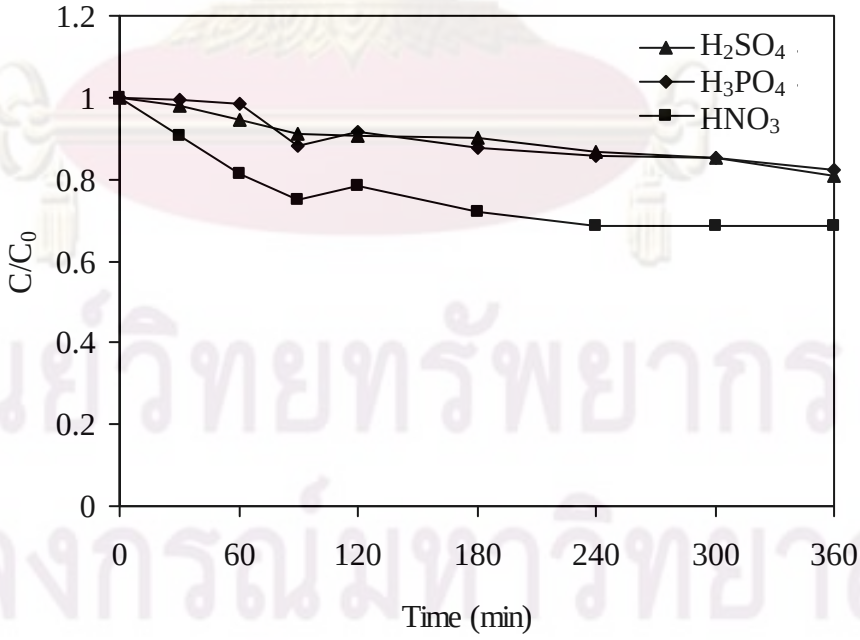

Figure 4.16 Photodegradation of 0.05 mM 2-chlophenol by 0.5%W/TiO_2 with different acid catalysts under blue light irradiation (1 g/L TiO_2, pH 5 and 25°C).

time was varied between 2 and 6 hours. It was found that the hydrothermal treatment could significantly intensify the absorptivity of the 0.5%W/TiO_2 particularly at high wavelengths as shown in Figure 4.17. The improvement increased as the treatment period increased from 2 to 4 hours; however, diminished when extended to 6 hours. Activity test with 2-chlorophenol indicated the 0.5%W/TiO_2 with 4 hours of hydrothermal treatment was more active than others (Figure 4.18). Hence, hydrothermal treatment of 4 hours was considered to be the optimum period. The XRD pattern of 0.5%W/TiO_2 autoclaved for 4 hours compare to 0.5%W/TiO_2 in Figure 4.19. It can be seen that for 0.5%W/TiO_2 without hydrothermal treatment, the TiO_2 sample had low anatase peak. This is because the precursor of TiO_2 was hydrolyzed at lower temperature, the rate of hydrolysis reaction is relative low and the hydrolysis was not completed, there was a large amount of un-hydrolyzed sols still remaining in the xerogel powders. These un-hydrolyzed sols prevented the phase transformation of amorphous to anatase by adsorbing sols on the surface of TiO_2 particles. Consequently, the as-prepared TiO_2 powders were amorphous or low crystallinity as reported by Yu et al (2005). In contrast, the TiO_2 samples after hydrothermal treatment appeared to have higher anatase peak. Hence, it can be concluded that hydrothermal treatment enhanced the phase transformation of the TiO_2 powders from amorphous to anatase at a low temperature and increased peak intensity

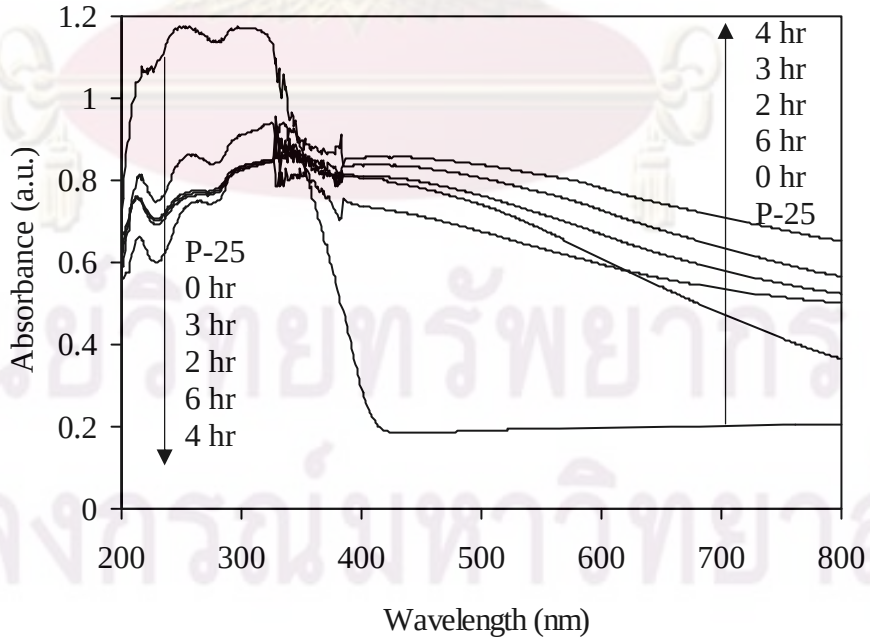

Figure 4.17 Absorption spectrographs of 0.5%W/TiO_2 prepared at the optimum sol-gel conditions with different hydrothermal treatment time.

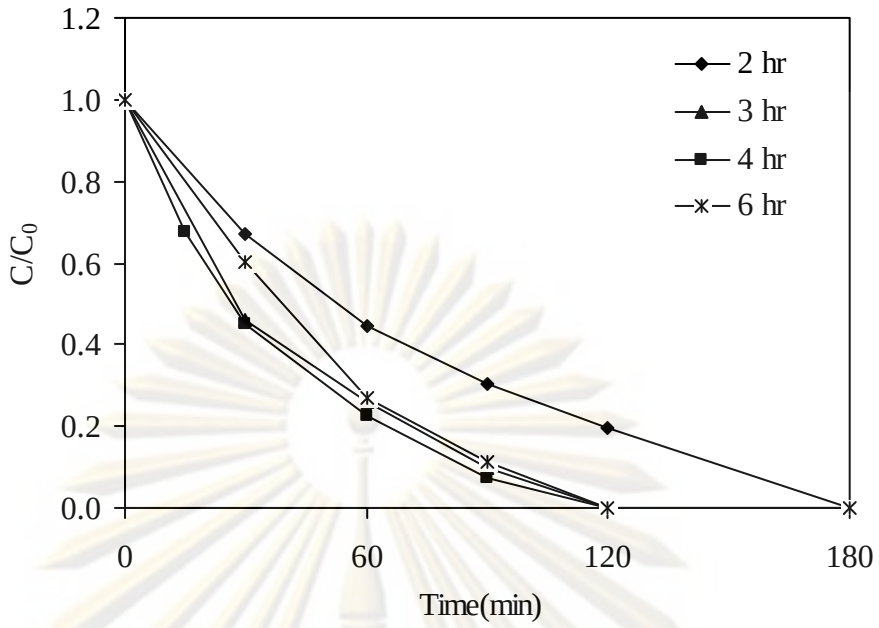

Figure 4.18 Effect of hydrothermal treatment time on the photodegradation of 0.01 mM 2-chlorophenol under blue light irradiation (1 g/L TiO_2, pH 5 and 25°C).

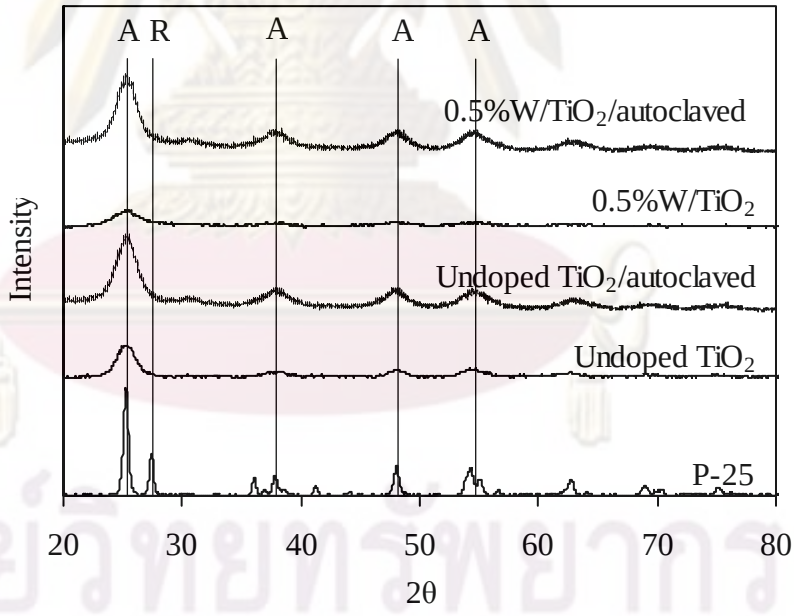

Figure 4.19 XRD pattern of TiO_2 synthesized under various conditions.

which was also reported by Mahata and Kundu (2009). It is important to note that, after hydrothermal treatment, the shift in anatase peak was not observed as in case of 0.5%W/TiO_2 synthesized by sol-gel process. This could be understood because the radius of W^{n+} ($4<n<6$) of 62-70 pm is virtually the same as Ti^{4+} atom of 62 pm. Thus, it could be concluded that some Ti^{4+} in the lattice of TiO_2 were substituted by W^{n+}.

The hydrothermal treatment also improved the catalytic property of undoped TiO_2 as shown in Figure 4.20; however, the improvement was less evident than those in the case of 0.5%W/TiO_2. In addition, the performance of hydrothermal-treated 0.5%W/TiO_2 was better than undoped TiO_2 and hydrothermal-treated undoped TiO_2 as shown in Figure 4.20. Furthermore, it is very interesting to observe that the photocatalysis activity of the 4 hours hydrothermal-treated 0.5%W/TiO_2 under blue light irradiation was nearly comparable to those of the P-25 under UV irradiation at 253.7 nm, i.e., 0.01 mM of 2-chlorophenol could be removed completely in 120 and 90 minutes, respectively. It is implied that the presence of transition metals and hydrothermal process increases the photocatalytic activity either by scavenging electrons that reduce the recombination of charges and therefore favors the •OH formation, or by modifying the surface properties of the material regarding the active sites, presence of defects etc., which could increase the adsorption and favor the interfacial reactions. This can significantly reduce the treatment cost of the photocatalytic process as the expensive UV irradiation can be replaced by the cheaper blue light irradiation.

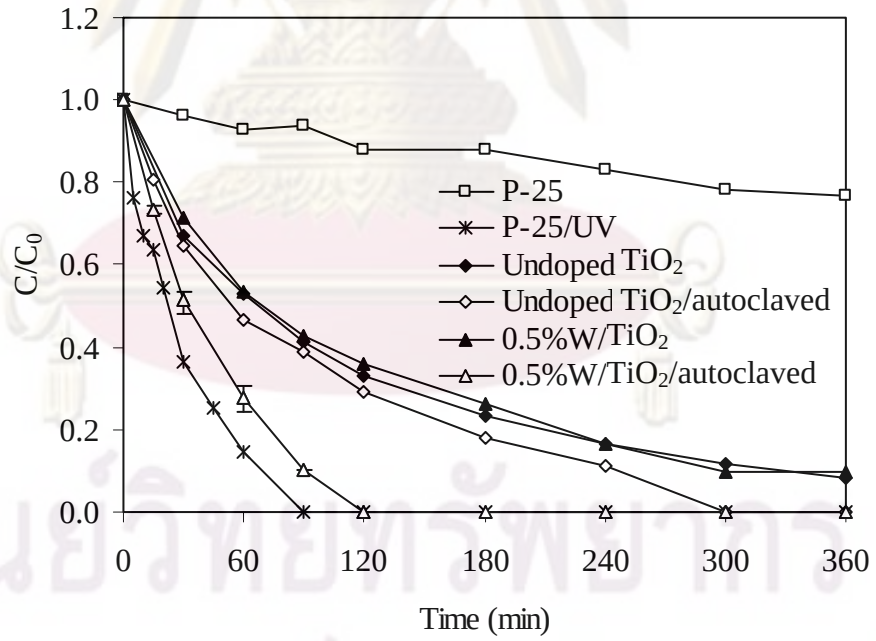

Figure 4.20 Photodegradation of 0.01 mM 2-chlophenol by TiO_2 synthesized under various conditions under blue-light irradiation as compared to Degussa P-25 under blue-light and UV irradiations (1 g/L TiO_2, pH 5 and 25°C).

The X-ray fluorescence (XRF) analysis was used to determine the elemental concentration of tungsten in the 0.5%W/TiO_2 with 4-hour hydrothermal treatment. The structure analysis result of XRF shows that 1.78% (w/w) tungsten was presented in the sample which was reasonable and corresponding very well with the doped mole ratio of 1.92% (w/w) (equivalent to 0.5% by mole).

4.1.3 Physical Properties of Synthetic Titanium Dioxide

Crystal size, band gap energy and weight fraction of anatase and rutile phase of the synthetic TiO_2 were calculated and summarized in Table 4.5. The crystal size estimated from Scherrer formula showed that tungsten had an effect on the crystal size, i.e., the crystal size decreased as compared to the undoped TiO_2. On the other hand, the hydrothermal treatment could significantly increase the crystal size. However, all synthetic TiO_2 samples had the crystal sizes smaller than the Degussa P-25. In addition, no rutile was found in the TiO_2 synthesized under the conditions used in this study, only the anatase phase was identified.

Morphologies of the undoped TiO_2 and 0.5%W/TiO_2 both with and without hydrothermal treatment were revealed by the SEM micrographs as shown in Figure 4.21. It reveals that the Degussa P-25 (Figure 4.21(a)) had better uniformity than the TiO_2 obtained from this study all of which exhibited nanogranular and rough surface. The morphologies of undoped TiO_2 and hydrothermal-treated 0.5%W/TiO_2 showed no significant difference as demonstrated in Figures 4.21(b) and 4.21(d). The nanoparticle size of the 0.5%W/TiO_2 was significantly larger than that estimated by the XRD measurements. This is due to the agglomeration of the nanocrystallines on the surface to form larger grains as shown by the SEM image in Figure 4.21(c). Formation of more aggregates could be related to the change of surface properties of the TiO_2 crystallites. The values of surface area, pore volume, and pore size are shown in Table 4.6. Among the synthetic TiO_2, the undoped TiO_2 had the high surface area (251.30 m^2/g). After doped with tungsten, the TiO_2 surface reduced to 201.50 m^2/g due to the agglomeration of the nanocrystallites as shown in the SEM image. It is very interesting to observe that the surface area became the highest after hydrothermal treatment. Moreover, it can be seen that all the samples had much higher surface area and pore volume whereas lower pore size than the Degussa P-25. In fact, Degussa P-25 powder, produced through hydrolysis of $TiCl_4$ in a hydrogen flame (Datye et al., 1995), does not contain pore in each TiO_2 crystallites. Therefore,

Table 4.5 Crystal size, band gap energy, and weight fraction of anatase and rutile phase of the synthetic TiO_2 compared to the Degussa P-25.

TiO_2	Crystal size (nm)	Band gap energy (eV)	% Anatase	% Rutile
Degussa P-25	34.426	3.20	69.55	30.45
Undoped TiO_2	4.209	1.20	100	0
0.5%W/TiO_2	2.993	1.18	100	0
Hydrothermal-treated 0.5%W/TiO_2	8.032	0.90	100	0

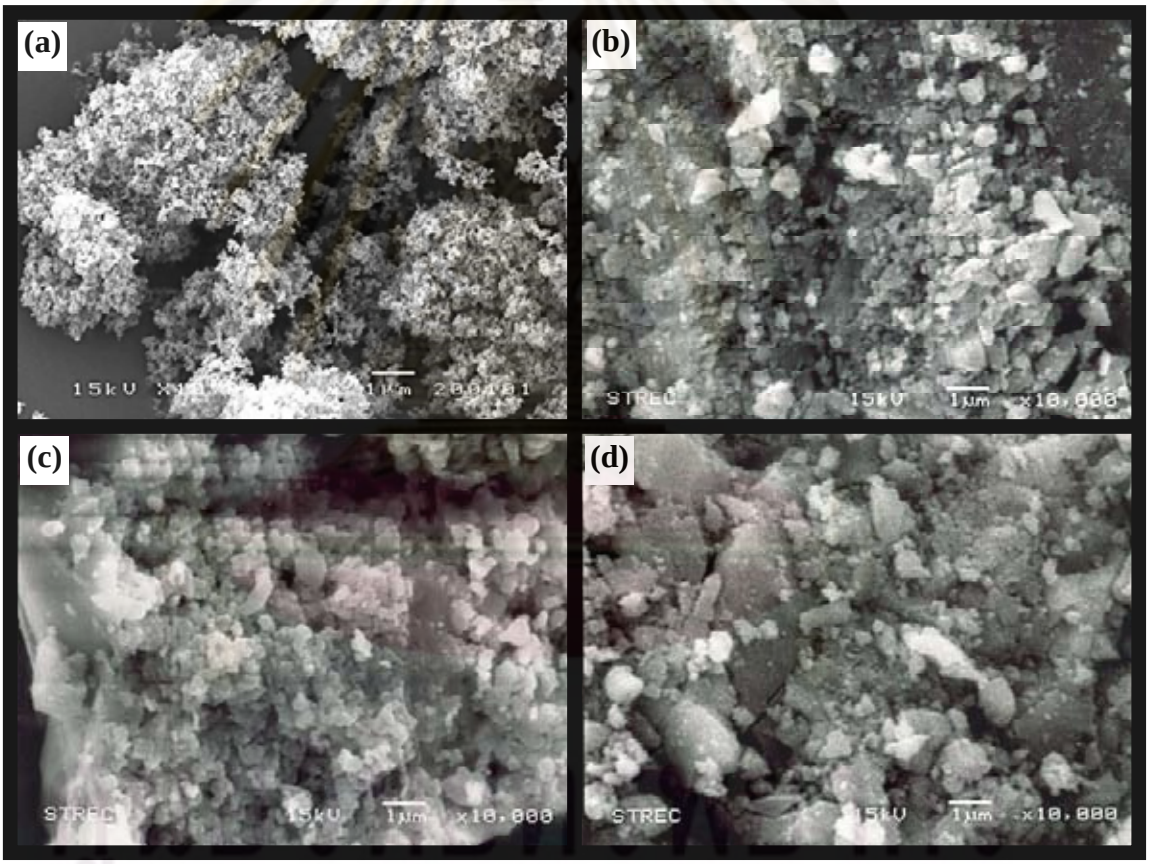

Figure 4.21 SEM micrographs of synthetic TiO_2 and Degussa P-25. (a) Degussa P-25, (b) undoped TiO_2, (c) 0.5%W/TiO_2, and (d) 0.5%W/TiO_2 with hydrothermal treatment.

Table 4.6 BET specific surface area, pore volume and size of the synthetic TiO_2 compared to Degussa P-25.

TiO_2 sample	Surface area (m^2/g)	Pore volume (cc./g)	Pore size (Å)
Degussa P-25 [a]	49.30	0.0900	83.00
Undoped TiO_2	251.30	0.1832	29.16
0.5%W/TiO_2	201.50	0.1245	24.72
Hydrothermal-treated 0.5%W/TiO_2	313.70	0.3337	42.56

[a] from Yu et al. (2006)

the formation of the pore structures in the samples could be attributed to the aggregations of TiO_2 crystallites. Finally, the synthetic TiO_2 was analyzed for their particle size distribution. From the particle size analysis as shown in Table 4.7 and Figure 4.22, it was found that the size distributions of all TiO_2 synthesized in this study were not significantly different. Particle sizes measured from this analysis were quite large due to the crystallite agglomeration. Nonetheless, it is believed that most particles would disperse into their primary sizes in aqueous suspension with sufficient mixing.

4.2 Adsorption of 2-Chlorophenol

This part aimed to characterize the adsorption behavior of 2-chlorophenol onto the TiO_2 surface. Different types of synthetic TiO_2 as well as the Degussa P-25 were used in this part. It was found that the contact time to reach adsorption equilibrium was approximately 20 minutes for all synthetic TiO_2 and approximately 30 minutes for Degussa P-25 as shown in Figure 4.23. The results revealed that Degussa P-25

Table 4.7 Comparison the particle size distribution between synthetic TiO_2 and Degussa P-25.

TiO_2 sample	Particle size distribution (μm)		
	D(v,0.1)	D(v,0.5)	D(v,0.9)
Undoped TiO_2	7.25	81.25	253.57
0.5%W/TiO_2	13.80	68.63	237.48
Hydrothermal-treated 0.5%W/TiO_2	6.85	93.44	290.77

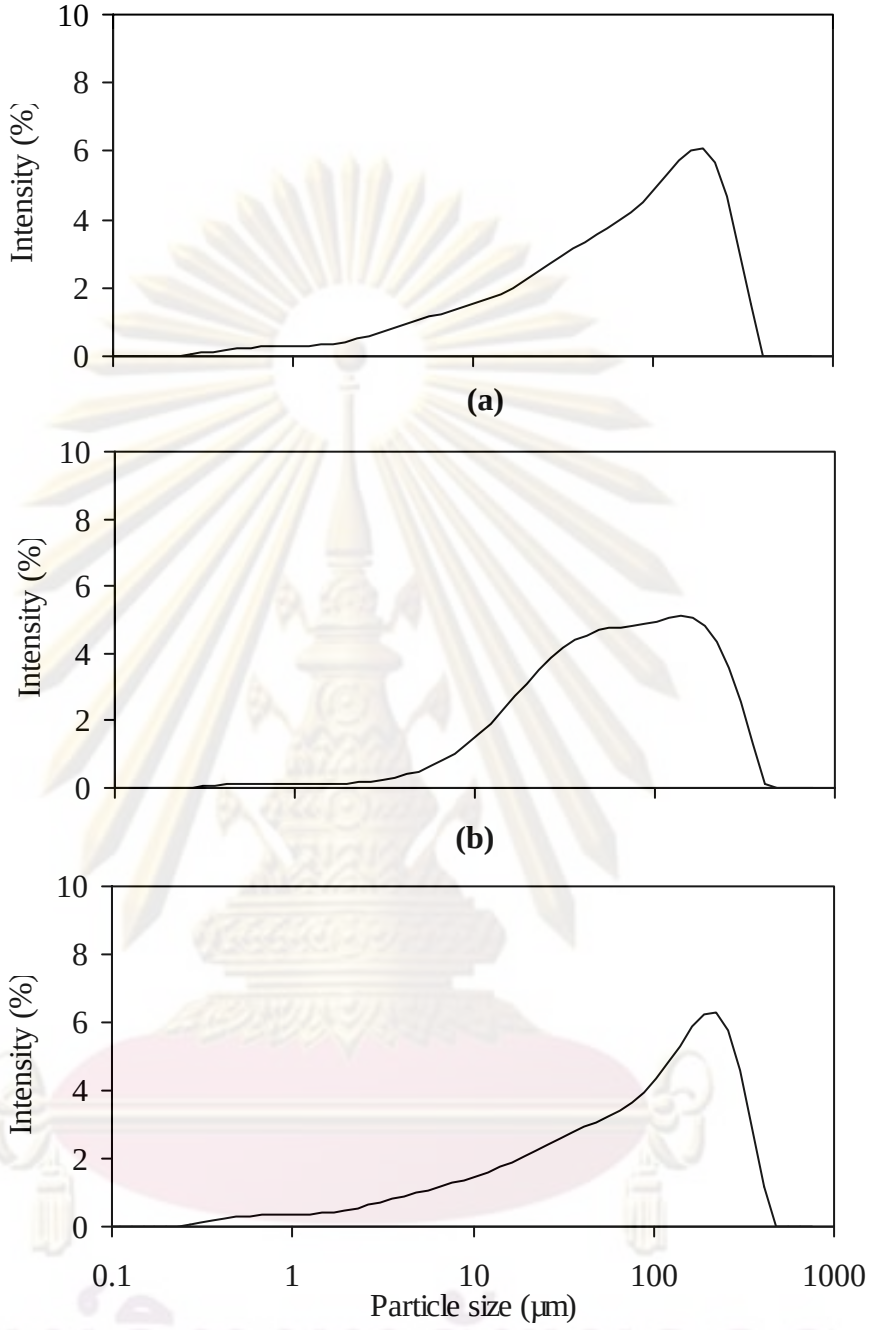

Figure 4.22 Particle size distribution of the synthetic TiO_2: (a) undoped TiO_2, (b) 0.5%W/TiO_2, and (c) hydrothermal-treated 0.5%W/TiO_2.

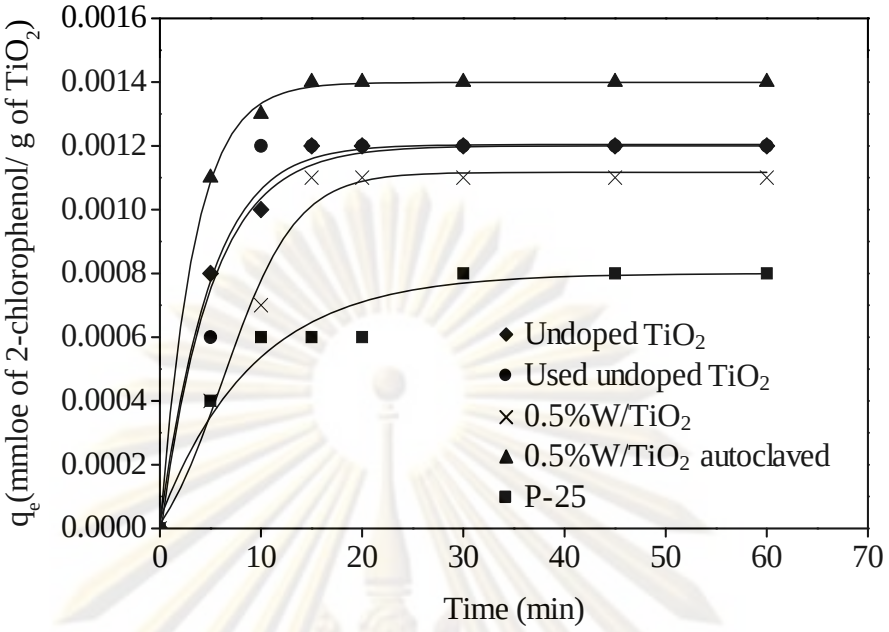

Figure 4.23 Adsorption of 2-chlorophenol on synthetic TiO_2 and Degussa P-25.

provided the lowest adsorption capacity for 2-chlorophenol whereas the 0.5%W/$TiO_2$with hydrothermal treatment had the highest capacity followed by undoped TiO_2 and 0.5%W/TiO_2, respectively. In addition, there was no significant difference in adsorption ability between fresh and used undoped TiO_2. This behavior might be explained by surface area and pore structure as shown previously in Table 4.6 and SEM morphology (Figure 4.21). Low surface area of 0.5%W/TiO_2 (201.5 m^2/g) resulted in a low active surface site to adsorb 2-chlorophenol as compared to 313.7 m^2/g for the 0.5%W/TiO_2 with autoclaving. Since the 0.5%W/TiO_2 with hydrothermal treatment had the highest photocatalytic activity (as will be discussed later), it's adsorption isotherm was investigated with the initial 2-chlorophenol ranging from 0.005 to 1.5 mM. The results were shown in Figure 4.24. It is obvious that the amount of 2-chlorophenol adsorbed on titanium surface increased with increasing initial concentration of 2-chlorophenol in water. Figure 4.25 shows the isotherm plot and indicates that 2-chlorophenol adsorbed on titanium surface increased with increasing of the equilibrium concentration of 2-chlorophenol in aqueous phase until reaching a plateau. Further analysis using the linearized forms of Langmuir and Freundlich adsorption isotherms following Equations 2.9 and 2.11 in Chapter 2 as shown in Figures 4.26 and 4.27, respectively.

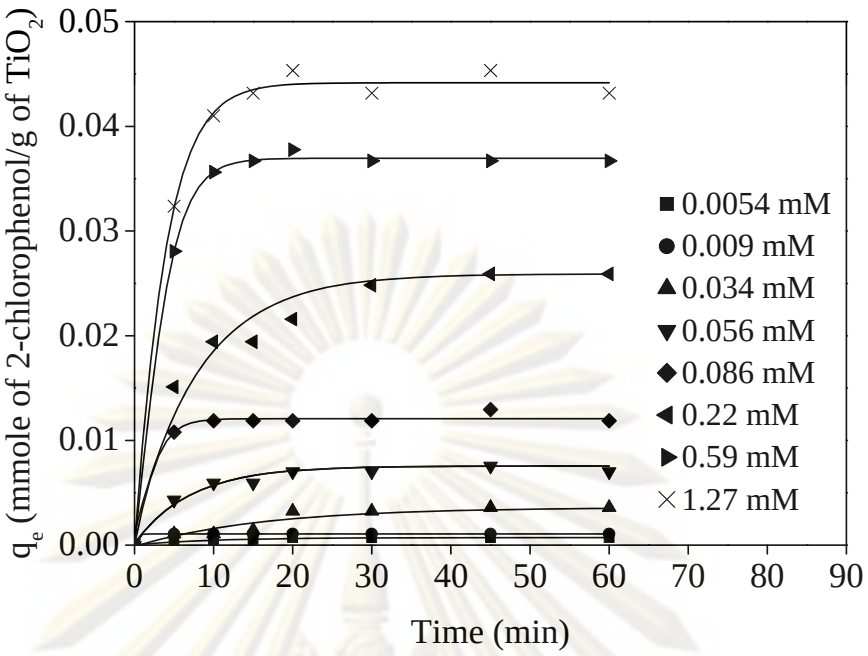

Figure 4.24 Adsorption of 2-chlorophenol onto the surface of 0.5%W/TiO_2 with hydrothermal treatment.

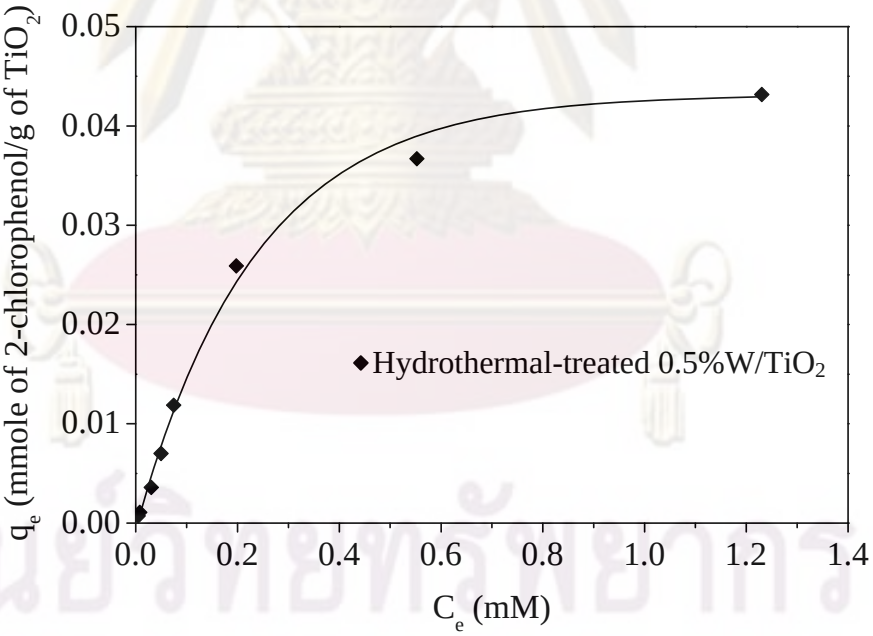

Figure 4.25 Isotherm plot of the 2-chlorophenol adsorption onto 0.5%W/TiO_2 with hydrothermal treatment.

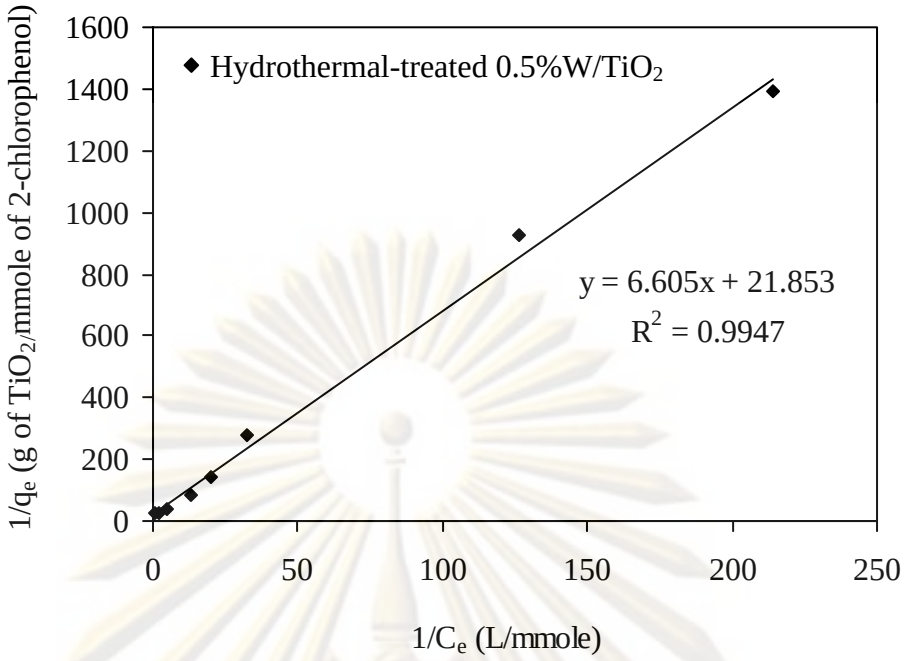

Figure 4.26 Langmuir adsorption isotherm plot for hydrothermal-treated 0.5%W/TiO_2.

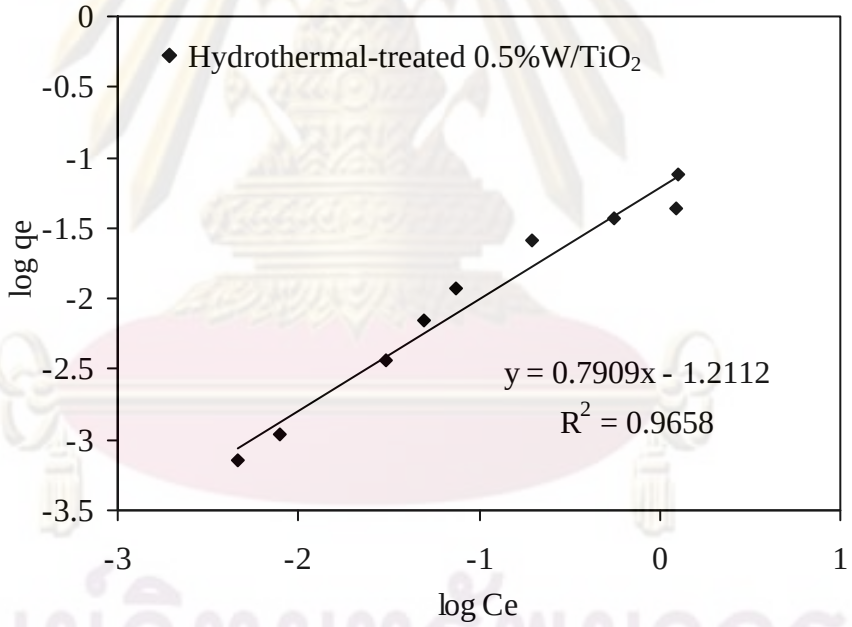

Figure 4.27 Freundlich adsorption isotherm plot for hydrothermal-treated 0.5%W/TiO_2.

The Langmuir parameters, q_{max} and b, and R^2 were 0.046 mmole of 2-chlorophenol/ g of TiO_2 and 3.309 L/mmole, and 0.9947, respectively, whereas the Freundlich parameters, K_F and n, and R^2 were 16.501 and 1.271, and 0.9563, respectively. From the R^2 values, it revealed that the Langmuir isotherm could describe the experimental data better than the Freundlich isotherm.

4.3 Kinetics Study

4.3.1 Direct Photolysis and Volatilization

In this part, Degussa P-25 was used to study the photodegradation of 2-chlorophenol at the initial concentration of 0.01 mM. The results in Figure 4.28 reveal that 2-chlorophenol had a low volatilization rate (1.5% in 6 hours); hence, its volatilization to the atmosphere could be neglected. In addition, direct photolysis with blue light irradiation was also minimal and could be neglected as well. Photodegradation of 2-chlorophenol in the presence of Degussa P-25 under UV and blue light irradiations were also investigated and shown in Figure 4.28. It was found that P-25 was very active under UV irradiation whereas much less active in blue light, i.e., 0.01 mM of 2-chlorophenol was completely removed in 90 minutes under UV irradiation whereas only 23.2% removal efficiency was obtained in 6 hours under blue light irradiation. It is important to mention that the initial concentration of 2-chlorophenol in the case of photocatalytic oxidation was the concentration after 30 minutes of dark adsorption to allow the 2-chlorophenol equilibrated between aqueous phase and solid surface.

.

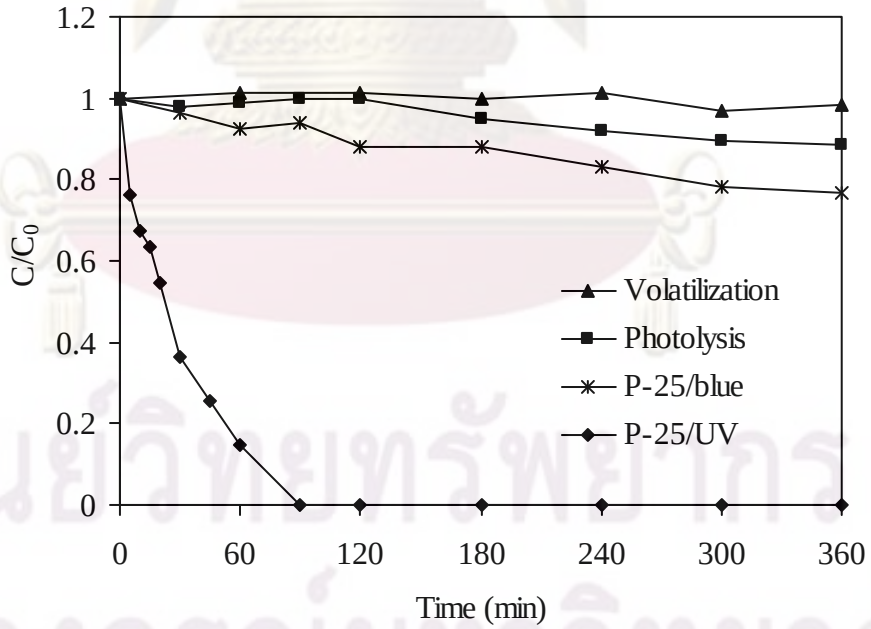

Figure 4.28 Volatilization, photolysis and photocatalytic oxidation of 2-chlorophenol irradiated by blue light or UV in present of Degussa P-25 (1 g/L TiO_2, 0.01 mM 2-chlorophenol, pH 5 and 25°C).

4.3.2 Effect of Titanium Dioxide Dose

To obtain the optimum TiO_2 dose on photodegradation under the study conditions, undoped TiO_2 was selected. The effect of TiO_2 dose on the photocatalysis of 2-chlorophenol is demonstrated in Figure 4.29. The results showed that the degradeation of 2-chlorophenol increased as a TiO_2 dose increased from 0.25 up to 1 g/L, i.e., from 43.5% at 0.25 g/L to 76.0 and 91.8% at 0.5 and 1.0 g/L, respectively. However, further increased to 1.5 g/L slightly decreased the efficiency of 2-chlorophenol degradation to 87.6%. This suggested that the degradation increased with increasing catalyst concentration, which is the characteristic of heterogeneous photocatalysis. An increase in catalyst amount actually increases the number of active sites on the photocatalyst surface thus causing an increase in the number of •OH radicals which can take part in actual degradation of 2-chlorophenol in solution. Beyond a certain limit of catalyst amount, the solution becomes turbid and thus blocks the light penetration into the mixture resulting in limiting the reaction and therefore percentage degradation starts decreasing (Macedo et al., 2007; Wang et al., 2008).

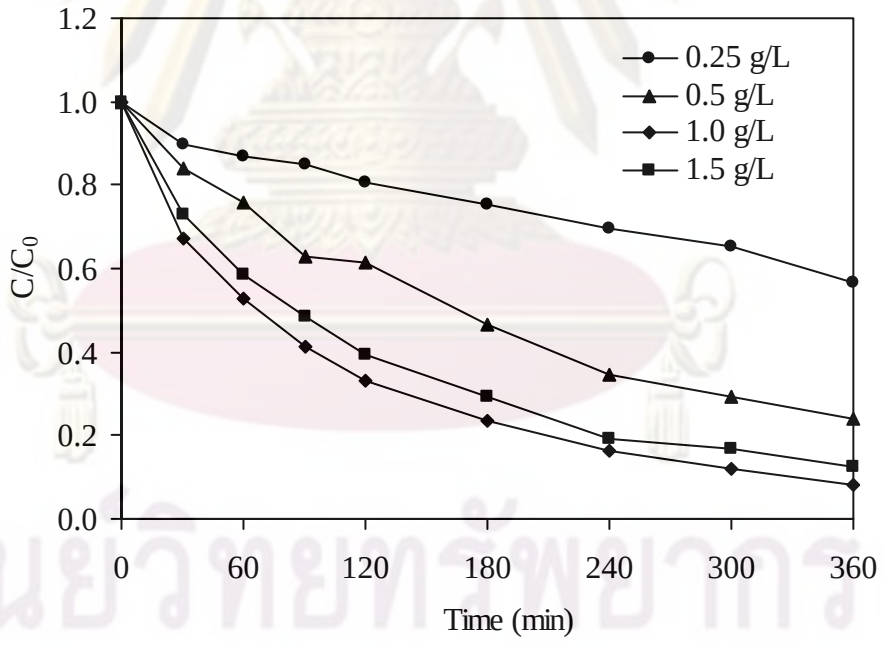

Figure 4.29 Effect of undoped TiO_2 dose on photocatalytic degradation of 2-chlorophenol irradiated by blue light (0.01 mM 2-chlorophenol, pH 5 and 25°C).

4.3.3 Effect of pH

In this part aimed to characterize the photocatalytic activity of synthetic TiO_2 under different pH under blue light irradiation. It was found that pH had a great effect on the photodegradation efficiency of 2-chlorophenol. Variation of solution pH changed the surface charge of TiO_2 particles and shifted the potentials of catalytic reactions. Point of zero charge (pzc) of the synthetic TiO_2 was shown in Figure 4.30 showing that the pzc of undoped TiO_2 was 4.5 and decreasing to 3.6 and 3.4 for 0.5%W/TiO_2 and hydrothermal-treated 0.5%W/TiO_2, respectively. Figure 4.31 summarizes the effect of pH on the photocatalytic oxidation of 2-chlorophenol in present of undoped TiO_2. It revealed that as the pH decreased sequentially from 8 to 7, 6 and 5, the oxidation of 2-chlorophenol became more efficient, i.e., the removal efficiencies increased from 49.4% to 59.0, 67.3 and 91.8%, respectively. This observation may be due to the electrical interaction between charged surface and ionic adsorbates. Since the pzc of the synthetic TiO_2 was 4.5, the TiO_2 surface was positively charged as the pH was less than 4.5 whereas became negatively charged when the pH was greater than 4.5. Additionally, since the pK_a of 2-chlorophenol is 8.53, 2-chlorophenols transform to 2-chlorophenol anion when the pH is greater than 8.53. Therefore, adsorption of 2-chlorophenol onto the TiO_2 surface is likely to be maximized at pH 4.5 where both species have no charge. As a result, the degradation became better as the solution pH decreasing toward the pzc of the TiO_2.

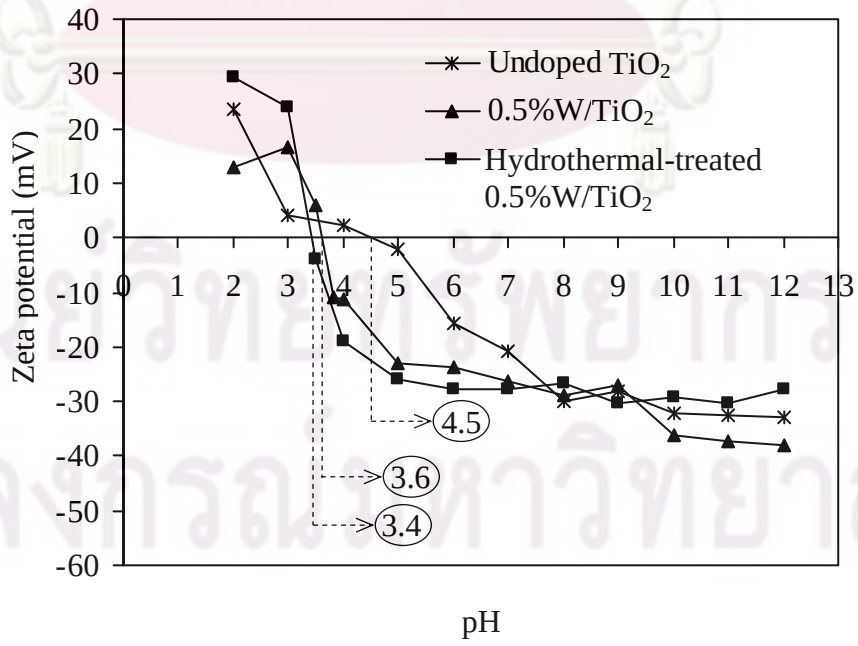

Figure 4.30 Point of zero charge of the synthetic TiO_2.

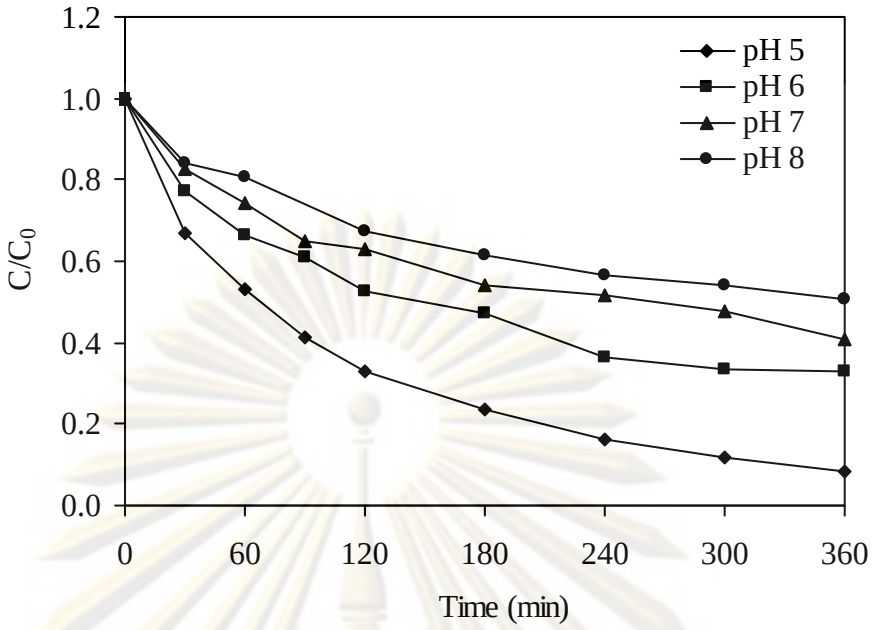

Figure 4.31 Effect of pH on photocatalytic degradation of 2-chlorophenol irradiated by blue light (1 g/L TiO_2, 2-chlorophenol 0.01 mM and 25°C).

This results agreed with Drzewicz et al (1999) who studied degradation of 2,4-dichlorophenol and found that the most efficient decomposition of 2,4-dichlorophenol occurred at pH 5 whereas the least efficient happened at the most alkaline solution which was pH 10.7.

4.3.4 Effect of Light Wavelength

It is interesting to determine the photo-respond of synthetic TiO_2 to the light at other wavelength rather than blue light because its absorption spectra also showed a superior trend to Degussa P-25. In this part, the blue, green and red lights were used to activate the synthetic TiO_2 to evaluate its photocatalytic activity and the results were summarized in Table 4.8 and Figure 4.32. For undoped TiO_2, it was found that the removal efficiencies in 6 hours of 0.01 mM of 2-chlorophenol were 91.8, 52.9,

Table 4.8 Effect of light color on the photocatalytic activity of the synthetic TiO_2.

TiO_2 sample	6-hour removal efficiency (%)		
	Blue light	Green light	Red light
Undoped TiO_2	91.8	52.9	20.9
0.5%W/TiO_2	90.5	33.8	17.4
Hydrothermal-treated 0.5%W/TiO_2	100.0	43.4	20.0

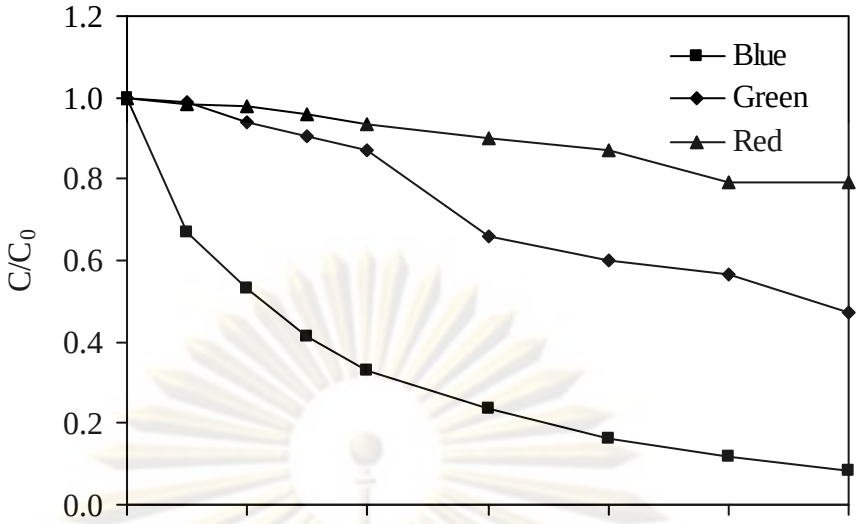

(a) Undoped TiO_2

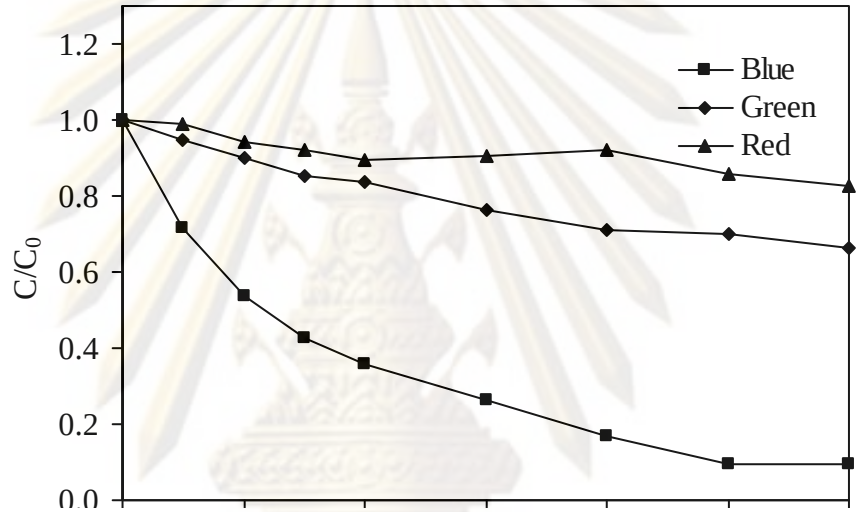

(b) 0.5%W/TiO_2

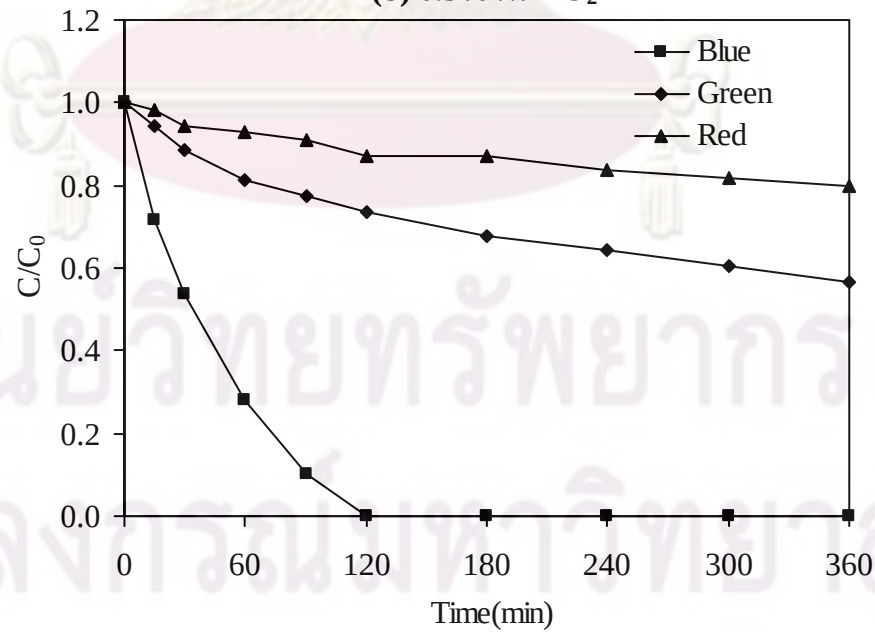

(c) 0.5%W/TiO_2 with hydrothermal treatment

Figure 4.32 Photocatalysis of 2-chlorophenol under different light irradiation (1 g/L undoped TiO_2, 2-chlorophenol 0.01 mM, pH 5 and 25°C).

and 20.9% under the blue, green and red lights, respectively. The 0.5%W/TiO_2 showed the lowest photocatalytic activity in every light wavelength. It is note that the nanocrystalline 0.5%W/TiO_2 had the highest degree of agglomeration as compared to other types. Interestingly, 0.5%W/TiO_2 with hydrothermal treatment could completely removed 2-chlorophenol in 120 minutes under blue light activation however the photocatalytic activity under green light activation was less than undoped TiO_2 while providing similar result in red light irradiation.

4.3.5 Kinetics Determination

TiO_2 photocatalytic reaction is known to be a heterogeneous reaction, and the oxidation reaction can be mainly achieved by •OH. Langmuir-Hinshelwood model as shown in equation 2.13 in Chapter 2 can be applied to determine the contribution of adsorption and oxidation in the reaction. In this experimental part, the photocatalytic activities of the undoped TiO_2 and 0.5%W/TiO_2 with hydrothermal treatment under blue light irradiation were investigated and compared. Figures 4.33 and 4.34 illustrate the degradation of 2-chlorophenol under different concentrations for undoped and 0.5%W/TiO_2 with hydrothermal treatment, respectively.

In order to determine the kinetics of 2-chlorophenol oxidation by photocatalytic oxidation by TiO_2, it is important to eliminate the competitive reaction from several intermediates being formed from 2-chlorophenol oxidation. This study decided to use the initial rate technique to determine the oxidation rate of 2-chlorophenol since there was no intermediate present at the initial stage. In practice, it is very difficult to obtain an accurate initial rate if the reaction does not follow zero-order reaction (as in this study) where the initial slope can be drawn easily and directly from the profile plot. This study tried to overcome this problem by fitting the experimental data with either pseudo-first or pseudo-second order to obtain the reaction rate constant and then calculated the initial rate. It was found that the degradation data at the initial stage of 120 minutes could be characterized better by pseudo-1st-order reaction as shown in Figures 4.33 and 4.34 (plots for pseudo-2nd-order reaction were not shown). The y-intercept and slope which represent "1/k_r" and "1/k_rK" were summarized in Table 4.9. Further analysis following the Langmuir-Hinshelwood model as shown in Figure 4.35 provided the k_r and K of 1.65×10^{-4} mM/min and 85.03 1/mM for undoped TiO_2 and 3.00×10^{-4} mM/min and

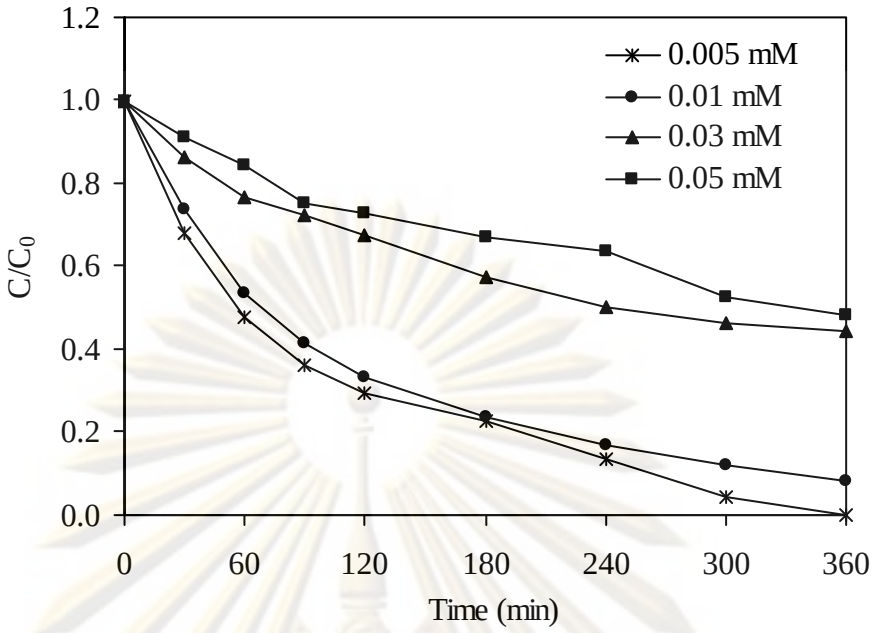

(a)

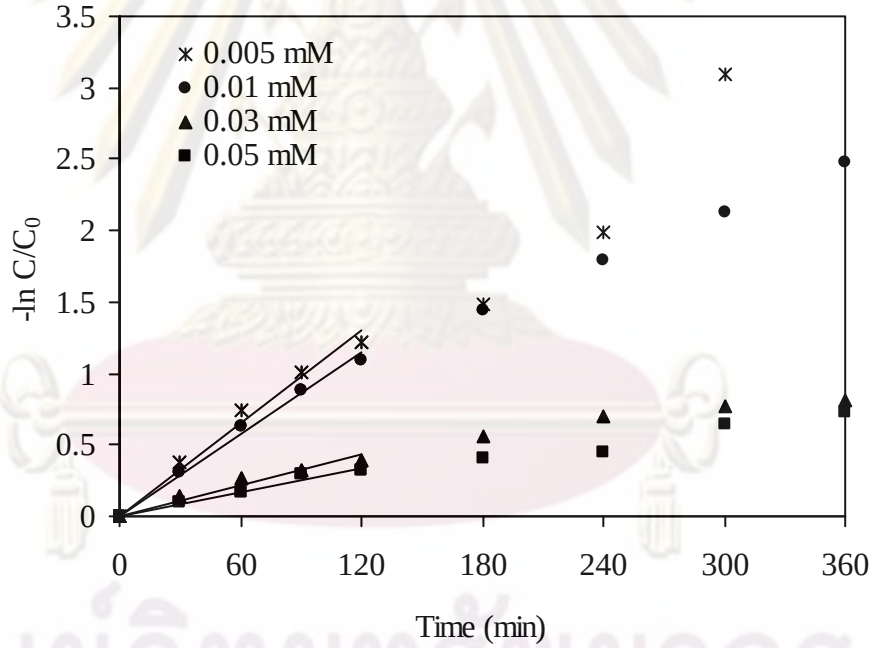

(b)

Figure 4.33 Photocatalysis of various initial concentration of 2-chlorophenol under blue light irradiation in present of undoped TiO_2: (a) degradation time-profile and (b) 1st-order plot (1 g/L TiO_2, pH 5 and 25°C).

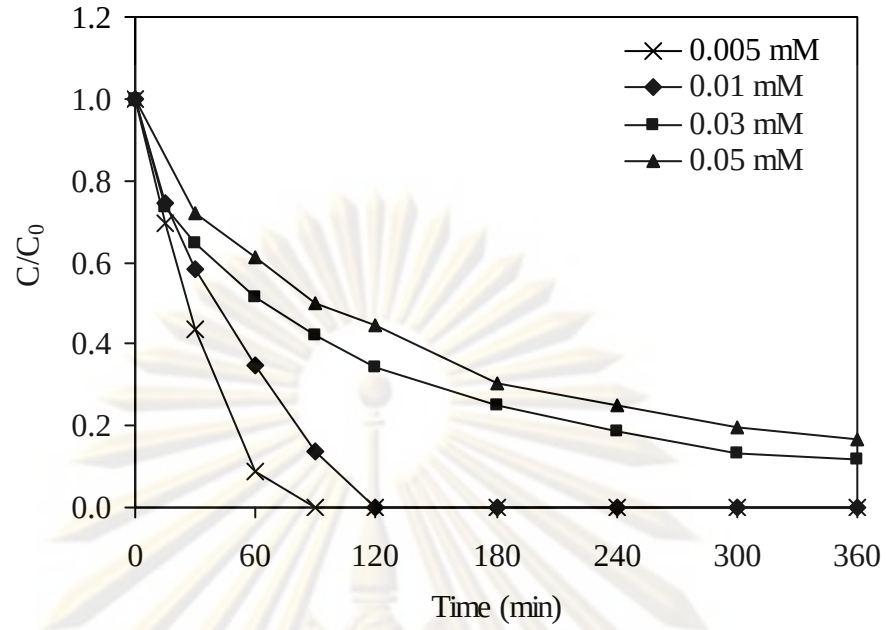

(a)

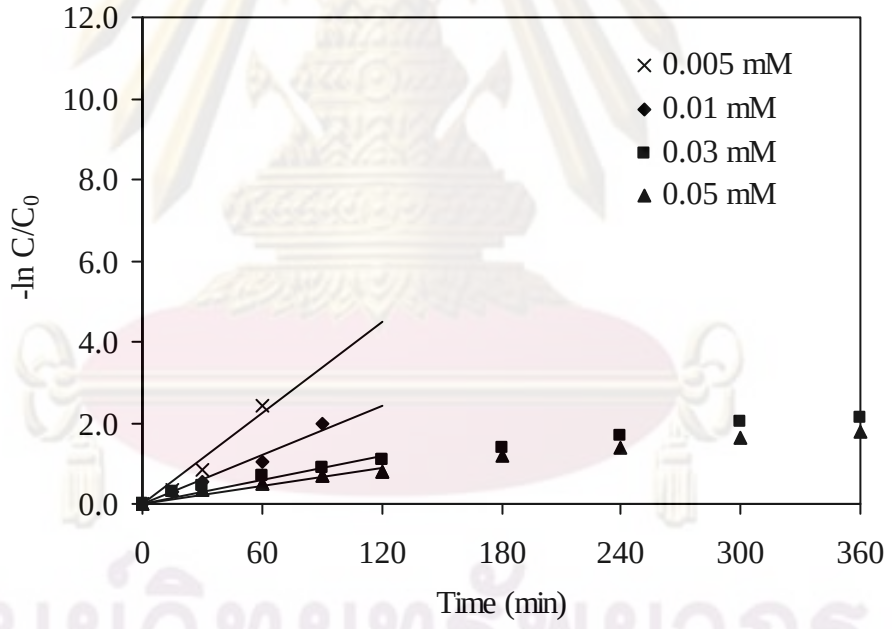

(b)

Figure 4.34 Photocatalysis of various initial concentration of 2-chlorophenol under blue light irradiation in present of 0.5%W/TiO_2 with hydrothermal treatment: (a) degradation time-profile and (b) 1st-order plot (1 g/L TiO_2, pH 5 and 25°C).

Table 4.9 Pseudo-first order rate constant for 2-chlorophenol photocatalytic oxidation under different initial concentrations.

Initial conc. (mM)	Undoped TiO_2			0.5%W/TiO_2 with hydrothermal-treated		
	$k_{observed}$ (min^{-1})	R^2	$Rate_{ini}$ (mM/min)	$k_{observed}$ (min^{-1})	R^2	$Rate_{ini}$ (mM/min)
0.005	0.0109	0.9798	4.93×10^{-5}	0.0375	0.9534	1.55×10^{-4}
0.01	0.0095	0.9930	8.12×10^{-5}	0.0204	0.9783	1.76×10^{-4}
0.03	0.0036	0.9439	9.97×10^{-5}	0.0097	0.9170	2.65×10^{-4}
0.05	0.0029	0.9765	1.37×10^{-4}	0.0074	0.9517	2.88×10^{-4}

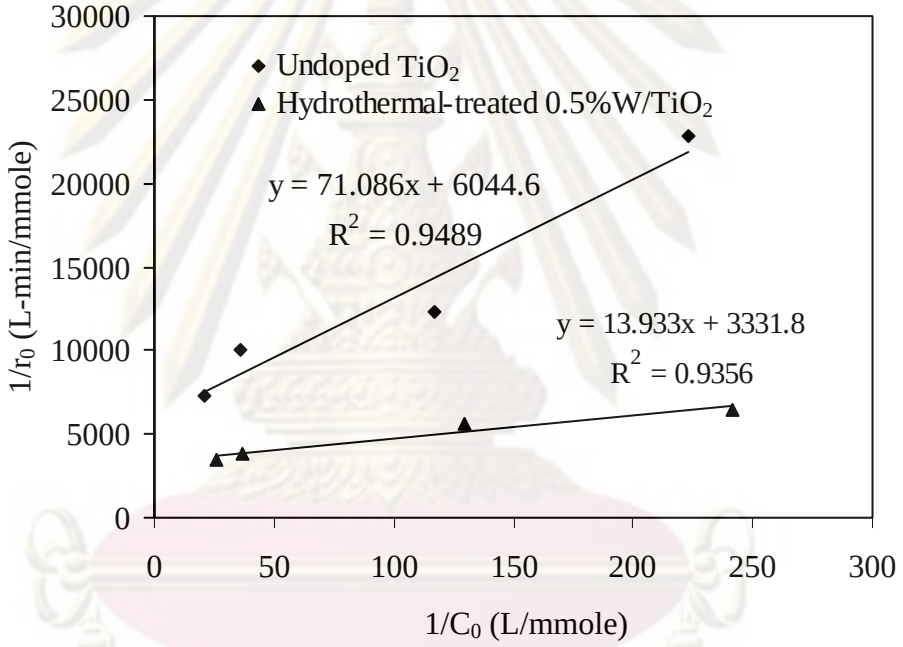

Figure 4.35 Langmuir-Hinshelwood plot of Table 4.9.

239.13 1/mM for hydrothermal-treated 0.5%W/TiO_2, respectively. It is obviously seen that the tungsten doping and hydrothermal treatment could significantly improve both photocatalytic activity and adsorption property of the TiO_2.

4.3.6 Reusability of Synthetic Titanium Dioxide

This part aimed to determine the reusability of the hydrothermal-treated 0.5%W/TiO_2 as the photocatalyst in the visible light region. After the catalysts were used to treat 2-chlorophenol for 6 hours, they were washed with the deionized water

several times and re-suspended in the 2-chlorophenol wastewater under blue-light irradiation. The experiment results revealed that the removal rate and efficiency of reused hydrothermal-treated 0.5%W/TiO_2 were almost the same as in the first cycle as shown in Figure 4.36. This implied that the photoactivity of hydrothermal-treated 0.5%W/TiO_2 could possible be sustained for a long period of time.

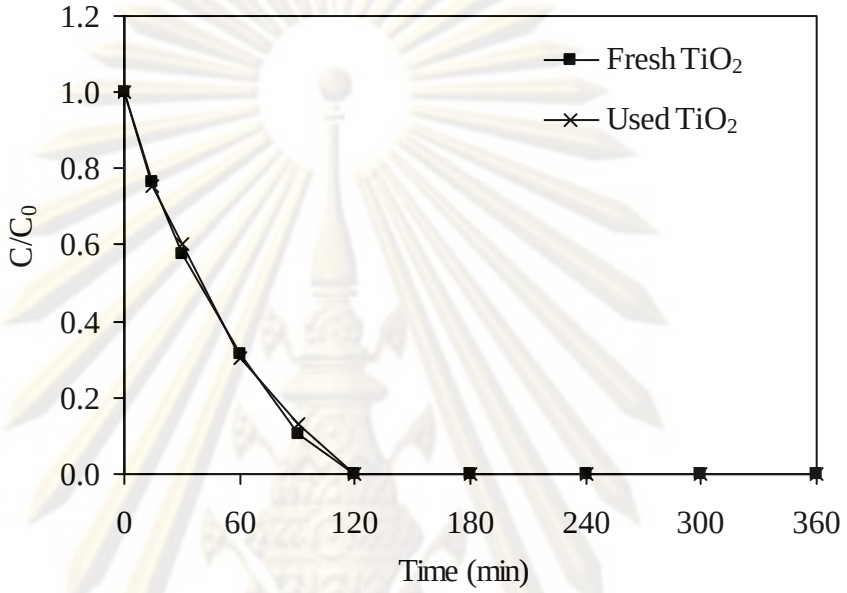

Figure 4.36 Photocatalysis of 2-chlorophenol under blue light irradiation in present of fresh and used hydrothermal-treated 0.5%W/TiO_2. (1g/L TiO_2, 2-chlorophenol 0.01 mM, at pH 5 and 25°C).

CHAPTER V

CONCLUSION

5.1 Conclusions

In this study, a new TiO_2 photocatalyst, which can be effectively activated by the blue light, has been synthesized and tested for its photocatalytic activity using 2-chlorophenol as the target compound. Important findings from this study can be summarized as follows:

- Optimum conditions for visible-light activated TiO_2 were:

a) Placing 70 mL anhydrous ethanol in a 250 mL flask and slowly adding 0.05 mole of tetra(n-butoxyl)titanium under the vigorous stirring condition to prepare a clear tetra(n-butoxyl)titanium ethanol solution (Solution I). The flask was then placed in a water bath controlled at 4°C.

b) At the same time, 20 mL of deionized water was mixed with 20 mL anhydrous ethanol to make an ethanol aqueous solution. Tungsten in the form of $Na_2WO_4.2H_2O$ at the W:Ti ratio of 0.5% on the mole basis was added and the mixture was continuously stirred until the doping chemical was completely dissolved (Solution II).

c) Solution II was dropwise added into Solution I under vigorous stirring condition and the precipitates would be formed. The mixture was control at 4°C through out the dropwise addition step and maintaining at 4°C for another 30 minutes during the following curing step.

d) Mixture was continuous stirred in the water bath for another 30 minutes without temperature control, i.e., allowed the temperature to gradually increase to room condition. The mixture was then added with 4 mL of concentrated HNO_3 and underwent hydrolytic condensation for 3 hours under vigorous stirred condition.

e) Hydrolyzed solution was then treated by hydrothermal process by autoclaving at 121°C and 103.4 kPa for 4 hours before placing into an oven to dry at 120°C for 2 hours to obtain solid titanium hydroxide.

f) Titanium hydroxide was pulverized into a powder form and calcined at 200°C with the ramp rate of 1°C/minute for 10 hours to become titanium dioxide doped with tungsten.

- Hydrothermal-treated 0.5%W/TiO_2 prepared under the optimum conditions had the photocatalytic activity under blue light irradiation almost comparable to those of the commercial Degussa P-25 under UV irradiation, i.e., 0.01 mM of 2-chlorophenol could be completely removed in 120 and 90 minutes by the hydrothermal-treated 0.5%W/TiO_2 under blue light irradiation and the Degussa P-25 under UV irradiation, respectively.

- Crystalline structure, a very important factor affecting the photoactivity of the TiO_2 under the UV irradiation, did not directly involve in the photocatalytic behavior of the TiO_2 under visible light irradiation.

- Photo-oxidation kinetics of 2-chlorophenol could be explained by the Langmuir-Hinshelwood model with k_r and K of 1.65×10^{-4} mM/min and 85.03 1/mM for undoped TiO_2 and 3.00×10^{-4} mM/min and 239.13 1/mM for hydrothermal-treated 0.5%W/TiO_2, respectively.

5.2 Recommendations for Future Study

- Investigate into more details of the chemical structure and phase composition of the hydrothermal-treated 0.5%W/TiO_2 to determine the causes which make this catalyst so active under the blue light irradiation.
- Study the photoactivity of the hydrothermal-treated 0.5%W/TiO_2 by using other target pollutants and compared the results to 2-chlorophenol case.
- Investigate the photoactivity of the hydrothermal-treated 0.5%W/TiO_2 under sunlight irradiation.
- Immobilize the hydrothermal-treated 0.5%W/TiO_2 on fixed surface for possible field applications both in air and water treatment.

REFERENCES

Albonetti, S., Blasioli, S., Bonelli, R., Mengou, J, E., Scirè, S., Trifirò, F. The role of acidity in the decomposition of 1, 2-dichlorobenzene over TiO_2-based V_2O_5/WO_3 catalysts. Applied Catalysis A: General 341 (2008): 18-25.

Ao, Y., Xu, J., Fu, D., Shen, X., Yuan, C. Low temperature preparation of anatase TiO_2-coated activated carbon. Colloids and Surfaces A: Physico chem. Eng. Aspects 312 (2008): 125-130.

APHA, Standard methods for the examination of water and wastewater, 18th edition, American Public Health Association, Washington D.C.: 1992.

Araña, J., Melián, E, P., López, V, M, R., Alonso, A, P., Rodríguez, J, M, D., Díaz, O, G., Peña, J, P. Photocatalytic degradation of phenol and phenolic compounds Part I. Adsorption and FTIR study. Journal of Hazardous Materials 146 (2007): 520-528.

Asahi, R, M., Morikawa, T., Ohwaki, T., Aoki, A., Yaga, Y. Visible-light photocatalysis in nitrogen-doped titanium oxides. Science 293 (2001): 269-271.

Barakat, M, A., Schaeffer, H., Hayes, G., Ismat, S, S. Photocatalytic degradation of 2-chlorophenol by nanoparticles Co-doped TiO_2. Applied Catalysis B: Environmental 57 (2005): 23-30.

Carotta, M, C., Gherardi, S., Malagù, C., Nagliati, M., Vendemiati, B., Martinelli, G., Sacerdoti, M., Lesci, I, G. Comparison between titania thick films obtained through sol-gel and hydrothermal synthetic processes. Thin Solid Films 515 (2007): 8339-8344.

Chao, H, E., Yun, Y, U., Xingfang, H, U., Larbot, A. Effect of silver doping on the phase transformation and grain growth of sol-gel titania powder. Journal of the European Ceramic Society 23 (2003): 1457-1464.

Chemat technology. sol-gel technology [online]. 1998. Available from: http://www.chemat.com/html/solgel.html [2010, July 20].

Chen, H, W., Ku, Y., Kuo, Y, L. Effect of Pt/TiO_2 characteristics on temporal behavior of o-cresol decomposition by visible light-induced photocatalysis. Water Research 41 (2007): 2069-2078.

Datye, A, K., Riegel, G., Bolton, J, R., Huang, M., Prairie, M, R. Microstructure characteristic of fumed titanium dioxide photocatalyst. Journal of Solid State Chemistry. 115 (1995): 236-239.

Drzewicz, P., Pahta, P., Gluszewski, W., Trojanowicz M. Effect of selected scavengers on radiolytic degradation of 2,4-dichlorophenol for environmental purposes. Journal of Radioanalytical and Nuclear Chemistry. 242 (1999): 601-609.

Durán, P., Capel, F., Tartaj, J., Gutierrez, D., Moure C. Heating-rate effect on the $BaTiO_3$ formation by thermal decomposition of metal citrate polymeric precursors. Solid State Ionics. 141-142 (2001): 529-539.

Fox, M, A., Dulay, M, T. Heterogeneous photocatalyst. Chemical reviews 93 (1993): 341-357.

Fujishima, A., Honda, K. Electrochemical photolysis of water at a semiconductor electrode. Nature 238 (1972): 37-38.

Fujishima, A., Rao, T, N., Tryk, D, A. Titanium dioxide photocatalysis. Journal of Photochemistry and Photobiology C: Photochemistry Reviews 1 (2000): 1-21.

Hathway, T., Rockafellow, E, M., Oh, Y, C., Jenks, W, S. Photocatalytic degradation using tungsten-modified TiO_2 and visible light: Kinetic and mechanistic effects using multiple catalyst doping strategies. Journal of Photochemistry and Photobiology A: Chemistry 207 (2009): 197-203.

Hoffmann, M, R., Martin, S, T., Choi, W., Bahnemann, D, W. Environmental applications of semiconductor photocatalyst. Chemical Reviews 95 (1995): 69-96.

Huang, L, H., Sun, C., Liu, Y, L. Pt/N-codoped TiO_2 nanotubes and its photocatalytic activity under visible light. Applied Surface Science 253 (2007): 7029-7035.

Ilisz, I., Dombi, A., Mogyorósi, K., Farkas, A., Dékány, I. Removal of 2-chlorophenol from water by adsorption combined with TiO_2 photocatalysis. Applied Catalysis B: Environmental 39 (2002): 247-256.

Ishibai, Y., Sato, J., Nishikawa, T., Miyagishi, S. Synthesis of visible-light active TiO_2 photocatalyst with Pt-modification: Role of TiO_2 substrate for high photocatalytic activity. Applied Catalysis B: Environmental 79 (2008): 117-121.

Kanna, M., Wongnawa, S. Mixed amorphous and nanocrystalline TiO_2 powders prepared by sol-gel method: Characterization and photocatalytic study. Materials Chemistry and Physics 110 (2008): 166-175.

Kato, K., Tsuzuki, A., Taoda, H., Torii, Y., Kato, T., Butsugan, Y. Crystal structures of TiO_2 thin coatings prepared from the alkoxide solution via the dip-coating technique affecting the photocatalytic decomposition of aqueous acetic acid. Journal of Materials Science 29 (1994): 5911-5915.

Khouw, C, B., Dartt, C, B., Labinger, J, A., Davis, M, E. Studies on the catalytic-oxidation of alkanes and alkenes by titanium silicates. Journal of Catalysis 149 (1994): 195-205.

Kontos, A, I., Arabatzis, I, M., Tsoukleris, D, S., Kontos, A, G., Bernard, M, C., Petrakis, D, E., Falaras, P. Efficient photocatalysts by hydrothermal treatment of TiO_2. Catalysis Today 101 (2005): 275-281.

Lei, W., Lu, W, Z., Zhu, J, H., Ye, X. Effects of heating rate on microstructures and microwave dielectric properties of $(1-x)ZnAl_2O_4$-$xTiO_2$ (x = 0.21) ceramics. Ceramics International 35 (2009): 277-280.

Lettmann, C., Hildenbrand, K., Kisch, H., Macyk, W., Maier, W, F. Visible light photodegradation of 4-chlorophenol with a coke-containing titanium dioxide photocatalyst. Applied Catalysis B: Environmental 32 (2001): 215-227.

Lhomme, L., Brosillon, S., Wolbert, D. Photocatalytic degradation of pesticides in pure water and a commercial agricultural solution on TiO_2 coated media. Chemosphere 70 (2008): 381-386.

Lin, C, F., Wu, C, H., Onn, Z, N. Degradation of 4-chlorophenol in TiO_2, WO_3, SnO_2, TiO_2/WO_3 and TiO_2/SnO_2 systems. Journal of Hazardous Materials 54 (2008): 1033-1039.

Lin, Y, M., Tseng, Y, H., Huang, J, H., Chao, C, C., Chan, C, C., Wang, I. Photocatalytic activity for degradation of nitrogen oxides over visible light responsive Titania-based photocatalysts. Environmental Science & Technology 40 (2006): 1616-1621.

Liu, J., Yang, R., Li, S. Preparation and characterization of the TiO_2-V_2O_5 photocatalyst with visible-light activity. Rare Metals 25 (2006): 636-642.

Lorret, O., Francová, D., Waldner, G., Stelzer, N. W-doped titania nanoparticles for UV and visible-light photocatalytic reactions. Applied Catalysis B: Environmental 91 (2009): 39-46.

Macedo, L, C., Zaia, D, A, M., Moore, G, J., Santana, H, D. Degradation of leather dye on TiO_2: A study of applied experimental parameters on photoelectrocatalysis. Journal of Photochemistry and Photobiology A: Chemistry 185 (2007): 86-93.

Mahata, S., Kundu, D. Hydrothermal synthesis of aqueous nano-TiO_2 sols. Materials Science-Poland 27 (2009): 463-470.

Meng, F., Fu, Z., Wang, W., Zhang, Q. Microstructural evolution of nanocrystalline Al_2O_3 sintered at a high heating rate. Ceramics International 36 (2010): 555-559.

Merabet, S., Bouzazab, A., Wolbert, D. Photocatalytic degradation of indole in a circulating upflow reactor by UV/TiO_2 process-Influence of some operating parameters. Journal of Hazardous Materials 166 (2009): 1244-1249.

Murakami, N., Chiyoya, T., Tsubota, T., Ohno, T. Switching redox site of photocatalytic reaction on titanium(IV) oxide particles modified with transition-metal ion controlled by irradiation wavelength. Applied Catalysis A: General 348 (2008): 148-152.

Navarrete, J., Lopez, T., Gomez, R., Figueras, F. Surface acidity of sulfated TiO_2-SiO_2 sol-gels. Langmuir 12 (1996): 4385-4390.

Rao, N, N., Dubey, A, K., Mohanty, S., Khare, P., Jain, R., Kaul, S, N. Photocatalytic degradation of 2-chlorophenol: a study of kinetics, intermediates and biodegradability. Journal of Hazardous Materials B 101 (2003): 301-314.

Saepurahman., Abdullah, M, A., Chong, F, K. Preparation and characterization of tungsten-loaded titanium dioxide photocatalyst for enhanced dye degradation. Journal of Hazardous Materials 176 (2010): 451-458.

Shchukin, D., Poznyak, S., Kulak, A., Pichat, P. TiO_2-In_2O_3 photocatalysts: preparation, characterizations and activity for 2-chlorophenol degradation in water. Journal of Photochemistry and Photobiology A: Chemistry 162 (2004): 423-430.

Smyth, J, R. TiO_2 group. Mineral Structure and Property Data [online]. 2009. Available from: http://ruby.colorado.edu/~smyth/min/tio2.html [2009, August 20].

Stakheev, A, Y., Shpiro, E, S., Apijok, J. XPS and XAES Study of TiO_2-SiO_2 mixed oxide system. Journal of Physical and Chemical 97 (1993): 5668-5672.

Son, H, S., Ko, G., Zoh, K, D. Kinetics and mechanism of photolysis and TiO_2 photocatalysis of triclosan. Journal of Hazardous Materials 166 (2009): 954-960.

Sonawane, R, S., Kale, B, B., Dongare, M, K. Preparation and photo-catalytic activity of Fe-TiO_2 thin films prepared by sol-gel dip coating. Materials Chemistry and Physics 85 (2004): 52-57.

Tian, H., Ma, J., Li, K., Li, J. Hydrothermal synthesis of S-doped TiO_2 nanoparticles and their photocatalytic ability for degradation of methyl orange. Ceramics International 35 (2009): 1289-1292.

Todorova, N., Giannakopoulou, T., Vaimakis, T., Trapalis, C. Structure tailoring of fluorine-doped TiO_2 nanostructured powders. Materials Science and Engineering B 152 (2008): 50-54.

Tsai, W, T., Lee, M, K., Su, T, Y., Chang, Y, M. Photodegradation of bisphenol-A in a batch TiO_2 suspension reactor. Journal of Hazardous Materials 168 (2009): 269-275.

Vargas, R., Núñez, O. The photocatalytic oxidation of dibenzothiophene (DBT). Journal of Molecular Catalysis A: Chemical 294 (2008): 74-81.

Wang, C, C., Lee, C, K., Lyu, M, D., Juang, L, C., Photocatalytic degradation of C.I. basic violet 10 using TiO_2 catalysts supported by Y zeolite: An investigation of the effects of operational parameters. Dyes and Pigments 76 (2008): 817-824.

Wang, Z., Chen, C., Wu, F., Zou, B., Zhao, M., Wang, J., Feng, C. Photodegradation of rhodamine B under visible light by bimetal codoped TiO_2 nanocrystals. Journal of Hazardous Materials 164 (2009): 615-620.

Wetchakun, N., Phanichphant, S. Effect of temperature on the degree of anatase-rutile transformation in titanium dioxide nanoparticles synthesized by the modified sol-gel method. Current Applied Physics 8 (2008): 343-346.

Xiao, G., Wang, X., Li, D., Fu, X. $InVO_4$-sensitized TiO_2 photocatalysts for efficient air purification with visible light. Journal of Photochemistry and Photobiology A: Chemistry 193 (2008): 213-221.

Xu, J., Ao, Y., Fu, D., Yuan, C. Low-temperature preparation of F-doped TiO_2 film and its photocatalytic activity under solar light. Applied Surface Science 254 (2008): 3033-3038.

Xu, J, C., Shi, Y, L., Huang, J, E., Wang, B., Li, H, L. Doping metal ions only onto the catalyst surface. Journal of Molecular Catalysis A: Chemical 219 (2004): 351-355.

Yang, J., Bai, H., Jiang Q., Lian, J. Visible-light photocatalysis in nitrogen-carbon-doped TiO_2 films obtained by heating TiO_2 gel-film in an ionized N_2 gas. Thin Solid Films 516 (2008): 1736-1742.

Yu, J., Yu, H., Cheng, B., Zhou, M., Zhao, X. Enhanced photocatalytic activity of TiO_2 powder (P25) by hydrothermal treatment. Journal of Molecular Catalysis A: Chemical 253 (2006): 112-118.

Yu, J., Zhou, M., Cheng, B., Yu, H., Zhao, X. Ultrasonic preparation of mesoporous titanium dioxide nanocrystalline photocatalysts and evaluation of photocatalytic activity. Journal of Molecular Catalysis A: Chemical 227 (2005):75-80.

Zhang, X., Zhang, F., Chan, K, Y. The synthesis of Pt-modified titanium dioxide thin films by microemulsion templating, their characterization and visible-light photocatalytic properties. Materials Chemistry and Physics 97 (2006): 384-389.

APPENDICES

APPENDIX A

Experimental Setup

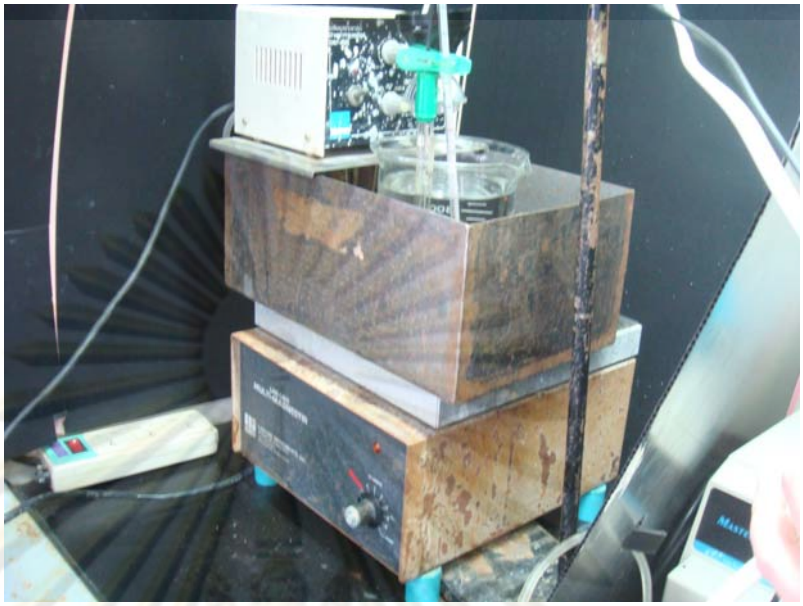

Figure A.1 Reactor setup (outside)

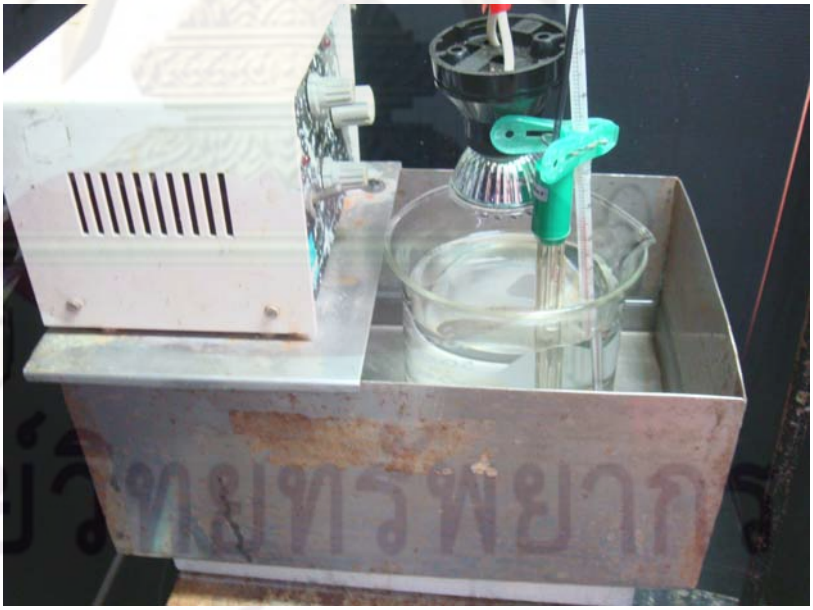

Figure A.2 Reactor setup (inside)

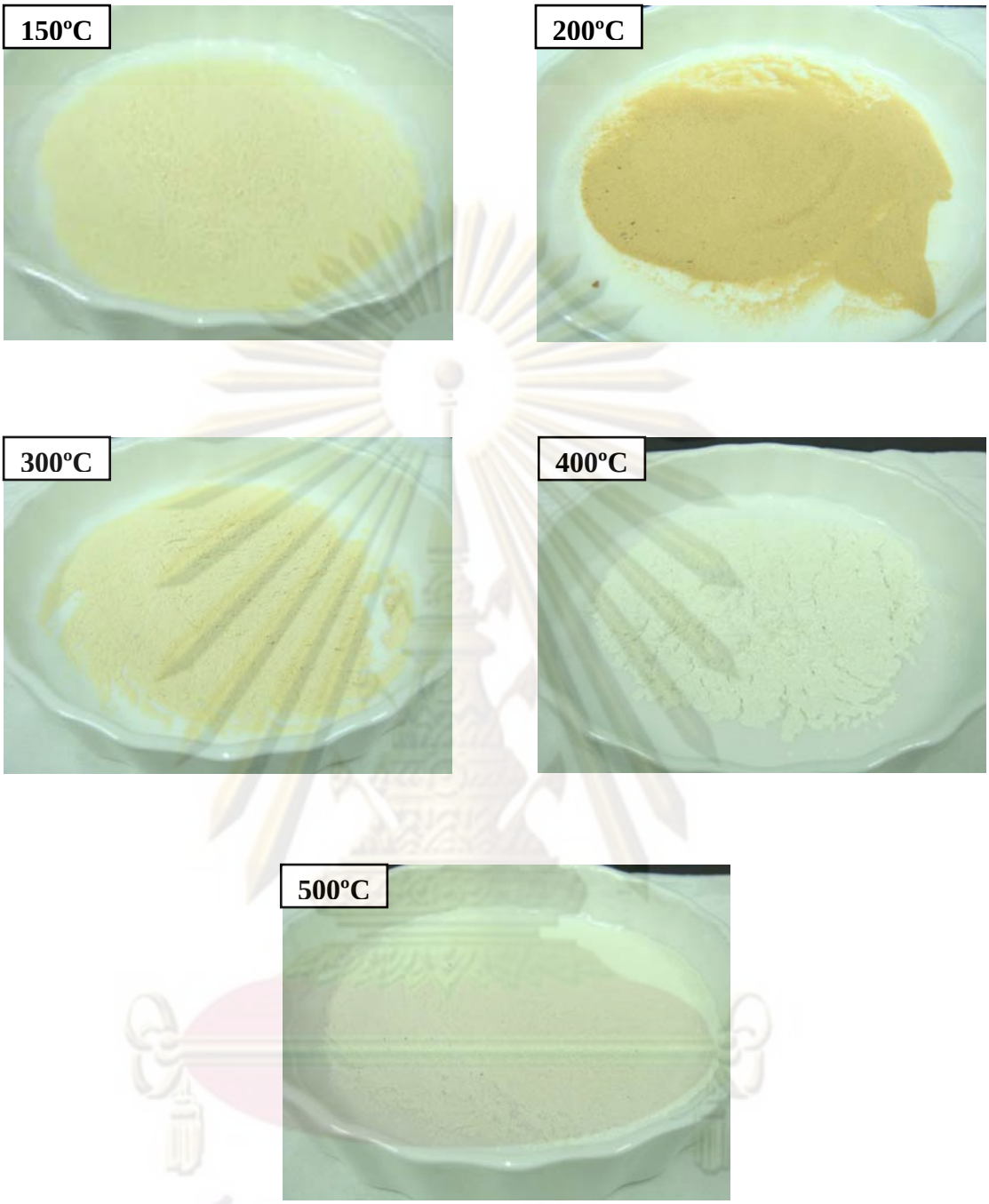

Figure A.3 The color of undoped TiO_2 calcined at different temperature

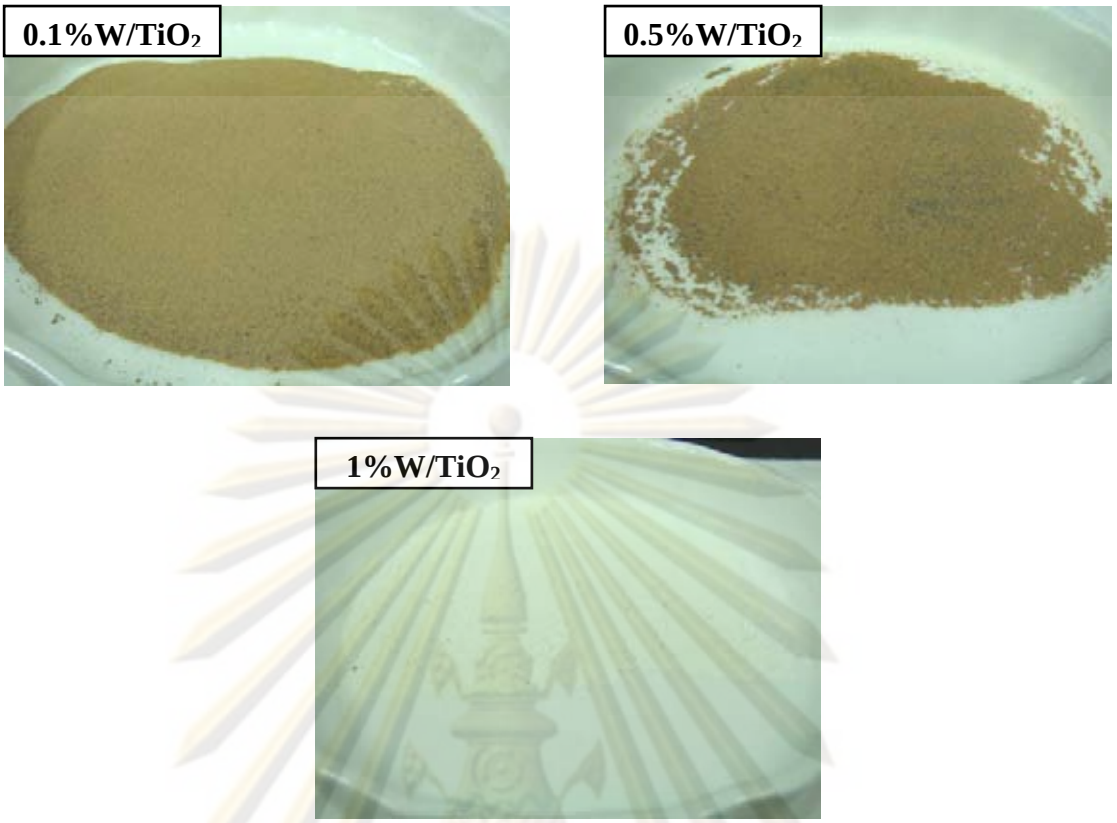

Figure A.4 The color of W/TiO_2 synthesized by sol-gel process

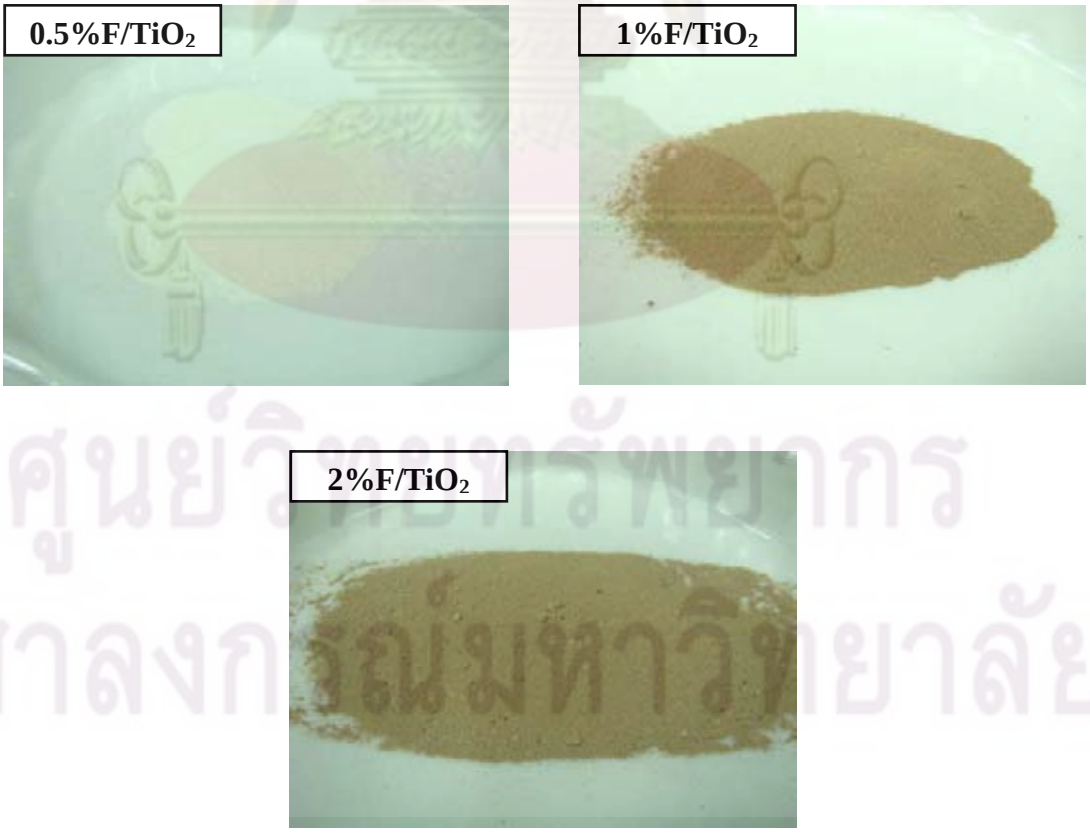

Figure A.5 The color of F/TiO_2 synthesized by sol-gel process

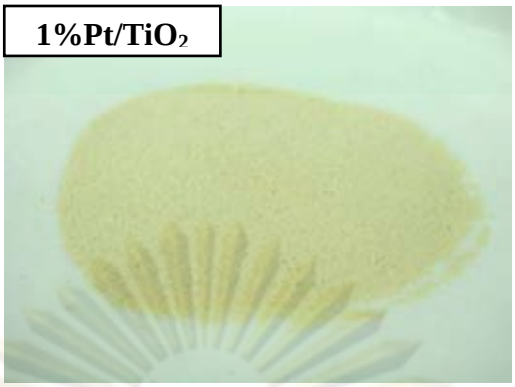

Figure A.6 The color of Pt/TiO_2 synthesized by sol-gel process

Figure A.7 The color of hydrothermal-treated $0.5\%W/TiO_2$ (autoclaved 4 hours)

APPENDIX B

Experimental Data

Table B.1 Photodegradation of 0.01 mM 2-chlorophenol by TiO_2 calcined at 200°C and 300°C under blue light irradiation.

Time (min)		Residual of 2-chlorophenol (mM)	
		200°C	300°C
Adsorption	0	0.009	0.012
	15	0.009	0.011
	30	0.009	0.011
Irradiation	0	0.009	0.011
	30	0.006	0.010
	60	0.005	0.010
	90	0.004	0.009
	120	0.003	0.009
	180	0.002	0.008
	240	0.001	0.007
	300	0.001	0.007
	360	0.001	0.006

Note: 1g/L TiO_2, pH 5, 25ºC, 2W (72 W/m^2) blue light, using NaOH and $HClO_4$ for pH adjustment

Table B.2 Photodegradation of 0.01 mM 2-chlorophenol of undoped TiO_2 at various ramp rate under blue light irradiation.

Time (min)		Residual of 2-chlorophenol (mM)		
		1ºC/min	4ºC/min	9ºC/min
Adsorption	0	0.012	0.014	0.014
	15	0.011	0.012	0.011
	30	0.011	0.012	0.012
Irradiation	0	0.011	0.012	0.012
	30	0.010	0.011	0.011
	60	0.010	0.011	0.011
	90	0.009	0.010	0.011
	120	0.009	0.010	0.010
	180	0.008	0.009	0.009
	240	0.007	0.009	0.009
	300	0.007	0.008	0.008
	360	0.006	0.008	0.008

Note: 1g/L TiO_2, pH 5, 25ºC, 2W (72 W/m^2) blue light, using NaOH and $HClO_4$ for pH adjustment

Table B.3 The photodegradation of 0.01 mM 2-chlorophenol at various temperature and duration time control in dissolution stage under blue light irradiation.

Time (min)		Residual of 2-chlorophenol (mM)			
		No control	**Mix step**	**4 ºC, 30 min**	**4 ºC, 1 hour**
Adsorption	0	0.009	0.011	0.009	0.009
	15	0.009	0.011	0.009	0.008
	30	0.008	0.010	0.009	0.009
Irradiation	0	0.008	0.010	0.009	0.009
	30	0.007	0.007	0.006	0.006
	60	0.006	0.006	0.005	0.005
	90	0.006	0.005	0.004	0.004
	120	0.005	0.004	0.003	0.003
	180	0.004	0.003	0.002	0.002
	240	0.003	0.003	0.001	0.001
	300	0.003	0.002	0.001	0.001
	360	0.002	0.001	0.001	0.001

Note: 1g/L TiO_2, pH 5, 25ºC, 2W (72 W/m^2) blue light, using NaOH and $HClO_4$ for pH adjustment

Table B.4 The photodegradation of 0.01 mM 2-chlorophenol at various doped TiO_2 compare to undoped TiO_2 and Degussa P-25 under blue light irradiation.

Time (min)		Residual of 2-chlorophenol (mM)				
		0.5%W/TiO_2	1%F/TiO_2	1%Pt/TiO_2	Undoped TiO_2	Degussa P-25
Adsorption	0	0.009	0.010	0.009	0.009	0.009
	15	0.008	0.010	0.009	0.009	0.008
	30	0.009	0.010	0.009	0.009	0.008
Irradiation	0	0.009	0.010	0.009	0.009	0.008
	30	0.006	0.008	0.008	0.006	0.008
	60	0.005	0.008	0.008	0.005	0.008
	90	0.004	0.007	0.007	0.004	0.008
	120	0.003	0.007	0.007	0.003	0.007
	180	0.002	0.006	0.006	0.002	0.007
	240	0.001	0.005	0.006	0.001	0.007
	300	0.001	0.005	0.006	0.001	0.007
	360	0.001	0.005	0.006	0.001	0.006

Note: 1g/L TiO_2, pH 5, 25ºC, 2W (72 W/m^2) blue light, using NaOH and $HClO_4$ for pH adjustment

Table B.5 The photodegradation of 0.05 mM 2-chlorophenol of 0.5%W/TiO_2 at acid catalyst under blue light irradiation.

Time (min)		Residual of 2-chlorophenol (mM)		
		H_2SO_4	H_3PO_4	HNO_3
Adsorption	0	0.039	0.045	0.059
	15	0.037	0.042	0.057
	30	0.037	0.042	0.057
Irradiation	0	0.037	0.042	0.004
	30	0.036	0.042	0.003
	60	0.035	0.041	0.003
	90	0.034	0.037	0.003
	120	0.034	0.038	0.003
	180	0.033	0.037	0.003
	240	0.032	0.036	0.003
	300	0.032	0.036	0.003
	360	0.030	0.035	0.003

Note: 1g/L TiO_2, pH 5, 25ºC, 2W (72 W/m^2) blue light, using NaOH and $HClO_4$ for pH adjustment

Table B.6 Effect of autoclave time on the photodegradation of 0.01 mM 2-chlorophenol under blue light irradiation.

Time (min)		Residual of 2-chlorophenol (mM)			
		2 hours	3 hours	4 hours	6 hours
Adsorption	0	0.010	0.010	0.010	0.012
	15	0.008	0.010	0.006	0.008
	30	0.007	0.009	0.006	0.008
Irradiation	0	0.007	0.009	0.006	0.008
	30	0.005	0.004	0.004	0.005
	60	0.003	0.002	0.002	0.003
	90	0.002	0.001	0.001	0.002
	120	0.001	0.000	0.000	0.002
	180	0.000	0.000	0.000	0.000
	240	0.000	0.000	0.000	0.000
	300	0.000	0.000	0.000	0.000
	360	0.000	0.000	0.000	0.000

Note: 1g/L TiO_2, pH 5, 25ºC, 2W (72 W/m^2) blue light, using NaOH and $HClO_4$ for pH adjustment

Table B.7 the photodegradation of 0.01 mM 2-chlorophenol on undoped TiO_2 and 0.5%W/TiO_2 with 4hours hydrothermal treatment under blue light irradiation.

Time (min)		Residual of 2-chlorophenol (mM)	
		hydrothermal-treated Undoped TiO_2	hydrothermal-treated 0.5%W/TiO_2
Adsorption	0	0.012	0.010
	15	0.011	0.007
	30	0.011	0.007
Irradiation	0	0.011	0.007
	15	0.009	0.005
	30	0.007	0.004
	60	0.005	0.002
	90	0.004	0.001
	120	0.003	0.000
	180	0.002	0.000
	240	0.001	0.000
	300	0.000	0.000
	360	0.000	0.000

Note: 1g/L TiO_2, pH 5, 25ºC, 2W (72 W/m^2) blue light, using NaOH and $HClO_4$ for pH adjustment

Table B.8 Adsorption of 2-chlorophenol on synthetic TiO_2 and Degussa P-25.

Adsorption Time (min)	q_e (mmole of 2-chlorophenol/g of TiO_2)				
	Undoped TiO_2	Used undoped TiO_2	0.5%W/TiO_2	0.5%W/TiO_2 hydrothermal-treated	Degussa P-25
0	0.0000	0.0000	0.0000	0.0000	0.0000
5	0.0004	0.0006	0.0008	0.0004	0.0011
10	0.0006	0.0012	0.0010	0.0007	0.0013
15	0.0006	0.0012	0.0012	0.0011	0.0014
20	0.0006	0.0012	0.0012	0.0011	0.0014
30	0.0008	0.0012	0.0012	0.0011	0.0014
45	0.0008	0.0012	0.0012	0.0011	0.0014
60	0.0008	0.0012	0.0012	0.0011	0.0014

Note: 1g/L TiO_2, pH 5, 25°C, using NaOH and $HClO_4$ for pH adjustment

Table B.9 Adsorption of 2-chlorophenol on hydrothermal-treated 0.5%W/TiO_2.

Adsorption Time (min)	q_e (mmole of 2-chlorophenol/g of TiO_2)				
	0.0054 mM	**0.009 mM**	**0.034 mM**	**0.056 mM**	**0.86 mM**
0	0	0	0	0	0
5	0.0004	0.0004	0.0011	0.0043	0.0108
10	0.0004	0.0011	0.0011	0.0059	0.0119
15	0.0005	0.0011	0.0014	0.0059	0.0119
20	0.0007	0.0011	0.0032	0.0070	0.0119
30	0.0007	0.0011	0.0032	0.0070	0.0119
45	0.0007	0.0011	0.0036	0.0075	0.0130
60	0.0007	0.0011	0.0036	0.0070	0.0119
Adsorption Time (min)	**q_e (mmole of 2-chlorophenol/g of TiO_2)**				
	0.22 mM	**0.59 mM**	**1.27 mM**		
0	0	0	0		
5	0.0151	0.0281	0.0324		
10	0.0194	0.0356	0.0410		
15	0.0194	0.0367	0.0432		
20	0.0216	0.0378	0.0453		
30	0.0248	0.0367	0.0432		
45	0.0259	0.0367	0.0453		
60	0.0259	0.0367	0.0432		

Note: 1g/L TiO_2, pH 5, 25ºC, using NaOH and $HClO_4$ for pH adjustment

Table B.10 Volitilization and photolysis photodegradation of 2-chlorophenol.

Time (min)	Residual of 2-chlorophenol (mM)	
	Voltilization	Photolysis
0	0.0067	0.0099
30	-	0.0097
60	0.0068	0.0098
90	-	0.0099
120	0.0068	0.0099
180	0.0067	0.0094
240	0.0068	0.0091
300	0.0065	0.0089
360	0.0066	0.0088

Note: 1g/L TiO_2, pH 5, 25ºC, 2W (72 W/m^2) blue light, using NaOH and $HClO_4$ for pH adjustment

Table B.11 Photodegradation of 2-chlorophenol irradiated by UV in present of Degussa P-25.

Time (min)		Residual of 2-chlorophenol (mM)
		Degussa P-25/UV
Adsorption	0	0.011
	30	0.010
	60	0.010
Irradiation	0	0.010
	5	0.008
	10	0.007
	15	0.006
	20	0.005
	30	0.004
	45	0.003
	60	0.001
	90	0.000
	120	0.000
	180	0.000
	240	0.000
	300	0.000
	360	0.000

Note: 1g/L TiO_2, pH 5, 25ºC, 4W UV light, using NaOH and $HClO_4$ for pH adjustment

Table B.12 Effect of undoped TiO_2 dose on photocatalytic degradation of 2-chlorophenol irradiated by blue light.

Time (min)		Residual of 2-chlorophenol (mM)			
		0.25 g/L	0.5 g/L	1.0 g/L	1.5 g/L
Adsorption	0	0.014	0.008	0.009	0.009
	15	0.014	0.008	0.009	0.009
	30	0.014	0.008	0.009	0.009
Irradiation	0	0.014	0.008	0.009	0.009
	30	0.013	0.006	0.006	0.007
	60	0.012	0.006	0.005	0.005
	90	0.012	0.005	0.004	0.004
	120	0.011	0.005	0.003	0.004
	180	0.011	0.004	0.002	0.003
	240	0.010	0.003	0.001	0.002
	300	0.009	0.002	0.001	0.002
	360	0.008	0.002	0.001	0.001

Note: 1g/L TiO_2, pH 5, 25ºC, 2W (72 W/m^2) blue light, using NaOH and $HClO_4$ for pH adjustment

Table B.13 Effect of pH on photocatalytic degradation of 2-chlorophenol irradiated by blue light.

Time (min)		Residual of 2-chlorophenol (mM)			
		pH 5	pH 6	pH 7	pH 8
Adsorption	0	0.009	0.012	0.012	0.009
	15	0.009	0.011	0.011	0.009
	30	0.009	0.011	0.011	0.008
Irradiation	0	0.009	0.011	0.011	0.008
	30	0.006	0.009	0.009	0.007
	60	0.005	0.007	0.008	0.007
	90	0.004	0.007	0.007	0.006
	120	0.003	0.006	0.007	0.005
	180	0.002	0.005	0.006	0.005
	240	0.001	0.004	0.005	0.005
	300	0.001	0.004	0.005	0.004
	360	0.001	0.004	0.004	0.004

Note: 1g/L TiO_2, 25ºC, 2W (72 W/m^2) blue light, using NaOH and $HClO_4$ for pH adjustment

Table B.14 Photocatalysis of 0.01 mM 2-chlorophenol under different light irradiation in present of undoped TiO_2.

Time (min)		Residual of 2-chlorophenol (mM)		
		Blue	**Green**	**Red**
Adsorption	0	0.009	0.009	0.015
	15	0.009	0.009	0.014
	30	0.009	0.009	0.014
Irradiation	0	0.009	0.009	0.014
	30	0.006	0.009	0.014
	60	0.005	0.008	0.014
	90	0.004	0.008	0.014
	120	0.003	0.008	0.013
	180	0.002	0.006	0.013
	240	0.001	0.005	0.012
	300	0.001	0.005	0.011
	360	0.001	0.004	0.011

Note: 1g/L TiO_2, pH 5, 25ºC, 2W (72 W/m^2 for blue light, 22 W/m^2 for green light and 34 W/m^2 for red light) using NaOH and $HClO_4$ for pH adjustment

Table B.15 Photocatalysis of 0.01 mM 2-chlorophenol under different light irradiation in present of 0.5%W/TiO_2.

Time (min)		Residual of 2-chlorophenol (mM)		
		Blue	Green	Red
Adsorption	0	0.009	0.007	0.009
	15	0.008	0.008	0.009
	30	0.009	0.008	0.009
Irradiation	0	0.009	0.008	0.009
	30	0.006	0.008	0.009
	60	0.005	0.007	0.008
	90	0.004	0.007	0.008
	120	0.003	0.007	0.008
	180	0.002	0.006	0.008
	240	0.001	0.006	0.008
	300	0.001	0.006	0.008
	360	0.001	0.005	0.007

Note: 1g/L TiO_2, pH 5, 25ºC, 2W (72 W/m^2 for blue light, 22 W/m^2 for green light and 34 W/m^2 for red light) using NaOH and $HClO_4$ for pH adjustment

Table B.16 Photocatalysis of 0.01 mM 2-chlorophenol under different light irradiation in present of hydrothermal-treated 0.5%W/TiO_2.

Time (min)		Residual of 2-chlorophenol (mM)		
		Blue	**Green**	**Red**
Adsorption	0	0.010	0.010	0.011
	15	0.007	0.010	0.010
	30	0.007	0.010	0.010
Irradiation	0	0.007	0.010	0.010
	15	0.005	0.009	0.010
	30	0.004	0.008	0.009
	60	0.002	0.008	0.009
	90	0.001	0.007	0.009
	120	0.000	0.007	0.009
	180	0.000	0.006	0.009
	240	0.000	0.006	0.008
	300	0.000	0.006	0.008
	360	0.000	0.005	0.008

Note: 1g/L TiO_2, pH 5, 25ºC, 2W (72 W/m^2 for blue light, 22 W/m^2 for green light and 34 W/m^2 for red light) using NaOH and $HClO_4$ for pH adjustment

Table B.17 Photocatalysis of various initial concentration of 2-chlorophenol under blue light irradiation in present of undoped TiO_2.

Time (min)		Residual of 2-chlorophenol (mM)			
		0.005 mM	**0.01 mM**	**0.03 mM**	**0.05 mM**
Adsorption	0	0.005	0.009	0.031	0.051
	15	0.004	0.009	0.028	0.048
	30	0.004	0.009	0.028	0.047
Irradiation	0	0.004	0.009	0.028	0.047
	30	0.003	0.006	0.024	0.043
	60	0.002	0.005	0.021	0.040
	90	0.002	0.004	0.020	0.035
	120	0.001	0.003	0.019	0.034
	180	0.001	0.002	0.016	0.032
	240	0.001	0.001	0.014	0.030
	300	0.000	0.001	0.013	0.025
	360	0.000	0.001	0.012	0.023

Note: 1g/L TiO_2, pH 5, 25ºC, 2W (72 W/m^2) blue light, using NaOH and $HClO_4$ for pH adjustment

Table B.18 Photocatalysis of various initial concentration of 2-chlorophenol under blue light irradiation in present of hydrothermal-treated 0.5%W/TiO_2.

Time (min)		Residual of 2-chlorophenol (mM)			
		0.005 mM	**0.01 mM**	**0.03 mM**	**0.05 mM**
Adsorption	0	0.005	0.010	0.030	0.050
	15	0.004	0.008	0.027	0.043
	30	0.004	0.008	0.027	0.039
Irradiation	0	0.004	0.008	0.027	0.039
	15	0.003	0.006	0.020	-
	30	0.002	0.004	0.018	0.028
	60	0.000	0.003	0.014	0.024
	90	0.000	0.001	0.012	0.019
	120	0.000	0.000	0.009	0.017
	180	0.000	0.000	0.007	0.012
	240	0.000	0.000	0.005	0.010
	300	0.000	0.000	0.004	0.008
	360	0.000	0.000	0.003	0.006

Note: 1g/L TiO_2, pH 5, 25ºC, 2W (72 W/m^2) blue light, using NaOH and $HClO_4$ for pH adjustment

Table B.19 the photodegradation of 0.01 mM 2-chlorophenol on fresh and used hydrothermal-treated 0.5%W/TiO_2 under blue light irradiation

Time (min)		Residual of 2-chlorophenol (mM)	
		Fresh	Used
Adsorption	0	0.010	0.010
	15	0.007	0.010
	30	0.007	0.010
Irradiation	0	0.007	0.010
	15	0.005	0.007
	30	0.004	0.006
	60	0.002	0.003
	90	0.001	0.001
	120	0.000	0.000
	180	0.000	0.000
	240	0.000	0.000
	300	0.000	0.000
	360	0.000	0.000

Note: 1g/L TiO_2, pH 5, 25ºC, 2W (72 W/m^2) blue light, using NaOH and $HClO_4$ for pH adjustment

Table B.20 Photocatalysis of 0.01 mM 2-chlorophenol on synthetic TiO_2 under UV irradiation.

Time (min)		Residual of 2-chlorophenol (mM)			
		Undoped TiO_2	Hydrothermal-treated undoped	0.5%W/TiO_2	Hydrothermal-treated 0.5%W/TiO_2
Adsorption	0	0.009	0.010	0.009	0.009
	15	0.008	0.010	0.007	0.005
	30	0.007	0.009	0.008	0.005
Irradiation	0	0.007	0.009	0.008	0.005
	15	-	0.009	-	-
	30	0.005	0.008	0.005	0.005
	60	0.004	0.007	0.005	0.004
	90	0.003	0.006	0.004	-
	120	0.002	0.005	0.002	0.002
	180	0.002	0.004	0.001	0.002
	240	0.001	0.003	0.000	0.001
	300	0.000	0.002	0.000	0.001
	360	0.000	0.002	0.000	0.001

Note: 1g/L TiO_2, pH 5, 25ºC, 2W (72 W/m^2) blue light, using NaOH and $HClO_4$ for pH adjustment

Table B.21 The photodegradation of 0.01 mM 2-chlorophenol on undoped under blue light irradiation.

Time (min)		Residual of 2-chlorophenol (mM)	
		Run 1	Run 2
Adsorption	0	0.009	0.009
	15	0.009	0.008
	30	0.009	0.008
Irradiation	0	0.009	0.008
	30	0.006	0.006
	60	0.005	0.005
	90	0.004	0.004
	120	0.003	0.003
	180	0.002	0.003
	240	0.001	0.002
	300	0.001	0.001
	360	0.001	0.001

Note: TiO_2 dose 1g/L, pH 5, temperature 25ºC, blue light 2W (72 W/m^2), using NaOH and $HClO_4$ for adjust pH

Table B.22 The photodegradation of 0.01 mM 2-chlorophenol on 0.5%W/TiO_2 under blue light irradiation.

Time (min)		Residual of 2-chlorophenol (mM)	
		Run 1	Run 2
Adsorption	0	0.009	0.009
	15	0.008	0.008
	30	0.009	0.008
Irradiation	0	0.009	0.008
	30	0.006	0.006
	60	0.005	0.005
	90	0.004	0.004
	120	0.003	0.003
	180	0.002	0.002
	240	0.001	0.002
	300	0.001	0.001
	360	0.001	0.001

Note: TiO_2 dose 1g/L, pH 5, temperature 25ºC, blue light 2W (72 W/m^2), using NaOH and $HClO_4$ for adjust pH

Table B.23 The photodegradation of 0.01 mM 2-chlorophenol on hydrothermal-treated undoped TiO_2 under blue light irradiation.

Time (min)		Residual of 2-chlorophenol (mM)	
		Run 1	Run 2
Adsorption	0	0.012	0.012
	15	0.011	0.011
	30	0.011	0.011
Irradiation	0	0.011	0.011
	30	0.010	0.009
	60	0.007	0.007
	90	0.006	0.005
	120	0.005	0.004
	180	0.004	0.003
	240	0.002	0.002
	300	0.001	0.001
	360	0.000	0.000

Note: TiO_2 dose 1g/L, pH 5, temperature 25ºC, blue light 2W (72 W/m^2), using NaOH and $HClO_4$ for adjust pH

Table B.24 Photocatalysis of various initial concentration of 2-chlorophenol under blue light irradiation in present of hydrothermal-treated 0.5%W/TiO_2.

Time (min)		Residual of 2-chlorophenol (mM)		
		Run 1	Run 2	Run 3
Adsorption	0	0.010	0.010	0.010
	15	0.007	0.008	0.009
	30	0.007	0.007	0.008
Irradiation	0	0.007	0.007	0.008
	15	0.005	0.005	-
	30	0.004	0.003	0.004
	60	0.002	0.002	0.002
	90	0.001	0.001	-
	120	0.000	0.000	0.000
	180	0.000	0.000	0.000
	240	0.000	0.000	0.000
	300	0.000	0.000	0.000
	360	0.000	0.000	0.008

Note: TiO_2 dose 1g/L, pH 5, temperature 25ºC, blue light 2W (72 W/m^2), using NaOH and $HClO_4$ for adjust pH

Table B.25 Particle size distribution of undoped TiO_2.

Size (μm)	Intensity (%)	Size (μm)	Intensity (%)
0.05	0.00	6.63	1.24
0.06	0.00	7.72	1.34
0.07	0.00	9.00	1.44
0.08	0.00	10.48	1.55
0.09	0.00	12.21	1.68
0.11	0.00	14.22	1.83
0.13	0.00	16.57	2.00
0.15	0.00	19.31	2.20
0.17	0.00	22.49	2.43
0.20	0.00	26.20	2.67
0.23	0.00	30.53	2.91
0.27	0.04	35.56	3.14
0.31	0.09	41.43	3.36
0.36	0.14	48.27	3.55
0.42	0.19	56.23	3.74
0.49	0.23	65.51	3.95
0.58	0.26	76.32	4.20
0.67	0.28	88.91	4.51
0.78	0.27	103.58	4.89
0.91	0.28	120.67	5.30
1.06	0.28	140.58	5.71
1.24	0.30	163.77	6.04
1.44	0.33	190.80	6.09
1.68	0.37	222.28	5.67
1.95	0.43	258.95	4.67
2.28	0.52	301.68	3.09
2.65	0.61	351.46	1.51
3.09	0.71	409.45	0.00
3.60	0.82	477.01	0.00
4.19	0.94	555.71	0.00
4.88	1.04	647.41	0.00
5.69	1.15	754.23	0.00

Table B.26 Particle size distribution of 0.5%W/TiO_2.

Size (μm)	Intensity (%)	Size (μm)	Intensity (%)
0.05	0.00	6.63	0.81
0.06	0.00	7.72	1.02
0.07	0.00	9.00	1.28
0.08	0.00	10.48	1.59
0.09	0.00	12.21	1.93
0.11	0.00	14.22	2.31
0.13	0.00	16.57	2.71
0.15	0.00	19.31	3.12
0.17	0.00	22.49	3.51
0.20	0.00	26.20	3.87
0.23	0.00	30.53	4.18
0.27	0.02	35.56	4.42
0.31	0.04	41.43	4.53
0.36	0.07	48.27	4.69
0.42	0.09	56.23	4.74
0.49	0.11	65.51	4.77
0.58	0.12	76.32	4.81
0.67	0.12	88.91	4.87
0.78	0.12	103.58	4.95
0.91	0.11	120.67	5.05
1.06	0.10	140.58	5.12
1.24	0.10	163.77	5.07
1.44	0.11	190.80	4.84
1.68	0.11	222.28	4.37
1.95	0.13	258.95	3.60
2.28	0.16	301.68	2.56
2.65	0.19	351.46	1.33
3.09	0.24	409.45	0.10
3.60	0.31	477.01	0.00
4.19	0.39	555.71	0.00
4.88	0.50	647.41	0.00
5.69	0.64	754.23	0.00

Table B.27 Particle size distribution of hydrothermal-treated 0.5%W/TiO_2.

Size (μm)	Intensity (%)	Size (μm)	Intensity (%)
0.05	0.00	6.63	1.18
0.06	0.00	7.72	1.27
0.07	0.00	9.00	1.38
0.08	0.00	10.48	1.49
0.09	0.00	12.21	1.61
0.11	0.00	14.22	1.75
0.13	0.00	16.57	1.90
0.15	0.00	19.31	2.07
0.17	0.00	22.49	2.25
0.20	0.00	26.20	2.43
0.23	0.00	30.53	2.61
0.27	0.03	35.56	2.79
0.31	0.09	41.43	2.94
0.36	0.15	48.27	3.08
0.42	0.21	56.23	3.23
0.49	0.27	65.51	3.41
0.58	0.31	76.32	3.63
0.67	0.33	88.91	3.94
0.78	0.34	103.58	4.34
0.91	0.35	120.67	4.81
1.06	0.35	140.58	5.32
1.24	0.37	163.77	5.86
1.44	0.39	190.80	6.25
1.68	0.43	222.28	6.28
1.95	0.48	258.95	5.76
2.28	0.55	301.68	4.61
2.65	0.62	351.46	2.90
3.09	0.71	409.45	1.19
3.60	0.80	477.01	0.00
4.19	0.89	555.71	0.00
4.88	0.99	647.41	0.00
5.69	1.08	754.23	0.00

Table B.28 Point of zero charge determination by zeta potential method of undoped TiO_2.

pH	Zeta potential
2	29.50
3	23.70
3.5	-4.03
4	-19.00
5	-25.80
6	-27.70
7	-27.90
8	-26.80
9	-30.50
10	-29.10
11	-30.30
12	-27.60

Table B.29 Point of zero charge determination by zeta potential method of 0.5%W/TiO_2.

pH	Zeta potential
2	13
3	16.7
3.5	5.9
3.84	-10.9
4	-11.1
5	-22.9
6	-23.9
7	-26.2
8	-28.9
9	-26.9
10	-36.1
11	-37.4

Table B.30 Point of zero charge determination by zeta potential method of hydrothermal-treated 0.5%W/TiO_2.

pH	Zeta potential
2	29.5
3	23.7
3.5	-4.03
4	-19
5	-25.8
6	-27.7
7	-27.9
8	-26.8
9	-30.5
10	-29.1
11	-30.3
12	-27.6

Table B.31 Adsorption and desorption isotherm of undoped TiO_2.

Undoped TiO_2			
P/P_0	**Volume**	**P/P_0**	**Volume**
Adsorption		**Desorption**	
0.0577	53.6081	0.8995	114.7889
0.0792	57.1624	0.7920	113.6731
0.1043	60.6064	0.6914	112.7534
0.1501	65.8068	0.5920	111.5669
0.2008	70.5686	0.4984	107.9111
0.2515	74.8686	0.3994	86.5709
0.3021	78.8553	0.2922	78.0865
0.4077	86.7019	0.1917	69.7797
0.5074	94.0329	0.0932	59.2656
0.6074	101.3778		
0.7074	108.1806		
0.7997	112.5729		
0.9054	114.7032		
0.9939	119.1955		

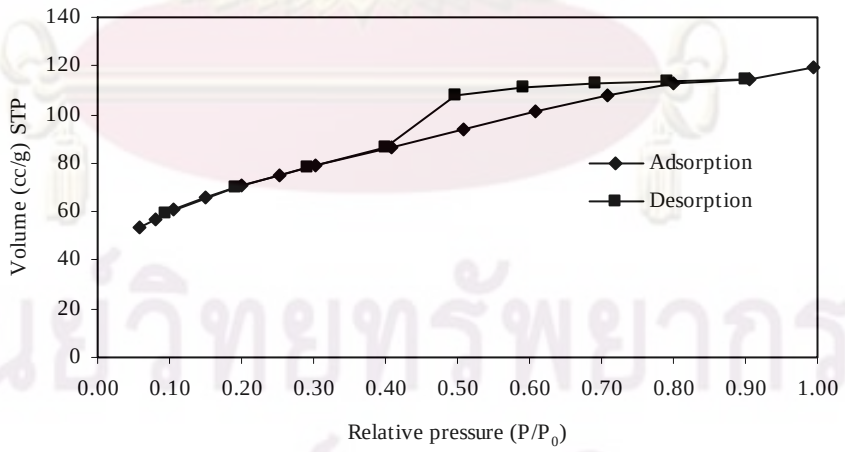

Figure B.1 Adsorption and desorption isotherm of undoped TiO_2.

Table B.32 Adsorption and desorption isotherm of 0.5%W/TiO_2.

0.5%W/TiO_2			
P/P_0	**Volume**	**P/P_0**	**Volume**
Adsorption		**Desorption**	
0.0584	48.4500	0.8912	72.1616
0.0809	51.0233	0.7907	71.7073
0.1062	53.3616	0.6905	71.3053
0.1537	56.7333	0.5903	70.8165
0.2049	59.4814	0.4912	69.9118
0.2564	61.6584	0.3999	65.9122
0.3074	63.3747	0.2958	62.9700
0.4052	65.8904	0.1980	59.1343
0.5065	67.7624	0.0909	52.0524
0.6070	69.3688		
0.7075	70.7484		
0.8083	71.6806		
0.9089	72.2882		
0.9967	80.9749		

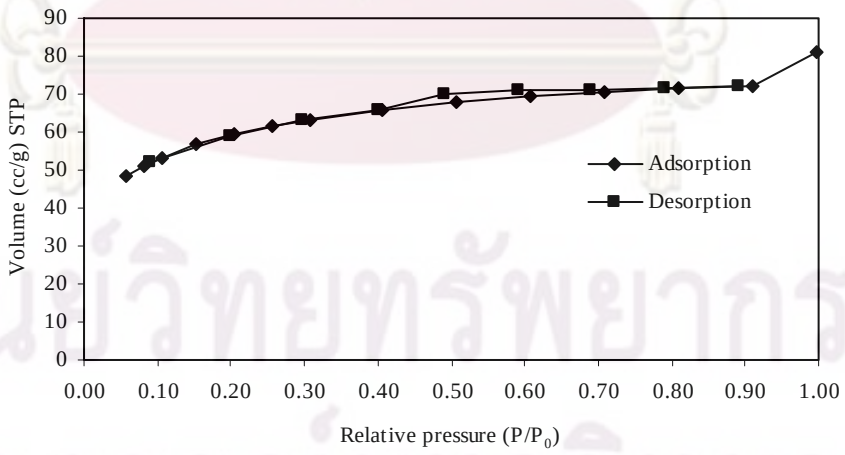

Figure B.2 Adsorption and desorption isotherm of 0.5%W/TiO_2.

Table B.33 Adsorption and desorption isotherm of hydrothermal-treated 0.5%W/TiO_2.

hydrothermal-treated 0.5%W/TiO_2			
P/P_0	**Volume**	**P/P_0**	**Volume**
Adsorption		**Desorption**	
0.0510	58.0385	0.9005	211.0169
0.0771	63.7190	0.7931	208.8683
0.1032	68.6185	0.6930	206.9103
0.1580	77.6586	0.5947	204.1074
0.1999	83.9810	0.5038	149.9670
0.2577	92.4298	0.3961	113.6686
0.2995	98.5467	0.2975	98.1910
0.3992	114.2499	0.1954	83.2356
0.5038	133.7554	0.0949	67.0282
0.5994	155.9137		
0.7014	184.0976		
0.8015	206.0261		
0.9013	210.9596		
0.9928	217.0818		

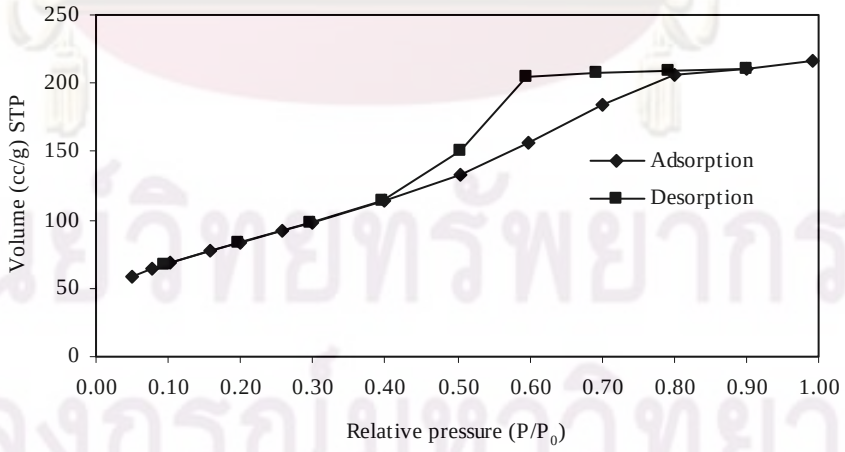

Figure B.3 Adsorption and desorption isotherm of hydrothermal-treated 0.5%W/TiO_2.

BIOGHAPHY

Miss Thapanan Putta was born on September 5th, 1982 in Uttaradit, Thailand. She received her Bachelor's degree in Industrial Technology from Department of Agricultural Machinery Technology, Faculty of Industrial Technology and Management, King Mongkut's University of Technology North Bangkok, Bangkok, Thailand in 2005. She received her Master's degree in Environmental Engineering from Department of Environmental Engineering, King Mongkut's University of Technology Thonburi in 2007. She pursued her Philosophy of Doctoral Degree studies in the International Postgraduate Program in Environmental Management (Hazardous Waste Management), Inter-Department of Environmental Management Chulalongkorn University, Bangkok, Thailand on May, 2007. She finished her Philosophy of Doctoral Degree in April, 2010.